MIT CEEPR

MIT Center for Energy and Environmental Policy Research

Working Paper Series

Spatial and Temporal Variation in the Value of Solar Power across United States Electricity Markets

PATRICK R. BROWN AND FRANCIS M. O'SULLIVAN

JULY 2019

CEEPR WP 2019-011

MASSACHUSETTS INSTITUTE OF TECHNOLOGY

Spatial and temporal variation in the value of solar power across United States electricity markets

Patrick R. Brown*[1] and Francis M. O'Sullivan[1,2,3]

[1]Energy Initiative, Massachusetts Institute of Technology, Cambridge, Massachusetts 02139, USA
[2]MIT Center for Energy and Environmental Policy Research
[3]Lincoln Clean Energy, LLC, Chicago, Illinois 60611, USA
*prbrown@mit.edu

Abstract

The cost of utility-scale photovoltaics (PV) has declined rapidly over the past decade. Yet increased renewable electricity generation, decreased natural gas prices, and deployment of emissions-control technology across the United States have led to concurrent changes in electricity prices and power system emissions rates, each of which influence the value of PV electricity. An ongoing assessment of the economic competitiveness of PV is therefore necessary as PV cost and value continue to evolve. Here, we use historical nodal electricity prices, capacity market prices, marginal power system emissions rates of CO_2 and air pollutants, and weather data to model the value of PV electricity at over 10 000 locations across the continental United States. We identify locations with persistently high PV value and calculate break-even PV costs based on the value of offset energy, capacity, CO_2 emissions, and public health costs arising from SO_2, NO_x, and $PM_{2.5}$ emissions. Under 2017 prices and grid conditions, PV breaks even at 50 % of nodes in New York and 60 % of nodes in the mid-Atlantic region based on the value of energy, capacity, and public health benefits, and at 100 % of nodes in Texas, the Midwest, and the mid-Atlantic under an additional 50 $/ton CO_2 price.

Graphical abstract

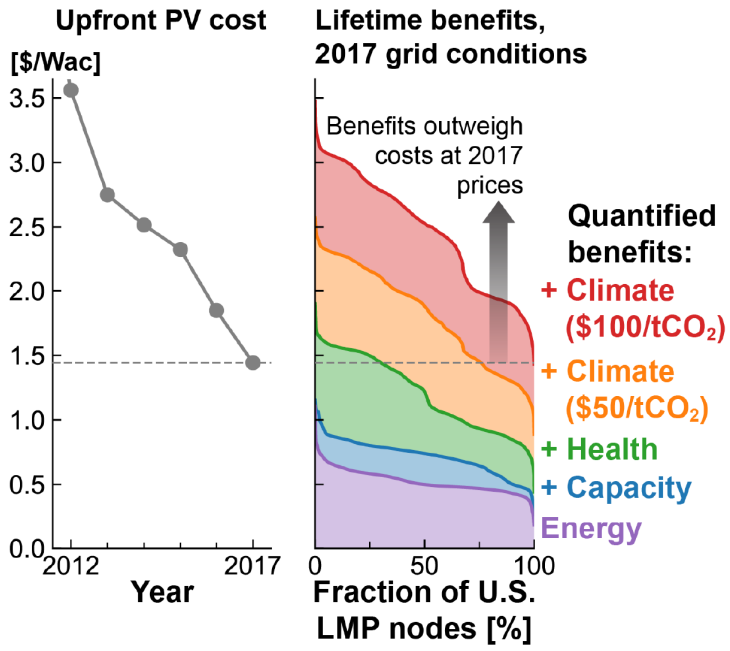

1 Introduction

Solar photovoltaics (PV) have demonstrated impressive reductions in cost and increases in deployment over the last decade: From 2010 to 2017, utility-scale system costs fell from 6 $\$/W_{ac}$ to $<1.5\,\$/W_{ac}$ and worldwide deployment increased from 40 GW to >400 GW. [1, 2] Yet numerous studies have noted that as the deployment of PV (or other zero-marginal-cost generation sources such as wind) increases, the value of PV electricity tends to decline as PV displaces higher-cost generators on the margin and reduces the wholesale price of electricity. [3, 4, 5, 6] This "merit-order effect" is most pronounced during times of day when solar energy generation is highest, causing the average market value of solar electricity to decline even more rapidly than the average electricity price. [7, 8, 9] At the same time, the adoption of emissions-control technology for coal generation over the last decade has reduced the marginal public health benefits of PV capacity, [10] and continued decarbonization of the power sector will further reduce these marginal benefits.

A number of strategies have been explored for mitigating the observed and projected value decline of variable renewables at the system level, including long-distance geographic

aggregation, [11] incorporation of energy storage and price-responsive demand, [11, 12] and use of high-capacity-factor system designs. [13, 14] Additional analyses have shown that siting renewables in locations with high electricity prices [15] or high power-system emissions rates [16, 17] can lead to larger benefits than siting in locations with the highest capacity factor or lowest levelized cost of energy (LCOE). However, the significant variability in prices and emissions rates within and across electricity markets, the effects of different market structures (particularly related to resource adequacy, i.e. capacity), and the large shifts in emissions rates and prices over the last decade have yet to be synthesized into a consistent framework that captures the spatial and temporal variability in the value of PV.

In this work we address the overarching question: How has the declining cost of PV aligned with changing conditions on the U.S. grid, and what does that imply for the competitiveness of PV today? More specifically: If a marginal addition of solar capacity had been installed at the site of a locational marginal electricity price (LMP) node in a given year between 2010–2017, what benefits would it have provided in terms of displaced energy, capacity, public health, and climate change costs in that year, and what upfront cost would the PV installation have had to achieve to break even over its lifetime, assuming that grid conditions in that year persist for the life of the PV installation?

To answer this question we assemble a large temporally- and spatially-synchronized dataset of historical day-ahead LMPs, system loads, capacity prices, marginal emissions rates and marginal damage rates from power system particulate matter emissions (resulting from SO_2, NO_x, and direct $PM_{2.5}$ emissions), and simulated solar generation, spanning more than 10 000 locations and eight years of operation. We identify significant variation in the value of PV electricity over time and across length scales substantially smaller than the size of Independent System Operators (ISOs). Marginal additions of PV capacity at recent upfront system costs are found to break even at large fractions of nodes for some regions on the basis of energy value, capacity value, and public health benefits alone, and at modest carbon prices for the remainder of locations.

1.1 Analytical approach

Our analysis covers six major U.S. ISOs: California ISO (CAISO), the Electric Reliability Council of Texas (ERCOT), Midwest ISO (MISO), the Pennsylvania-New Jersey-Maryland Interconnection (PJM), New York ISO (NYISO), and ISO-New England (ISONE), with node locations shown in **Figure 1**a. At each pricing node for which geographic information and a complete day-ahead LMP timeseries could be obtained for a given year (a sample size ranging

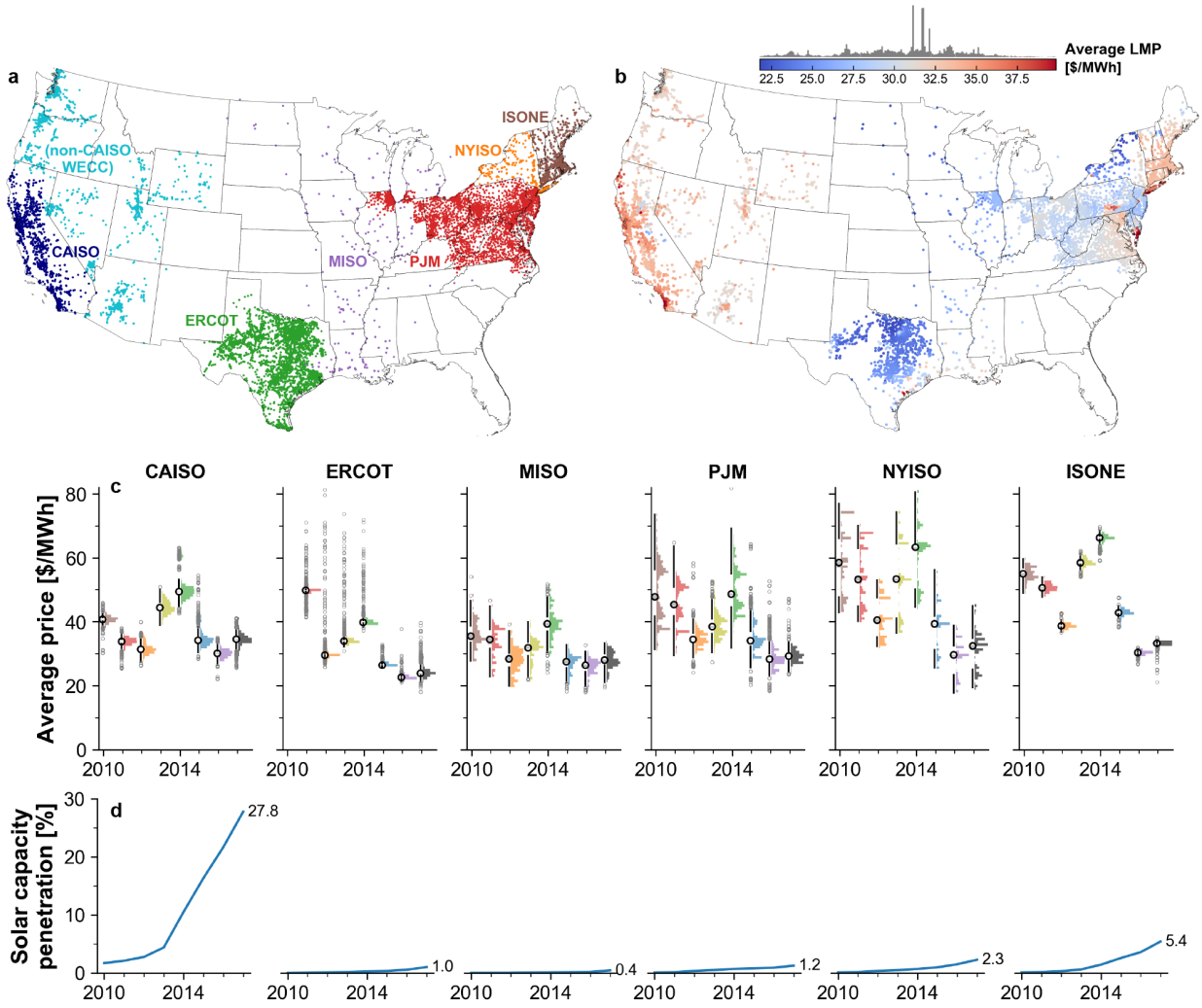

Figure 1: Variation in locational marginal electricity price (LMP) and solar penetration over the time period analyzed. a, Map of all pricing nodes considered in this study, with the corresponding ISO for each node indicated by the node color. Nodes labeled "non-CAISO WECC" lie outside of the CAISO system territory but have LMP and geographic data reported by CAISO. LMP data for a given node are not necessarily available for all years. **b**, Map of average nodal LMP on the day-ahead wholesale market in 2017. **c**, Yearly statistics for day-ahead nodal LMP by ISO for 2010–2017. **d**, Solar capacity penetration for each ISO between 2010 and 2017, given by cumulative installed solar generation capacity (utility-scale and distributed) divided by peak electricity demand within the ISO in each year. Data are from EIA, OpenPV, and the respective ISOs. [18, 19] Each column on each subplot in **c** corresponds to a single ISO-year and includes two components: on the left, summary statistics including the median (empty black circle), bootstrapped 95 % confidence interval for the median (gray bar), inter-quartile range (IQR, 25 %–75 %; white area between black whiskers), whiskers from the edge of the IQR to 1.5×IQR or the max/min value, whichever is closer (black lines), and outliers beyond the edge of the whiskers (gray circles); on the right, colored 101-bin histograms showing the distribution of values for each ISO-year. Sample sizes for each ISO-year are given in Table SI.1. Y-axis limits for **c** exclude some outlying nodes.

from ~7400 nodes in 2010 to ~13 700 nodes in 2017, as shown in Figure SI.1 and Table SI.1), the output of a utility-scale PV generator is simulated using historical irradiance data from the National Solar Radiation Database (NSRDB) [20] as inputs to a PV generation model based on the open-source PVLIB toolbox. [21, 22] The model accounts for PV module orientation, inverter DC/AC ratio, system and inverter losses, and temperature-induced module efficiency losses. This analysis assumes the use of 1-axis-tracking crystalline silicon (c-Si) PV arrays with a north/south axis of rotation (tracking from east to west throughout each day) and assumes must-run (i.e. non-curtailable) PV operation. A companion analysis uses this dataset to explore the impact of temporal PV output shaping—through tracking, curtailment, and orientation optimization—on the wholesale market value of PV energy. [23]

Modeled PV generation is validated at the monthly timescale against reported generation from hundreds of utility-scale PV plants, [18, 24] and at the hourly timescale against reported generation from a ~1 MW PV array at the site of the National Renewable Energy Laboratory (NREL). [25] Full validation results are described in the Supplementary Information (SI Note 3 and Figures SI.10 to SI.19).

At each node we assess four separate components of the value of a modeled PV generator: energy (from the LMP), capacity (i.e. resource adequacy), public health benefits (arising from the offset of SO_2, NO_x, and $PM_{2.5}$ emissions), and climate change mitigation arising from CO_2 emissions abatement. (The climate impact of abatement of non-CO_2 greenhouse gases is not included here; if included it would increase the modeled value of PV for climate change mitigation.) Yearly energy revenue in $\$/kW_{ac}$ per year at each node is given by the summed product of the time-synchronized PV AC power generation and LMP. Capacity revenue is given by combining historical capacity market clearing or contract prices with the calculated "capacity credit" for PV—the amount of firm generation capacity that a unit of PV capacity can displace while maintaining system reliability at the same level, indicating the fraction of the PV unit's peak capacity for which it is compensated on the capacity market. Capacity credit is here calculated from the modeled PV capacity factor during hours of peak net load (load minus utility-scale solar and wind generation). [26, 27, 15] Monetized public health benefits are calculated using the EASIUR model [28, 29, 30] and are given by the summed product of historical marginal damages from power system emissions and hourly modeled PV power generation. [31, 16]. Climate benefits are given by the summed hourly marginal emissions abatement [31, 32] multiplied by a chosen carbon price. Marginal emissions rates and damages are differentiated geographically by U.S. Environmental Protection Agency (EPA) Emissions & Generation Resource Integrated Database (eGRID) region [33] and

temporally by year, hour of day, and season (summer, winter, and spring/fall). [34] All monetary values are given in 2017 U.S. dollars (inflated from nominal input data using the Consumer Price Index [35]), and electric power and capacity factors are given in terms of AC output from the PV inverter. Additional details on the calculations and input data are given in the Methods and Supplementary Information.

1.2 Limitations of this analysis

Before describing our results, we first note several important caveats. First, the PV system services considered here include a combination of private benefits (resulting from market earnings from the LMP and capacity market) and public benefits (from air pollution and greenhouse gas mitigation); [36] we do not consider the impact of explicit subsidies (such as the investment tax credit or renewable energy credits procured to meet renewable portfolio standards) or implicit subsidies (such as net energy metering), which would entail a public-to-private wealth transfer from taxpayers and ratepayers to the solar owner. There are two potential interpretations within which the private and public benefits considered here can be put on equal footing. The first interpretation is to consider these values in a hypothetical policy environment where market-based policies capture the external cost of emissions, such that the total revenues calculated here are equivalent to private monetary gains by the solar owner. The second interpretation is from the point of view of a centralized power system planner. In this interpretation all benefits are public; net revenue represents the net benefit to society of avoided expenditures for energy and capacity provision and realized public health and climate benefits. We note that PV can result in further benefits and costs on the distribution system, including impacts (positive and negative) on distribution system losses, congestion, and upgrade requirements or deferral. These factors have been explored in other studies, [37, 38, 39] but require significantly more data on distribution system structure than is publicly available from the ISO sources used here.

Second, as we take the historical LMPs, loads, and marginal emissions rates as fixed, our results are relevant for assessing how a marginal unit of PV capacity—a "price-taker" in the context of the energy and capacity markets—competes with existing incumbent generators, and the impact of replacing existing generation with new PV generation. In the framework of Lamont [4] and Baker et al, [40] we thus address the "short-run" value of solar, as opposed to the medium- or long-run value, where the generation mix and associated price of electricity would be allowed to respond to additions of solar capacity. If a significant amount of PV generation capacity is installed at a given node or within the node's balancing area, LMPs and

the value of PV electricity at that location, as well as the PV capacity credit and marginal emissions offset, would decline due to the merit-order effect noted above. Other studies have employed econometric methods to assess the degree of causal relationship between solar deployment and solar value decline at the level of states or ISOs; [41, 42, 43] the data presented here could be used to increase the spatial resolution of such studies in subsequent work.

Third, we do not consider the impact of solar forecasting for participation in the day-ahead market; in effect we assume that the hourly day-ahead availability of each PV generator is perfectly predictable. A real PV plant would likely balance its participation in the day-ahead and real-time markets based on its confidence in output forecasts, expected divergence between day-ahead and real-time prices, and the magnitude of penalties imposed for deviation from scheduled generation. We also note that while most utility-scale PV plants sign multi-year power purchase agreements (PPAs) rather than rely solely on market revenues, the PPA value should scale with changes in the market value in a competitive market (with additional adjustments from applicable subsidies and the value of electricity price hedging, which are not included here).

Fourth, the health and climate benefits assessed here are sensitive to assumptions, particularly regarding the value of a statistical life (VSL) and discount rate. Climate benefits are difficult to quantify given the presence of positive and negative feedbacks, nonlinear tipping points, and the intergenerational nature of climate impacts, [44] and the appropriateness of using cost-benefit analysis to assess environmental impacts or existential risks such as climate change is open to debate. [45, 46] We do not assert that the prices assumed here for abated health and climate damages are the "right" prices; we simply explore the implications of assuming values widely used in the literature. [16, 10] The quantitative values of our results will change for different assumptions regarding these prices, but the directionality of the trends will be the same. The impact of alternative assumptions on the results presented here can be explored using the open-source computer code included in the Supplementary Information.

Finally, the presence of an emissions cap and trade program can complicate an assessment of the marginal emissions offset of solar. Under a firmly binding cap, a ton of emissions offset by solar would be replaced by a ton of emissions from another source. There are two cap and trade programs for carbon emissions active in the regions explored here: the California cap and trade program, and the Regional Greenhouse Gas Initiative (RGGI) for Connecticut, Delaware, Maine, Maryland, Massachusetts, New Hampshire, New Jersey, New York, Rhode

Island, and Vermont (covering all of ISONE and NYISO and part of PJM). As shown in Figure SI.3, over the time period analyzed, market clearing prices for CO_2 have been low: less than 15 \$/ton for California (within \$3 of the floor price in all years) and less than 7 \$/ton for RGGI in all years. [47, 48] SO_2 emissions are also subject to a cap and trade program under the EPA Acid Rain Program, but prices have been consistently low over the time period analyzed: 42 \$/ton in 2010 and 3 \$/ton or less in subsequent years, compared to a maximum of 1074 \$/ton in 2006 and a median public health cost ranging from 8000 \$/ton to 47 000 \$/ton over the regions and time period analyzed. [49, 31] For the assessment of the climate benefits of a marginal unit of PV generation, we subtract the clearing price for CO_2 in the California cap and trade program and RGGI for nodes covered by these markets from the chosen carbon price, as the clearing price is already factored into the LMP value. Effectively we negate the effect of existing cap and trade regulations on energy prices, then re-apply a uniform hypothetical carbon price across the ISOs. We do not model the effects of a higher carbon price on the merit-order dispatch stack; if formally implemented, a higher carbon price would make lower-emissions generators more likely to be dispatched, thus decreasing the marginal emissions rate of CO_2 and other pollutants and decreasing the emissions benefit of PV. No correction is made for the market clearing price of SO_2 given the very low price of SO_2 allowances over the time period analyzed compared to the social cost.

2 Results and discussion

2.1 PV energy value

Figure 2a displays a map of the modeled yearly energy revenue for PV arrays on the day-ahead wholesale market in 2017, and Figure 2b,c displays trends in revenue and value factor differentiated by ISO for each year from 2010–2017. Maps of the spatial distribution of revenue and value factor for each year, as well as maps and trends for the average value of solar electricity in \$/MWh, are displayed in Figures SI.23 to SI.25 in the Supplementary Information.

It is notable that the sunniest locations are not always the most profitable locations to install solar: the median nodal LMP revenue in the northeast (ISONE and NYISO) is greater than the median nodal LMP revenue in Texas (ERCOT) in three out of the seven years analyzed, despite the ~20 % higher median PV capacity factor in ERCOT. Two observations indicate that variation in solar revenue between sites is dictated more by variation in nodal LMP than by variation in capacity factor. First, the yearly variability in revenue (Figure 2b)

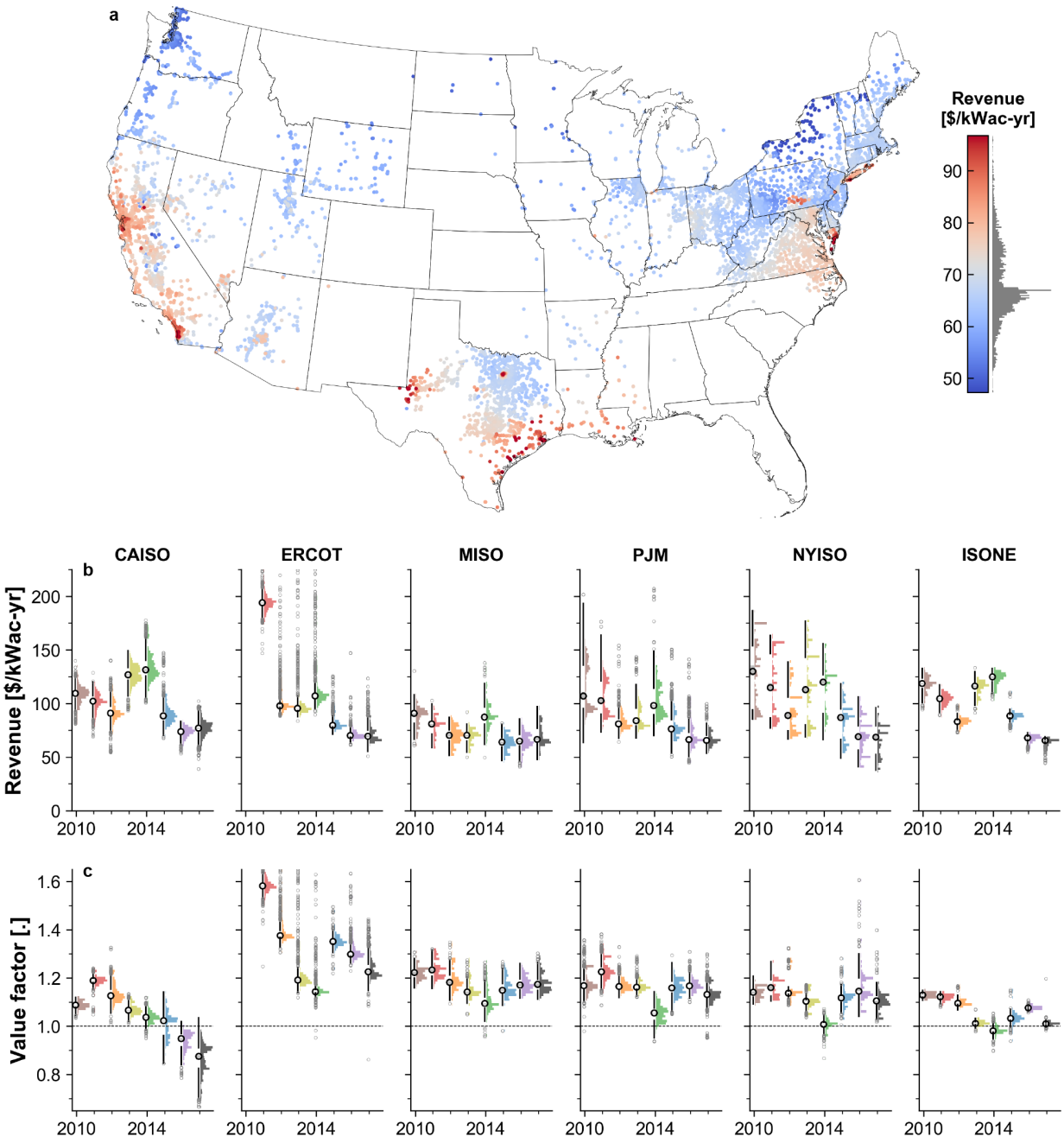

Figure 2: Modeled yearly PV revenue (a) on the day-ahead wholesale electricity market in 2017, and yearly statistics for PV revenue (b) and value factor (c) by ISO for 2010–2017. Each marker in **a** represents one pricing node. Statistics in **b-c** are displayed in the same format as Figure 1c. The value factor is the ratio of the average value of a MWh of solar electricity to the average price of electricity over the year.

is much greater than yearly variability in capacity factor (Figure SI.20a): median revenues over all ISOs and nodes range from 67 \$/kW$_{ac}$ per year in 2017 to 110 \$/kW$_{ac}$ per year in 2014 (a 65 % difference), while median capacity factors range from 22.5 % in 2011 to 24.7 % in 2016 (a 10 % difference) and median LMPs range from 28.1 \$/MWh in 2016 to 48.5 \$/MWh in 2014 (a 73 % difference). Second, spatial trends in yearly revenue (Figure 2a) more closely match spatial trends in average LMP than capacity factor (Figure 1b, Figure SI.21), and variance arising from congestion is larger than variance arising from capacity factor in most of the ISOs analyzed (Figure SI.30). These effects manifest most strongly in the observation of "hotspots" within the PJM ISO along the east coast where the yearly solar revenue is in some years more than double the median across the ISO as a whole.

While we focus on the years 2010–2017 for the bulk of this study given more complete data coverage across all ISOs for these years, PJM and NYISO provide LMP data dating back to 2001 and 2000, respectively. As shown in Figures SI.26 to SI.28, the hotspots noted above, particularly on Long Island and the Delmarva peninsula, have been observed for more than a decade, and the same collection of nodes tend to remain at the high extreme of the nodal revenue distribution from year to year. Disaggregation of the LMP into the marginal costs of energy, congestion, and losses (Figures SI.29 to SI.31) shows that these hotspots are driven by high congestion prices, which increase energy-only revenues by more than 50 \$/kW$_{ac}$ per year for some years. While the observed revenue dispersion is long-lived, the magnitude of the revenue at these nodes tends to rise and fall in line with trends in the ISO median value, driven by year-to-year variation in the energy price.

There is also notable variation in value factor between the different ISOs. ERCOT demonstrates the highest median value factor in each year (Figure 2c); given ERCOT's low solar penetration, high air conditioning load during sunny periods, and high price cap for electricity (associated with ERCOT's unique status as the only "energy-only" electricity market among the ISOs considered here), PV generation is likely to coincide with high-price periods in the ERCOT system, increasing its value factor. CAISO demonstrates the most pronounced decline in value factor over the period studied—from a median value factor of 1.09 in 2010 (1.06–1.12 at the central 95 % of nodes) to 0.87 in 2017 (0.72–0.96 at the central 95 % of nodes)—coinciding with its ∼15× increase in solar capacity penetration over this time period (Figure 1d).

2.2 PV capacity value

In markets where the LMP is administratively capped at an upper limit, additional payments to generators are necessary to ensure that there is adequate incentive to install sufficient generation capacity to meet demand across all hours. These "capacity payments" are made either through bilateral contracts between grid operators and individual generators (in the case of CAISO), or through a capacity market that clears seasonally or yearly (in the case of MISO, PJM, NYISO, and ISONE). **Figure 3**a shows the historical capacity prices for the five ISO capacity markets considered here, [50, 51, 52, 53, 54] and Figure 3b shows the nodal distribution of calculated capacity credits for 1-axis-tracking PV over 2010–2017. Where possible, capacity credits are shown using both ISO-defined critical hours (red curves) and the highest 7.04 % of net-load hours (blue curves) per year, where 7.04 % is the average of the number of hours used by MISO, PJM, NYISO, and ISONE for PV capacity credit assessment. [55, 56, 57, 58]

As shown in Figure 3b and Figure SI.33 and noted in [26, 27], the capacity credit is sensitive to the number of hours counted as critical; in general the higher the number of hours considered, the lower the capacity credit for PV. The high fraction of hours and explicit inclusion of winter evenings in the ISO-defined capacity credit calculations for NYISO and ISONE, in conjunction with the relatively low capacity factor of PV in the Northeast, leads to a low capacity credit for these ISOs. As CAISO does not specify specific hours for the PV capacity credit calculation, we only include the capacity factor calculated over peak-net-load hours, which has fallen from a median value of 53 % in 2010 to 25 % in 2017 as increased PV generation has pushed peak-net-load hours to the morning and evening.

Figure 3c shows the calculated capacity revenues over time, using the ISO-defined critical hours for MISO, PJM, NYISO, and ISONE and the top 7.04 % of net-load hours for CAISO. For most nodes and years the capacity revenue is small compared to the energy revenue (Figure 2b), but for some nodes—particularly those centered around New York City, and the Boston area in 2017—the capacity revenue can reach 40 % to 80 % of the energy revenue. The PJM and NYISO markets demonstrate the most within-ISO variability in capacity revenues, driven by large variation in capacity prices between their constituent capacity zones: in NYISO the interquartile range (IQR) of capacity revenues is $\geq 25\,\$/\mathrm{kW_{ac}}$ per year in each year, and in both PJM and NYISO the IQR is $\geq 42\,\$/\mathrm{kW_{ac}}$ per year in at least one year.

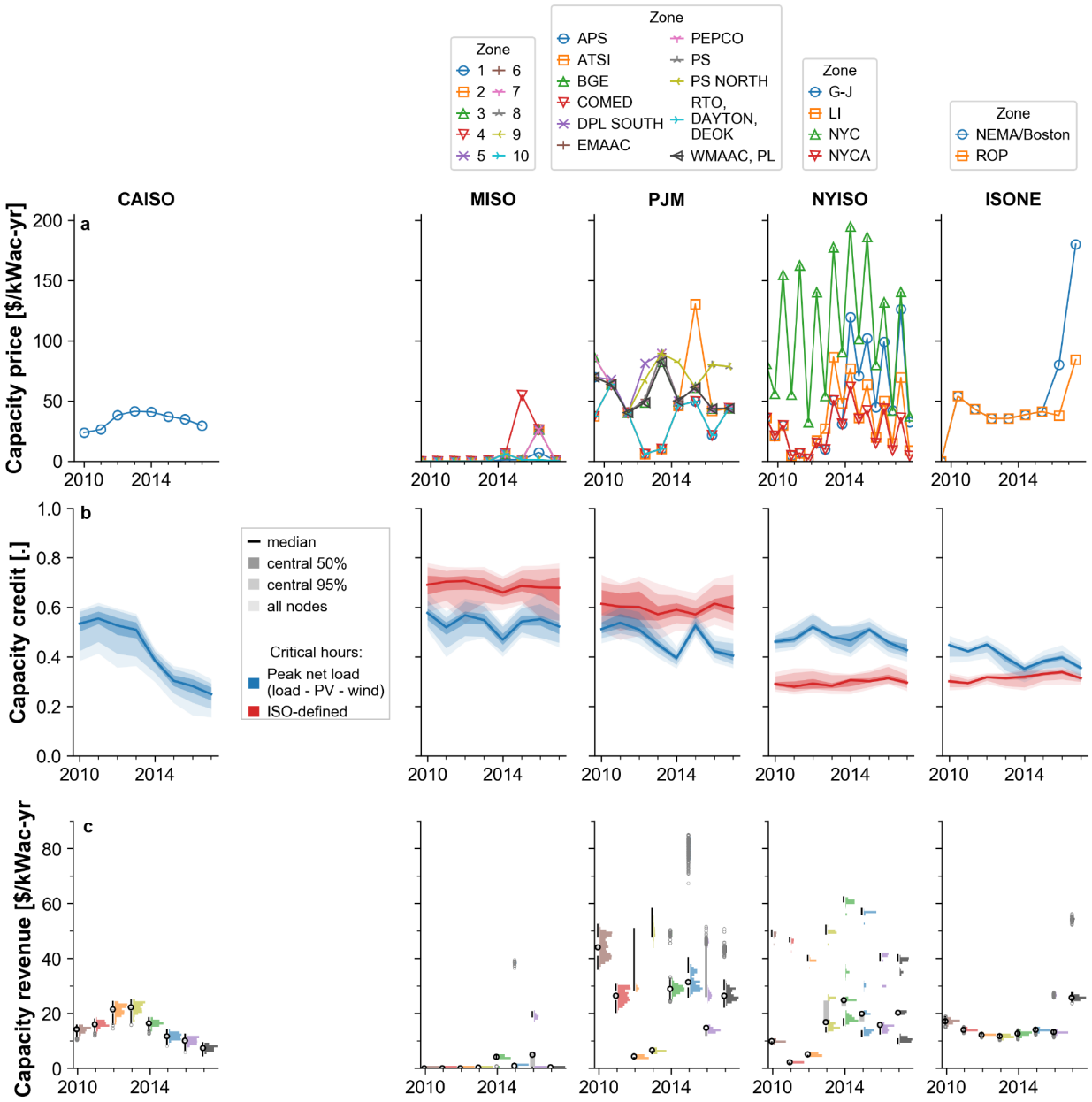

Figure 3: Capacity value of PV by ISO. a, Historical capacity price by ISO resource-adequacy zone. [50, 51, 52, 53, 54] Zone maps are shown in Figure SI.7 in the Supplementary Information. Prices for CAISO are weighted average (median for 2010–2011 due to data availability) capacity contract prices; prices for MISO, PJM, NYISO, and ISONE are market-clearing prices. ERCOT is not included in this analysis as it does not have a capacity market. Intervals before the capacity market became active in a given ISO (before the 2010/2011 season in ISONE and before the 2013/2014 season in MISO) are assigned a price of zero. Data for CAISO, MISO, PJM, and ISONE reflect annual capacity auction prices, while data for NYISO include both summer and winter capacity auction prices. Markers are located at the beginning of the corresponding compliance period; lines between markers are guides to the eye. **b**, Distribution of modeled PV capacity credits across all nodes in each ISO from 2010–2017, given by the average capacity factor of a modeled 1-axis-tracking PV array during "critical-load hours" over each year. Red curves indicate capacity credit calculated assuming ISO-specified critical-load hours; blue curves indicate capacity credit calculated with the top 7.04 % of net load hours (ISO-wide demand minus modeled utility-scale solar and ISO-reported wind production) taken as critical-load hours. **c**, Distribution of modeled PV capacity revenues by ISO over time for PV arrays at all modeled ISO nodes. Revenues are calculated using the top 7.04 % of net load hours for CAISO and the ISO-specified hours for MISO, PJM, NYISO, and ISONE.

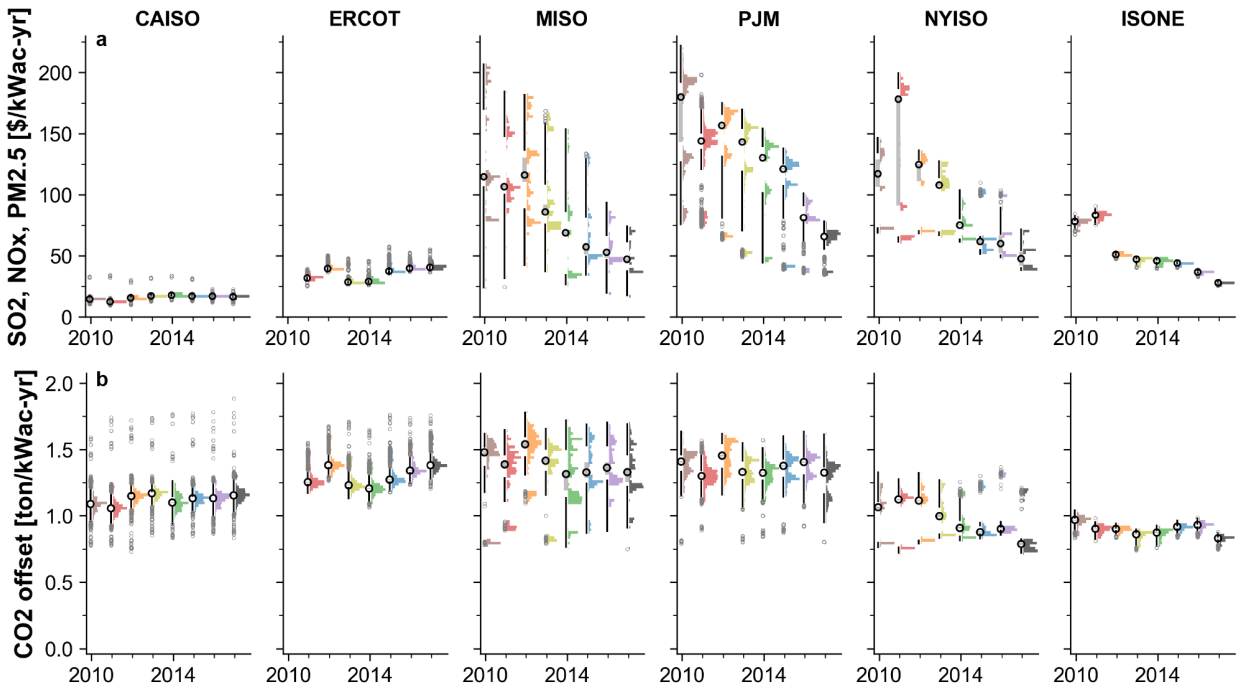

Figure 4: Public health and climate benefits from PV generation by ISO. a, Distribution of modeled public health benefits associated with SO_2, NO_x, and $PM_{2.5}$ mitigation by 1-axis-tracking PV arrays across nodes within each ISO. Marginal damage rates are calculated using the EASIUR model. [31] **b**, Modeled CO_2 abatement associated with PV generation at nodes within each ISO. Marginal emissions rates are from [31]. Marginal damages and emissions rates are differentiated by operational year, eGRID region, season, and hour of day; nodes are assigned to eGRID regions based on their geographic location (Figures 1 and SI.4).

2.3 PV health and climate benefits

Marginal public health benefits from PV generation arising from SO_2, NO_x, and $PM_{2.5}$ emissions mitigation have been declining with time in MISO, PJM, NYISO, and ISONE (**Figure 4**a), as noted by Millstein et al. [10] In spite of this decline, median public health benefits in 2017 are still substantial, equating to roughly 70 % of median 2017 energy revenue in MISO, 100 % in PJM, and 70 % in NYISO (Figure 2b). The majority of public health benefits over the time period analyzed have resulted from SO_2 mitigation, as shown in Figure SI.35, which disaggregates benefits by pollutant. Some of the highest-health-benefit nodes—such as those in New York City—do not necessarily have high marginal emissions rates, but have large associated damages resulting from their high population density.

CO_2 emissions offsets associated with PV generation, shown in Figure 4b, have been more stable than SO_2, NO_x, and $PM_{2.5}$ offsets over the time period analyzed, suggesting that the decline in air pollutant emissions has primarily resulted from the adoption of tighter air-quality standards and installation of SO_2- and NO_x-control technologies. While *average* CO_2

emissions rates across ISOs have declined as a result of increased natural gas and renewables generation (Figure SI.5), [59] the distribution of marginal generators has undergone little change, [10] leading to a relatively small change in marginal CO_2 emissions rates over time (Figure SI.6). [31]

2.4 PV system breakeven costs

To assess the competitiveness of an investment in PV capacity at a given node, we calculate the net present value (NPV) of PV electricity assuming that the value of PV services described above (energy, capacity, and emissions mitigation) for a given year is maintained for the duration of the plant's life, solving for the "breakeven" upfront cost that would set the NPV to zero.

The NPV is given by

$$\mathrm{NPV} = \sum_{t=1}^{L} \frac{\left(\left(R + C_{\mathrm{CO_2}} M_{\mathrm{CO_2}}\right)(1-d)^t - C_{OM}\right)(1-T) + \frac{D_t}{(1+i)^t} C_{PV} T}{(1+\rho)^t} - C_{PV} \qquad (1)$$

where L is the lifetime of the PV array; R is the yearly PV revenue, including contributions from energy (Figure 2b), capacity (Figure 3c), and public health (Figure 4a) where noted; $C_{\mathrm{CO_2}}$ is the price on carbon emissions; $M_{\mathrm{CO_2}}$ is the annual marginal CO_2 displaced per unit of PV capacity in a given ISO (Figure 4b); d is the annual degradation rate in PV output; C_{OM} is the annual operations and maintenance cost; T is the combined federal and state tax rate; D_t is the percentage of the upfront cost depreciated in year t using the 5-year Modified Accelerated Cost Recovery System (MACRS), assuming the PV owner can completely monetize the tax benefits of depreciation; i is the annual inflation rate; ρ is the real weighted average cost of capital (WACC); and C_{PV} is the upfront system cost. [60] Numerical values and sources for financial parameters are given in **Table 1**. The effects of federal, state, and local subsidies are not included here. Calculated breakeven costs are sensitive to input assumptions, particularly regarding the WACC, as shown in Figure SI.37.

Figure 5b shows the distribution in calculated breakeven PV cost across all nodes in 2017 considering different collections of PV services, compared to observed upfront PV system costs (Figure 5a). [1] Under the stated financial assumptions and considering the value of energy, capacity, and public health benefits (green curves, leaving out climate benefits), PV would break even at the 2017 upfront cost of 1.44 $\$/\mathrm{W_{ac}}$ at 30 % of the modeled nodes, ranging from 0 % of nodes in CAISO, MISO, and ISONE to ~50 % in NYISO and ~60 % in PJM. At a carbon price of 50 $\$/\mathrm{tonCO_2}$ (corresponding to the central value for 2020

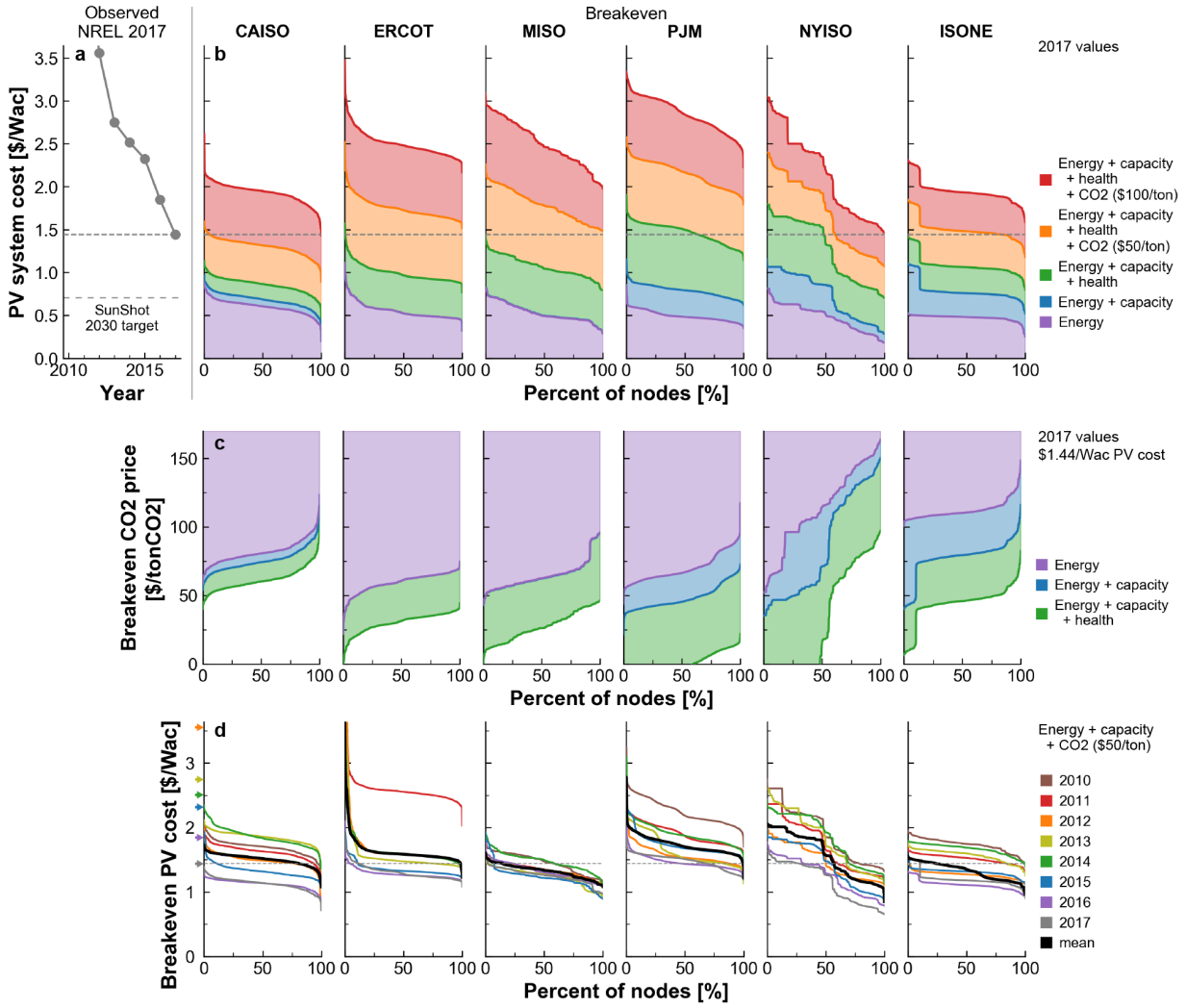

Figure 5: Observed capital cost and distribution of breakeven costs for PV arrays across all modeled nodes. Observed PV capital costs (**a**) are taken from Fu et al [1] for a 100 MW 1-axis-tracking PV array. The U.S. Department of Energy SunShot PV cost target for 2030 is included in **a** for context. [66] Each trace in **b** shows the percentage of nodes across each ISO that would break even below the corresponding upfront system cost on the y-axis, assuming that the nodal revenue in 2017 persists for the lifetime of the system. Colored traces and areas indicate the cumulative inclusion of revenue from the wholesale energy (LMP) market (purple), capacity market (blue), public health benefits (green), carbon mitigation assuming a 50 \$/ton CO_2 price (orange), and carbon mitigation assuming an additional 50 \$/ton CO_2 price (100 \$/ton total) (red). Dotted lines are included at 1.44 $\$/W_{ac}$, the 2017 observed PV system cost, to guide the eye. **c**, Breakeven CO_2 prices for PV in 2017, assuming an upfront system cost of 1.44 $\$/W_{ac}$. Note that in **c**, PV breaks even at CO_2 prices above the plotted line; in plots of the breakeven PV system cost (**b**,**d**), PV breaks even at upfront costs below the plotted line. **d**, Breakeven upfront costs for energy, capacity, and climate benefits for 2010–2017 profile years, assuming a 50 \$/ton CO_2 price. In **d**, colored arrows along the leftmost y-axis indicate the observed upfront PV system costs for each year shown in **a**. The black trace labeled "mean" is the nodal average breakeven cost, including all available years of data for each node. Figure SI.38 in the Supplementary Information shows yearly breakeven costs under alternative carbon price assumptions.

Table 1: Default assumptions for net-present-value calculation.

Parameter	Symbol	Value	Units	Reference
PV array lifetime	L	30	[years]	[1]
Revenue (energy, capacity, health)	R	*calculated*	[\$/kW$_{ac}$ per year]	
CO_2 price	C_{CO_2}	[0, 50, 100]	[\$/tonCO_2]	
CO_2 displacement	M_{CO_2}	*calculated*	[ton/kW$_{ac}$ per year]	
Degradation rate	d	-0.5	[%/yr]	[61, 62]
Operations & maintenance cost	C_{OM}	20	[\$/kW$_{ac}$ per year]	[1]
Federal & state tax rate	T	28	[%]	[63]
5-year MACRS depreciation in year t	D_t	*variable*	[%]	[64]
Inflation rate	i	2.5	[%]	[1]
Real weighted average cost of capital	ρ	7.0	[%]	[65]

historically used by the U.S. federal government [67]), PV would break even at ~75 % of the modeled nodes, ranging from 5 % in CAISO to 100 % in ERCOT, MISO, and PJM. A small reduction in upfront PV cost would deliver large gains: with a 10 % reduction in PV upfront cost, PV would break even at 90 % of modeled nodes and 50 % of CAISO nodes. (For comparison, PV costs have dropped 18 % per year on average since 2010. [1]) At a carbon price of 100 \$/tonCO_2, which approaches the floor price estimated to be necessary to achieve the goals of the 2015 Paris agreement (floor price estimates in the literature range from 116 \$/tonCO_2 to at least 220 \$/tonCO_2 [68, 69, 70, 71, 72]), PV at today's upfront cost would break even at 100 % of nodes in all ISOs.

If only market revenues from energy and capacity are counted (neglecting social benefits from abated emissions), median breakeven costs in 2017 range from 0.50 \$/W$_{ac}$ in MISO to 0.85 \$/W$_{ac}$ in NYISO. An alternative metric is the breakeven carbon price: as shown in Figure 5c, at the 2017 upfront PV cost of 1.44 \$/W$_{ac}$, median breakeven carbon prices range from 0 \$/tonCO_2 in PJM to 60 \$/tonCO_2 in CAISO in 2017 if energy, capacity, and public health values are included, and from 45 \$/tonCO_2 in PJM to ~80 \$/tonCO_2 in ISONE if only energy and capacity are included.

As noted above, energy and capacity revenues and the value of abated emissions demonstrate a large amount of variability from year to year, so the breakeven costs for 2017 shown in Figure 5b,c do not hold for all years. Some of the drivers of this variability—such as variations in gas price, hydropower availability, and capacity price—are relatively cyclical, while others—such as the decline in PV value factor and capacity credit in CAISO and the decline in marginal health benefits associated with the adoption of emissions-control measures—reflect longer-term trends that appear unlikely to change direction. To illustrate

the effect of year-to-year price variations, Figure 5d shows the calculated breakeven PV costs using different yearly profiles for energy and capacity prices, including a 50 $/ton CO_2 price but leaving out marginal health benefits (which, as noted above, appear unlikely to return to the high levels witnessed early in the decade). Breakeven costs for 2017 are near the bottom of the distribution over the years analyzed, as natural gas prices (and correspondingly LMPs) in 2017 were at the low end of their distribution over 2010–2017. Averaging the calculated energy, capacity, and climate benefits over 2010–2017 (heavy black lines in Figure 5d), PV breaks even at 2017 PV costs at ~85 % of modeled nodes, from ≤25 % in MISO and ISONE to ~55 % in NYISO, 80 % in CAISO, and ≥ 98 % in ERCOT and PJM.

3 Conclusions

While the marginal value and upfront system cost of PV have both declined over the last decade, the results described here suggest that cost decline has outpaced value decline, such that in 2017 the net benefits of utility-scale PV outweigh the cost across the majority of U.S. electricity markets when the social benefits of particulate matter and CO_2 emissions abatement are included. Current cap-and-trade market prices for CO_2 and SO_2 emissions are much lower than estimates of the social cost of emissions, suggesting that emissions caps should be lowered (or that emissions floor prices should be raised) in order to provide appropriate incentives for low-carbon generation sources such as PV. A next-best alternative to instituting appropriate emissions prices is to tailor PV deployment support mechanisms to reflect spatial differences in the benefits of PV generation. Persistent transmission congestion over the time period analyzed results in variation in the energy, capacity, health, and climate benefits of a unit of PV generation capacity depending on its location of interconnection with the electric grid. As shown in Figure 4a, nodal public health benefits from PV generation in the New York ISO have varied by roughly a factor of 2 across the state in any given year from 2010–2017, but existing renewable energy credits reward generation equally, irrespective of its location within the state.

The analysis described here applies primarily to utility-scale generators on the transmission grid, which are exposed to the spatially- and temporally-varying signals provided by the LMP. Residential and small commercial electricity customers on the distribution grid typically are not exposed to such signals, leading to installation incentives that are not necessarily matched to the system value of PV energy. Passing the spatial and temporal signals from the LMP (along with appropriate emissions prices) as far into the distribution system as

possible could help steer PV deployment to congested high-price locations, reducing prices for other electricity consumers and ensuring that distributed and utility-scale solar generators can compete on equal footing. [73]

It is important to emphasize that the breakeven costs shown here are for a marginal unit of PV capacity. As grid conditions change—through continued deployment of renewables, expansion of transmission capacity, retirement of existing plants, shifts in the price of natural gas, variations in hydropower availability, changes in climate and demand patterns, and evolution in other factors—there will be associated changes in LMP, net load, and marginal emissions rate profiles, leading to corresponding changes in the breakeven cost for PV and other technologies. Current electricity market designs, particularly regarding resource adequacy, will also need to be adjusted to adapt to generation mixes dominated by low- and zero-marginal-cost sources. [74, 75] On the whole, the upfront cost whereat PV breaks even is expected to decline with increasing PV penetration, [6] necessitating continued cost reductions for PV. Nevertheless, the experience so far in CAISO, where despite its 5–10× higher PV penetration than the other ISOs, PV would still break even at most nodes at an upfront cost within 10 % of observed 2017 costs, suggests that there is still considerable room for competitive PV expansion across the continental U.S., particularly in the interior and mid-Atlantic regions. The strategies presented here for assessing the locational value of PV electricity can be extended to other distributed energy resources such as wind power [76] and energy storage, [60] and incorporation of spatial, temporal, and technological resolution will become increasingly important as the electric power system evolves and relies increasingly on variable renewable energy resources.

4 Methods

4.1 Data sources

Meteorological data: Meteorological data including global horizontal irradiance (GHI, W/m^2), direct normal irradiance (DNI, W/m^2), diffuse horizontal irradiance (DHI, W/m^2), surface air temperature (°C), and surface wind speed at 2 m height (m/s) are taken from the National Solar Radiation Database Physical Solar Model (NSRDB PSM). [20] These data are derived from satellite observations and are available on a 4 km × 4 km grid across the continental United States, at 30 min resolution for historical data from 1998–2017 and at 60 min resolution for a typical meteorological year (TMY). The meteorological data for a given timestamp are assumed to remain constant until the next timestamp; for example, the reported insolation,

wind speed, and temperature at 8:00 are assumed to remain constant until 8:30. Historical meteorological data are used for all calculations; Figures SI.9 and SI.21 show the observed difference between historical and TMY capacity factors.

Electricity price: Complete sets of hourly day-ahead locational marginal price (LMP) data for electricity at all reported pricing nodes are obtained from the respective ISOs. [77, 78, 79, 80, 81, 82, 83] For simplicity, all nodes within California are labeled as "CAISO", even though the CAISO footprint does not cover the entire state of California. Only nodes with serially complete LMP availability for a given calendar year are utilized. All dollar values are converted to 2017 U.S. dollars using the historical consumer price index. [35]

The geographic locations of pricing nodes for CAISO, MISO, PJM, and NYISO are obtained from publicly-available sources. Node latitudes and longitudes for CAISO and MISO are available directly. [84, 85] For PJM, node locations are inferred from a list of the closest nodes to each zip code within the PJM service area; [86] the location of each node is taken as the centroid of the centers of all of the zip codes that list that node. For NYISO, node locations are resolved at the city or county level; [87] if a single node is listed for multiple cities or counties, the location of that node is taken as the centroid of the centers of all the cities or counties that list that node. Node locations for ERCOT and ISONE are not publicly available, and were obtained through correspondence with ISO representatives. Only pricing nodes with both LMP and geographic information are used in this analysis. A map of nodal data availability is given in Figure SI.1.

Capacity market clearing prices are obtained from the respective ISOs. [50, 51, 52, 53, 54] Pricing nodes are assigned to capacity zones based on their geographic locations (for MISO, NYISO, and ISONE) [85, 88] or published node-to-zone listings (for CAISO and PJM). [84, 89]

Load: Hourly load used in the calculation of PV capacity credit is taken from the FERC Form 714 Database. [90] The MISO coverage area has changed over the analyzed time period; MISO load in each year is taken as the sum of loads for MISO, SMEPA (South Mississippi Electric Power Association), Cleco, and Entergy.

Marginal emissions and damages: Marginal emissions rates for CO_2, SO_2, NO_x, and $PM_{2.5}$, and marginal public health damages for SO_2, NO_x, and $PM_{2.5}$, are taken from [31] and described in detail in [32, 16]. Emissions rates are disaggregated by EPA eGRID region, [33] year, season (Summer, May–September; Winter, November–March; Transitional, April and October), and hour of day. Marginal damages are calculated using the EASIUR model [28, 29, 30] assuming a value of a statistical life (VSL) of 8.6 million USD2010 and a relative

risk of 1.06 per 10 µg/m^3 increase in $PM_{2.5}$ concentration. Marginal damages calculated using the AP2 model, which are not used in the analysis but are provided for comparison with results from the EASIUR model, are shown in Figure SI.36. [91, 92, 93, 31]

PV capacity: PV capacity penetration in Figure 1d includes utility-scale PV capacity reported in EIA Form 860 [18] and distributed PV capacity reported by the OpenPV project. [19] The EIA Form 860 database only includes installations greater than 100 kW in capacity, so to prevent double-counting between the two data sets, only installations with capacity less than 100 kW are included from OpenPV. Capacity penetration is calculated by dividing the sum of utility-scale PV and distributed PV capacity by the peak ISO-wide demand in each year. The DC/AC ratio χ is assumed to be 1 for installations reported in the OpenPV dataset. For the purpose of PV capacity quantification in Figure 1d, CAISO includes all of California; ERCOT includes all of Texas; PJM includes all of Ohio, Pennsylvania, New Jersey, Delaware, Maryland, West Virginia, and Virginia; MISO includes all of North Dakota, South Dakota, Minnesota, Wisconsin, Iowa, Illinois, Indiana, Michigan, Arkansas, Louisiana, and Mississippi; NYISO includes all of New York; and ISONE includes all of Maine, Vermont, New Hampshire, Massachusetts, Rhode Island, and Connecticut.

4.2 PV generation

4.2.1 Model formulation

Time-resolved alternating-current (AC) PV power generation for a PV generator at each pricing node is simulated using the open-source PVLIB Python toolbox originally developed at Sandia National Laboratories, [94, 21, 22] with input meteorological data taken from NSRDB as described above. Numerical assumptions for PV system characteristics are listed in **Table 2**. Assumptions generally match those used in the PVWatts model for crystalline silicon modules [95, 96] and recent PV industry trends. [97, 1]

For a given node location, the solar position and extraterrestrial DNI are calculated at each timestamp, and airmass is determined from the calculated solar position. For 1-axis tracking, the tracker angle ψ is calculated at each timestamp from the solar position, axis tilt (θ), and axis azimuth (ϕ), subject to the maximum tracker angle ψ_{max} and ground coverage ratio κ. "Backtracking" – a reduction in the tracker angle ψ during times close to sunrise and sunset to prevent shading between parallel rows of panels – is employed for all tracking simulations. [98] Direct and diffuse plane-of-array (POA) irradiance are calculated according to the Reindl diffuse sky model, [99, 100] taking into account the solar position, array orientation, measured

Table 2: Default assumptions for PV generation model.

Parameter	Symbol	Value	Units
Axis tilt, 1-axis tracking array	θ	0	degrees from horizontal [°]
Axis azimuth	ϕ	180	degrees clockwise from north [°]
DC/AC ratio	χ	1.3	fraction [.]
DC system losses	η_{system}	14	percent [%]
Nominal inverter losses	$\eta_{inverter}$	4	percent [%]
Temperature coefficient	γ	-0.4	percent relative to 25 °C [%/°C]
Maximum tracker angle	ψ_{max}	60	degrees from center [°]
Ground coverage ratio	κ	0.33	fraction [.]
Ground albedo	α	0.2	fraction [.]
Antireflection coating index	n_{ar}	1.3	fraction [.]

irradiance (GHI, DNI, and DHI) from NSRDB, airmass, extraterrestrial DNI, [101, 102] and ground albedo (which contributes to diffuse POA irradiance at nonzero tilt angles). Off-normal reflection losses for direct POA irradiance are calculated from Fresnel's equation as in [95] assuming indexes of refraction $n_{air} = 1$ for air, n_{ar} given in Table 2 for the antireflection coating, and $n_{glass} = 1.526$ for glass. Global POA irradiance is calculated from the sum of direct (after reflection losses), sky diffuse, and ground diffuse POA irradiance. PV cell temperature is calculated using the Sandia PV Array Performance Model [103] assuming open rack mounting with polymer backplane modules, taking into account surface air temperature and wind speed from NSRDB and global POA irradiance. DC power output as a fraction of nameplate DC capacity P_{dc}^0 is given by

$$\frac{P_{dc}}{P_{dc}^0} = \frac{I_G^{POA}}{1000} \left(1 + \gamma \left(T_{cell} - 25\,^\circ\mathrm{C}\right)\right) \left(1 - \eta_{system}\right) \tag{2}$$

where I_G^{POA} is global POA irradiance (W/m^2), γ is the temperature coefficient of the PV cell, T_{cell} is the calculated PV cell temperature, and η_{system} is the DC system losses. AC power output as a fraction of nameplate AC capacity is calculated as in PVWatts [95] incorporating the DC/AC ratio χ and nominal inverter losses $\eta_{inverter}$. When $(P_{dc}/P_{dc}^0) \times \chi > 1$, the AC output is clipped to the nameplate AC capacity. All capacities and capacity factors are presented in terms of nameplate alternating-current (AC) capacity and AC capacity factor. Figure SI.8 in the Supplementary Information shows the sensitivity of calculated AC capacity factor to changes in each of the variables listed in Table 2.

4.2.2 Model validation

To assess the accuracy of the PV generation model and the suitability of the model assumptions noted above, modeled PV capacity factors are validated against two sets of empirical data: monthly reported generation from hundreds of utility-scale PV plants from the EIA Form 860 and Form 923 databases; [18, 24] and hourly reported generation for a single PV installation from the PVDAQ database. [25] Monthly validation is relevant for assessing the accuracy of PV revenue calculations, which scale with capacity factor; hourly validation is additionally relevant for average value and value factor calculations, which depend on the temporal profile of PV generation throughout each day.

Monthly validation: The EIA Form 860 database includes information on plant location, nameplate AC capacity, installation date, and technical design parameters for every utility-scale power plant in the U.S. For PV plants, these data include PV module technology, array tilt angle (θ), tracking strategy employed, and nameplate DC capacity (which, when divided by the nameplate AC capacity, gives the DC/AC ratio χ). The EIA Form 923 database reports monthly electricity generation for the majority of the plants included in the EIA 860 database. For each PV plant shared between the Form 860 and Form 923 databases, we simulate the plant capacity factor using the reported system parameters and historical insolation at the site of the plant and compare the simulated results (averaged over each calendar month) with the historical reported monthly generation of the plant over the years 2014–2016. The data are subsetted to include only those plants with DC/AC ratio between 0.5 and 2.5 and either a single fixed-tilt orientation or one-axis tracking; dual-axis-tracking plants, plants employing concentration or multiple orientations, and plants lacking orientation data are dropped from the sample. All 1-axis tracking installations are assumed to have $\theta = 0°$. Plants with less than 0.1 MWh of reported generation in any month of a given year and plants with an annual reported capacity factor of less than 5 % for a given year are also dropped from the sample, as well as plants with less than a full year of operation for any given year. The cleaned validation dataset includes 542 plants for 2014, 800 plants for 2015, and 1170 plants for 2016. The temperature coefficient γ is assumed to be $-0.4\,\%/°\mathrm{C}$ for plants employing crystalline silicon PV modules and $-0.2\,\%/°\mathrm{C}$ for plants employing thin-film PV modules. Other simulation parameters not reported in the Form 860 database are taken from Table 2.

Figures SI.10 to SI.12 in the Supplementary Information display the locations of the plants in the validation set and reported and simulated generation for 2014–2016. Simulation accuracy is assessed in terms of the Pearson correlation coefficient (CC), mean absolute error

(MAE), mean bias error (MBE), relative mean bias error (rMBE), root mean square error (RMSE), and relative root mean square error (rRMSE) between the monthly simulated and reported capacity factor for each plant in each year. Validation metrics are displayed in Figures SI.13 to SI.15 and discussed in SI Note 3.

Hourly validation: The PVDAQ database includes time-resolved power generation data for over 100 PV installations across the U.S., with varying levels of detail regarding the system design parameters for each installation. We select system number 1332, a 1.135 $\mathrm{MW_{ac}}$ fixed-tilt PV array at the site of the National Renewable Energy Laboratory, for hourly validation purposes, as it is the largest array in the database and includes data on system azimuth (180°), tilt (16.8°), and DC/AC ratio (1.02). Hourly validation results are discussed in SI Note 3; Figures SI.16 and SI.17 display simulated and measured PV output for the validation site over the years 2014–2016, and Figures SI.18 and SI.19 display simulation accuracy statistics (CC, MAE, MBE, rBME, RMSE, and rRMSE) binned by month and by hour of day.

4.3 Energy, capacity, and emissions abatement value

4.3.1 Wholesale energy value

Annual energy revenue R^{energy} in \$/$\mathrm{kW_{ac}}$ per year for a PV generator at a given node is given by

$$R^{energy} = \sum_{t=0}^{N} \frac{P_t}{P_{max}} \Pi_t \left(\frac{\tau}{60}\right) \tag{3}$$

where t is a timestamp, N is the number of timestamps in the year (e.g. 17520 for 30 min timestamps in a non-leap year), P_t is the modeled AC power output of the PV system in timestamp t, P_{max} is the peak AC power output of the PV system, Π_t is the LMP in timestamp t, and τ is the period of the timestamp in minutes (i.e. 30 min for historical PV output). As the native period of the LMP (60 min) is longer than that of the modeled PV output (30 min), the LMP is resampled to match the period of the PV output, with new timestamps taking the value at the most recent existing timestamp (i.e. forward-filled).

The average value of PV electricity V in \$/MWh at a given node is given by

$$V = \frac{\sum_{t=0}^{N} P_t \Pi_t}{\sum_{t=0}^{N} P_t}. \tag{4}$$

The PV value factor VF at a given node is given by

$$\mathrm{VF} = \frac{V}{\overline{\Pi}} = \left(\frac{\sum_{t=0}^{N} P_t \, \Pi_t}{\sum_{t=0}^{N} P_t} \right) \times \frac{N}{\sum_{t=0}^{N} \Pi_t}. \tag{5}$$

4.3.2 Capacity value

The capacity credit of PV can be calculated using a number of different methods. [104, 26, 105, 106, 107] The most rigorous method is to calculate the system-wide loss of load expectation (LOLE) following the addition of the specific PV generator, then to determine the equivalent capacity of a conventional firm generator that, if added to the system in place of the PV generator, would result in the same LOLE. [106] This calculation requires a large amount of system- and generator-specific operational data. A commonly-used approximation method with fewer data requirements, which has historically been used by MISO, PJM, NYISO, and ISONE in addition to several studies in the literature, [26, 105, 108, 109, 15, 110] is to identify the capacity credit as the capacity factor of the PV generator during a specified subset of (typically high-load or high-loss-of-load-probability) hours over a given time period. Here we use the capacity-factor approximation method, which has been shown to agree reasonably well with the more rigorous LOLE-based method for PV. [27]

PV capacity credit ξ for a given node and year is given by

$$\xi = \frac{\sum_{t=0}^{N} \alpha_t \, P_t}{\sum_{t=0}^{N} \alpha_t \, P_{max}}, \tag{6}$$

where α_t is 1 if t is a critical-load hour and 0 otherwise. Two different rules for identifying critical-load hours α_t are used here. In the *peak net-load* method, a specified percentage of hours with the highest net load are labeled as critical, where net load is ISO-wide demand minus simulated utility-scale solar generation and ISO-reported wind generation (where available) in the specified year. ISO-wide solar generation is simulated as described above for purposes of monthly model validation, using utility-scale solar plant locations and system parameters from the EIA Form 860 database for plants located with each ISO boundary. [18] Hourly wind generation is taken from the respective ISOs, and is available since 2010 for ERCOT and MISO and since 2011 for CAISO, ERCOT, and PJM. [111, 112, 79, 80, 113, 114] For NYISO and for years outside these ranges, wind is ignored and net load is taken as demand minus solar generation. Figures SI.32 and SI.33 show the capacity credit under different peak-hour thresholds and load assumptions.

In the *ISO-specified* method, critical hours are defined by the ISOs as follows:

- MISO: Hours beginning at 2pm, 3pm, 4pm from June–August (276 hours) [55]
- PJM: Hours beginning at 2pm, 3pm, 4pm, 5pm from June–August (368 hours) [56]
- NYISO: Hours beginning at 2pm, 3pm, 4pm, 5pm from June–August, and hours beginning at 4pm, 5pm, 6pm, 7pm from December–February (728 hours in a non-leap year) [57]
- ISONE: Hours beginning at 1pm, 2pm, 3pm, 4pm, 5pm in June–September, and hours beginning at 5pm, 6pm in October–May (1096 hours in a non-leap year) [58]

For both methods, the capacity credit for a given node and year is calculated using modeled PV generation during the specified year. Some ISOs and literature studies [110, 115] use multiple years of operational data to calculate PV capacity credit; here, for consistency across ISOs and to maintain any historical correlation between PV availability and net load, we use the production profile P_t for a single year to assess the capacity credit and revenue for that year. Modeled nodal PV output P_t at 30 min resolution is downsampled via trapezoidal integration to match the 60 min resolution of system load and wind generation (e.g. PV output for the 8:00 bin is given by the integral of PV output between 8:00–9:00).

PV capacity revenue $R^{capacity}$ ([\$/kW$_{\text{ac}}$ per year]) is given by

$$R^{capacity} = 12\,\frac{\sum_{t=0}^{N} \alpha_t\, P_t\, \Pi_t^{capacity}}{\sum_{t=0}^{N} \alpha_t\, P_{max}}, \tag{7}$$

where $\Pi_t^{capacity}$ is the historical capacity price in \$/kW$_{\text{ac}}$ per month, and the factor of 12 converts the revenue from \$/kW$_{\text{ac}}$ per month to \$/kW$_{\text{ac}}$ per year.

4.3.3 Emissions mitigation

The annual marginal CO_2 emissions abatement M_{CO_2} in ton/kW$_{\text{ac}}$ per year at a given node is given by

$$M_{CO_2} = \sum_{t=0}^{N} \frac{P_t}{P_{max}}\, m_t \tag{8}$$

where m_t is the hourly marginal CO_2 emissions rate in the eGRID region containing the node. Annual marginal abated public health cost H in \$/kW$_{\text{ac}}$ per year at a given node is given by

$$H = \sum_{z \in [\text{SO}_2, \text{NOx}, PM_{2.5}]} \sum_{t=0}^{N} \frac{P_t}{P_{max}} h_t^z \tag{9}$$

where h_t^z is the hourly marginal damage rate of species z in the eGRID region containing the node.

Acknowledgments

P.R.B. and the work reported here are supported by the U.S. Department of Energy (DOE) Office of Energy Efficiency and Renewable Energy (EERE) Postdoctoral Research Award through the EERE Solar Energy Technologies Office (SETO) under DOE contract number DE-SC00014664. P.R.B. acknowledges A. Botterud, J. Jean, S. Burger, J. Jenkins, S. Kurtz, R. van Haaren, D. Weiss, E. Dimantchev, and E. Gençer for insightful discussions, A. Brocks for assistance with capacity market data, and J. Jenkins and S. Burger for assistance with node locations. P.R.B. also acknowledges the administrators and staff of the MIT Supercloud and the authors of the open-source software packages and public data sources used in this analysis, and representatives from ERCOT and ISONE for access to data not available publicly. All views expressed in this paper are those of the authors and do not necessarily reflect the views of DOE, EERE, SETO, or acknowledged individuals.

Author Contributions

P.R.B. and F.M.O'S. conceived of the study. P.R.B. collected all data, performed all calculations and analysis, and wrote the paper. F.M.O'S. provided comments on the manuscript.

Declaration of Interests

Both authors are affiliated with the MIT Energy Initiative, which receives funding from a variety of external sources including utility companies, oil and gas producers, renewable energy companies, private philanthropic organizations, and environmental non-profits, listed at http://energy.mit.edu/membership/#current-members. None of these organizations were involved

with the development of the work reported here. F.M.O'S. is Senior Vice President of Lincoln Clean Energy, LLC, a developer and owner of wind and solar projects in the United States.

References

[1] Fu, R., Chung, D., Lowder, T., Feldman, D., and Ardani, K. (2017). U.S. Solar Photovoltaic System Cost Benchmark: Q1 2017. Technical report, National Renewable Energy Laboratory. http://dx.doi.org/10.2172/1390776.

[2] REN21 (2018). Renewables 2018 Global Status Report. Technical report, Renewable Energy Poicy Network for the 21st Century. http://dx.doi.org/978-3-9818911-3-3.

[3] Sensfuß, F., Ragwitz, M., and Genoese, M. (2008). The merit-order effect: A detailed analysis of the price effect of renewable electricity generation on spot market prices in Germany. Energy Policy *36*, 3076–3084. http://dx.doi.org/10.1016/j.enpol.2008.03.035.

[4] Lamont, A.D. (2008). Assessing the long-term system value of intermittent electric generation technologies. Energy Economics *30*, 1208–1231. http://dx.doi.org/10.1016/j.eneco.2007.02.007.

[5] Woo, C.K., Moore, J., Schneiderman, B., Ho, T., Olson, A., Alagappan, L., Chawla, K., Toyama, N., and Zarnikau, J. (2016). Merit-order effects of renewable energy and price divergence in California's day-ahead and real-time electricity markets. Energy Policy *92*, 299–312. http://dx.doi.org/10.1016/j.enpol.2016.02.023.

[6] Wiser, R., Mills, A., Seel, J., Levin, T., and Botterud, A. (2017). Impacts of Variable Renewable Energy on Bulk Power System Assets, Pricing, and Costs. Technical report, Lawrence Berkeley National Laboratory and Argonne National Laboratory. https://emp.lbl.gov/publications/impacts-variable-renewable-energy.

[7] Mills, A. and Wiser, R. (2012). Changes in the Economic Value of Variable Generation at High Penetration Levels: A Pilot Case Study of California. Technical report, Lawrence Berkeley National Laboratory. http://emp.lbl.gov/sites/all/files/lbnl-5445e.pdf.

[8] Hirth, L. (2013). The market value of variable renewables. The effect of solar wind power variability on their relative price. Energy Economics *38*, 218–236. http://dx.doi.org/10.1016/j.eneco.2013.02.004.

[9] Mills, A.D. and Wiser, R.H. (2013). Changes in the economic value of photovoltaic generation at high penetration levels: A pilot case study of California. IEEE Journal of Photovoltaics *3*, 1394–1402. http://dx.doi.org/10.1109/JPHOTOV.2013.2263984.

[10] Millstein, D., Wiser, R., Bolinger, M., and Barbose, G. (2017). The climate and air-quality benefits of wind and solar power in the United States. Nature Energy *2*, 17134. http://dx.doi.org/10.1038/nenergy.2017.134.

[11] Mills, A.D. and Wiser, R.H. (2015). Strategies to mitigate declines in the economic value of wind and solar at high penetration in California. Applied Energy *147*, 269–278. http://dx.doi.org/10.1016/j.apenergy.2015.03.014.

[12] Braff, W.A., Mueller, J.M., and Trancik, J.E. (2016). Value of storage technologies for wind and solar energy. Nature Climate Change *6*, 964–969. http://dx.doi.org/10.1038/nclimate3045.

[13] Hirth, L. and Müller, S. (2016). System-friendly wind power. How advanced wind turbine design can increase the economic value of electricity generated through wind power. Energy Economics *56*, 51–63. http://dx.doi.org/10.1016/j.eneco.2016.02.016.

[14] Johansson, V., Thorson, L., Goop, J., Göransson, L., Odenberger, M., Reichenberg, L., Taljegard, M., and Johnsson, F. (2017). Value of wind power Implications from specific power. Energy *126*, 352–360. http://dx.doi.org/10.1016/j.energy.2017.03.038.

[15] Callaway, D., Fowlie, M., and McCormick, G. (2018). Location, location, location: The variable value of renewable energy and demand-side efficiency resources. Journal of the Association of Environmental and Resource Economists *5*, 39—-75. http://dx.doi.org/10.1086/694179.

[16] Siler-Evans, K., Lima, I., Morgan, M.G., and Apt, J. (2013). Regional variations in the health, environmental, and climate benefits of wind and solar generation. Proceedings of the National Academy of Sciences *110*, 11768–11773. http://dx.doi.org/10.1073/pnas.1221978110.

[17] Buonocore, J.J., Luckow, P., Norris, G., Spengler, J.D., Biewald, B., Fisher, J., and Levy, J.I. (2016). Health and climate benefits of different energy-efficiency and renewable energy choices. Nature Climate Change *6*, 100–106. http://dx.doi.org/10.1038/nclimate2771.

[18] U.S. Energy Information Administration (2018). Form EIA-860 detailed data. https://www.eia.gov/electricity/data/eia860/.

[19] National Renewable Energy Laboratory (2018). The OpenPV Project. https://openpv.nrel.gov/.

[20] Habte, A., Sengupta, M., and Lopez, A. (2017). Evaluation of the National Solar Radiation Database (NSRDB): 1998-2015. Technical report, National Renewable Energy Laboratory. http://www.nrel.gov/docs/fy17osti/67722.pdf.

[21] Holmgren, W.F., Hansen, C.W., and Mikofski, M.A. (2018). PVLIB Python: a Python Package for Modeling Solar Energy Systems. Journal of Open Source Software *3*, 884. http://dx.doi.org/10.21105/joss.00884.

[22] PV Performance Modeling Collaborative (2018). PVLIB Toolbox. https://pvpmc.sandia.gov/applications/pv_lib-toolbox/.

[23] Brown, P.R. and O'Sullivan, F.M. (2019). Shaping photovoltaic array output to align with changing wholesale electricity price profiles. *Submitted*.

[24] U.S. Energy Information Administration (2018). Form EIA-923 detailed data. https://www.eia.gov/electricity/data/eia923/.

[25] National Renewable Energy Laboratory (2018). PVDAQ (PV Data Acquisition). https://developer.nrel.gov/docs/solar/pvdaq-v3/.

[26] Pelland, S. and Abboud, I. (2008). Comparing Photovoltaic Capacity Value Metrics: A Case Study for the City of Toronto. Progress in Photovoltaics: Research and Applications *16*, 715–724. http://dx.doi.org/10.1002/pip.864.

[27] Madaeni, S.H., Sioshansi, R., and Denholm, P. (2012). Estimating the capacity value of concentrating solar power plants: A case study of the Southwestern United States. IEEE Transactions on Power Systems *27*, 1116–1124. http://dx.doi.org/10.1109/TPWRS.2011.2179071.

[28] Center for Climate and Energy Decision Making (2015). EASIUR: Marginal Social Costs of Emissions in the United States. https://barney.ce.cmu.edu/$\sim$jinhyok/easiur/.

[29] Heo, J., Adams, P.J., and Gao, H.O. (2016). Public Health Costs of Primary PM2.5 and Inorganic PM2.5 Precursor Emissions in the United States. Environmental Science and Technology *50*, 6061–6070. http://dx.doi.org/10.1021/acs.est.5b06125.

[30] Heo, J., Adams, P.J., and Gao, H.O. (2016). Reduced-form modeling of public health impacts of inorganic PM2.5and precursor emissions. Atmospheric Environment *137*, 80–89. http://dx.doi.org/10.1016/j.atmosenv.2016.04.026.

[31] Azevedo, I.L., Horner, N.C., Siler-Evans, K., and Vaishnav, P.T. (2017). Electricity Marginal Factors Estimates. Technical report, Center For Climate and Energy Decision Making. Pittsburgh: Carnegie Mellon University. https://cedm.shinyapps.io/MarginalFactors/.

[32] Siler-Evans, K., Azevedo, I.L., and Morgan, M.G. (2012). Marginal emissions factors for the U.S. electricity system. Environmental Science and Technology *46*, 4742–4748. http://dx.doi.org/10.1021/es300145v.

[33] U.S. Environmental Protection Agency (EPA) (2018). Emissions and Generation Resource Integrated Database (eGRID). https://www.epa.gov/energy/emissions-generation-resource-integrated-database-egrid.

[34] Vaishnav, P., Horner, N., and Azevedo, I.L. (2017). Was it worthwhile? Where have the benefits of rooftop solar photovoltaic generation exceeded the cost? Environmental Research Letters *12*, 094015. http://dx.doi.org/10.1088/1748-9326/aa815e.

[35] U.S. Department of Labor - Bureau of Labor Statistics (2018). Consumer Price Index. https://data.bls.gov/timeseries/CUUR0000SA0.

[36] Borenstein, S. (2012). The Private and Public Economics of Renewable Electricity Generation. Journal of Economic Perspectives *26*, 67–92. http://dx.doi.org/10.1257/jep.26.1.67.

[37] MIT Energy Initiative (2015). The Future of Solar Energy. Technical report, Massachusetts Institute of Technology, Cambridge, MA. mitei.mit.edu/futureofsolar.

[38] Cohen, M.A. and Callaway, D.S. (2016). Effects of distributed PV generation on California's distribution system, Part 1: Engineering simulations. Solar Energy *128*, 126–138. http://dx.doi.org/10.1016/j.solener.2016.01.002.

[39] Cohen, M.A., Kauzmann, P.A., and Callaway, D.S. (2016). Effects of distributed PV generation on California's distribution system, part 2: Economic analysis. Solar Energy *128*, 139–152. http://dx.doi.org/10.1016/j.solener.2016.01.004.

[40] Baker, E., Fowlie, M., Lemoine, D., and Reynolds, S.S. (2013). The Economics of Solar Electricity. Annual Review of Resource Economics *5*, 387–426. http://dx.doi.org/10.1146/annurev-resource-091912-151843.

[41] Clò, S., Cataldi, A., and Zoppoli, P. (2015). The merit-order effect in the Italian power market: The impact of solar and wind generation on national wholesale electricity prices. Energy Policy *77*, 79–88. http://dx.doi.org/10.1016/j.enpol.2014.11.038.

[42] Bushnell, J. and Novan, K. (2018). Setting with the Sun: The Impacts of Renewable Energy on Wholesale Power Markets. https://ei.haas.berkeley.edu/research/papers/WP292.pdf.

[43] Craig, M.T., Jaramillo, P., Hodge, B.M., Williams, N.J., and Severnini, E. (2018). A retrospective analysis of the market price response to distributed photovoltaic generation in California. Energy Policy *121*, 394–403. http://dx.doi.org/10.1016/j.enpol.2018.05.061.

[44] Lontzek, T.S., Cai, Y., Judd, K.L., and Lenton, T.M. (2015). Stochastic integrated assessment of climate tipping points indicates the need for strict climatepolicy. Nature Climate Change *5*, 441–444. http://dx.doi.org/10.1038/nclimate2570.

[45] Ackerman, F. and Heinzerling, L. (2002). Pricing the Priceless: Cost-Benefit Analysis of Environmental Protection. University of Pennsylvania Law Review *150*, 1553. http://dx.doi.org/10.2307/3312947.

[46] Morgan, M.G., Vaishnav, P., Dowlatabadi, H., and Azevedo, I.L. (2017). Rethinking the Social Cost of Carbon Dioxide. Issues in Science and Technology *33*. https://issues.org/rethinking-the-social-cost-of-carbon-dioxide/.

[47] California Air Resources Board (2018). Archived Auction Information and Results. https://www.arb.ca.gov/cc/capandtrade/auction/auction_archive.htm.

[48] Regional Greenhouse Gas Initiative (2018). Allowance Prices and Volumes. https://www.rggi.org/Auctions/Auction-Results/Prices-Volumes.

[49] U.S. Environmental Protection Agency (EPA) (2018). SO2 AllowanceAuctions. https://www.epa.gov/airmarkets/so2-allowance-auctions.

[50] California Public Utilities Commission (2019). Resource Adequacy. https://www.cpuc.ca.gov/RA/.

[51] Midwest ISO (MISO) (2019). Resource Adequacy. https://www.misoenergy.org/planning/resource-adequacy/#nt=%2Fplanningdoctype%3APRADocument&t=10&p=0&s=&sd=.

[52] PJM Interconnection (2019). Capacity Market (RPM). https://www.pjm.com/markets-and-operations/rpm.aspx.

[53] New York ISO (NYISO) (2019). Strip Auction Summary. http://icap.nyiso.com/ucap/public/auc_view_strip_detail.do.

[54] ISO New England (ISONE) (2018). Forward Capacity Auction Results. https://www.iso-ne.com/isoexpress/web/reports/auctions/-/tree/fca-results.

[55] Midwest ISO (MISO) (2018). Business Practices Manual No. 11 - Resource Adequacy. Technical report, Midwest Independent System Operator (MISO). https://www.misoenergy.org/legal/business-practice-manuals/.

[56] PJM Interconnection (2017). Manual 21: Rules and procedures for determination of generating capability. Technical report, PJM Interconnection. https://www.pjm.com/library/manuals.aspx.

[57] New York ISO (NYISO) (2018). Manual 4 - Installed Capacity Manual. Technical report, New York Independent System Operator (NYISO). https://www.nyiso.com/manuals-tech-bulletins-user-guides.

[58] ISO New England (ISONE) (2019). Market Rule 1,Section 13 - Forward Capacity Market. Technical report, ISO New England (ISONE). https://www.iso-ne.com/participate/rules-procedures/tariff/market-rule-1.

[59] Schivley, G., Azevedo, I., and Samaras, C. (2018). Assessing the evolution of power sector carbon intensity in the United States. Environmental Research Letters *13*. http://dx.doi.org/10.1088/1748-9326/aabe9d.

[60] Salles, M.B.C., Huang, J., Aziz, M.J., and Hogan, W.W. (2017). Potential arbitrage revenue of energy storage systems in PJM. Energies *10*, 1100. http://dx.doi.org/10.3390/en10081100.

[61] Jordan, D.C. and Kurtz, S.R. (2013). Photovoltaic degradation rates – an analytical review. Progress in Photovoltaics: Research and Applications *21*, 12–29. http://dx.doi.org/10.1002/pip.1182.

[62] Jordan, D.C., Kurtz, S.R., Vansant, K., and Newmiller, J. (2016). Compendium of photovoltaic degradation rates. Progress in Photovoltaics: Research and Applications *24*, 978–989. http://dx.doi.org/10.1002/pip.2744.

[63] Fu, R., Feldman, D., and Margolis, R. (2018). U.S. Solar Photovoltaic System Cost Benchmark: Q1 2018. Technical report, National Renewable Energy Laboratory. http://dx.doi.org/10.7799/1325002.

[64] U.S. Department of the Treasury Internal Revenue Service (2018). How To Depreciate Property. Technical report, U.S. Department of the Treasury - Internal Revenue Service. https://www.irs.gov/forms-pubs/about-publication-946.

[65] Feldman, D. and Bolinger, M. (2016). On the Path to SunShot: Emerging Opportunities and Challenges in Financing Solar. Technical report, National Renewable Energy Laboratory and Lawrence Berkeley National Laboratory. https://www.nrel.gov/docs/fy16osti/65638.pdf.

[66] Cole, W., Frew, B., Gagnon, P., Richards, J., Sun, Y., Zuboy, J., Woodhouse, M., and Margolis, R. (2017). SunShot 2030 for photovoltaics (PV): Envisioning a low-cost PV future. Technical report, National Renewable Energy Laboratory. https://www.nrel.gov/docs/fy17osti/68105.pdf.

[67] Interagency Working Group on Social Cost of Greenhouse Gases - United States Government (2016). Technical Support Document: Technical Update of the Social Cost of Carbon for Regulatory Impact Analysis Under Executive Order 12866. Technical report, Interagency Working Group on Social Cost of Greenhouse Gases. https://19january2017snapshot.epa.gov/sites/production/files/2016-12/documents/sc_co2_tsd_august_2016.pdf.

[68] Rogelj, J., McCollum, D.L., Reisinger, A., Meinshausen, M., and Riahi, K. (2013). Probabilistic cost estimates for climate change mitigation. Nature *493*, 79–83. http://dx.doi.org/10.1038/nature11787.

[69] Van Den Bergh, J.C. and Botzen, W.J. (2014). A lower bound to the social cost of CO 2 emissions. Nature Climate Change *4*, 253–258. http://dx.doi.org/10.1038/nclimate2135.

[70] Moore, F.C. and Diaz, D.B. (2015). Temperature impacts on economic growth warrant stringent mitigation policy. Nature Climate Change *5*, 127–131. http://dx.doi.org/10.1038/nclimate2481.

[71] Cai, Y., Lenton, T.M., and Lontzek, T.S. (2016). Risk of multiple interacting tipping points should encourage rapid CO2 emission reduction. Nature Climate Change *6*, 520–525. http://dx.doi.org/10.1038/nclimate2964.

[72] Nordhaus, W.D. (2017). Revisiting the social cost of carbon. Proceedings of the National Academy of Sciences *114*, 1518–1523. http://dx.doi.org/10.1073/pnas.1609244114.

[73] MIT Energy Initiative (2016). Utility of the Future. Technical report, Massachusetts Institute of Technology, Cambridge, MA. https://energy.mit.edu/uof.

[74] Taylor, J.A., Dhople, S.V., and Callaway, D.S. (2016). Power systems without fuel. Renewable and Sustainable Energy Reviews *57*, 1322–1336. http://dx.doi.org/10.1016/j.rser.2015.12.083.

[75] Milligan, M., Frew, B.A., Bloom, A., Ela, E., Botterud, A., Townsend, A., and Levin, T. (2016). Wholesale electricity market design with increasing levels of renewable generation: Revenue sufficiency and long-term reliability. Electricity Journal *29*, 26–38. http://dx.doi.org/10.1016/j.tej.2016.02.005.

[76] Mills, A.D., Millstein, D., Jeong, S., Lavin, L., Wiser, R., and Bolinger, M. (2018). Estimating the Value of Offshore Wind Along the United States' Eastern Coast. Technical report, Lawrence Berkeley National Laboratory. https://emp.lbl.gov/publications/estimating-value-offshore-wind-along.

[77] California ISO (CAISO) (2018). California ISO Oasis. http://oasis.caiso.com/mrioasis/logon.do.

[78] Electric Reliability Council of Texas (ERCOT) (2018). Market Prices. http://www.ercot.com/mktinfo/prices.

[79] Midwest ISO (MISO) (2018). Market Reports. https://www.misoenergy.org/markets-and-operations/real-time--market-data/market-reports/.

[80] Midwest ISO (MISO) (2018). Market Report Archives. https://www.misoenergy.org/markets-and-operations/real-time--market-data/market-reports/market-report-archives/.

[81] PJM Interconnection (2018). Daily Day-Ahead LMP. http://www.pjm.com/markets-and-operations/energy/day-ahead/lmpda.aspx.

[82] New York ISO (NYISO) (2018). Pricing Data. http://www.nyiso.com/public/markets_operations/market_data/pricing_data/index.jsp.

[83] ISO New England (ISONE) (2018). Hourly Day-Ahead LMPs. https://www.iso-ne.com/isoexpress/web/reports/pricing/-/tree/lmps-da-hourly.

[84] California ISO (CAISO) (2018). Market price maps. http://www.caiso.com/PriceMap/Pages/default.aspx.

[85] Midwest ISO (MISO) (2018). LMP contour map. https://api.misoenergy.org/MISORTWD/lmpcontourmap.html.

[86] PJM Interconnection (2014). Markets & Operations - One-Time Data Requests. http://www.pjm.com/$\sim$/media/markets-ops/energy/lmp-model-info/zip-code-mapping.ashx.

[87] New York ISO (NYISO) (2018). Planning Documents & Resources - Planning Data and Reference Docs. https://www.nyiso.com/public/markets_operations/services/planning/documents/index.jsp.

[88] New York ISO (NYISO) (2019). NYISO Pricing Information.

[89] PJM Interconnection (2019). Pricing Nodes.

[90] U.S. Federal Energy Regulatory Commission (2018). Form No. 714 - Annual Electric Balancing Authority Area and Planning Area Report. https://www.ferc.gov/docs-filing/forms/form-714/data.asp.

[91] Muller, B.N.Z., Mendelsohn, R., and Nordhaus, W. (2011). Environmental Accounting for Pollution in the United States Economy. American Economic Review *101*, 1649–1675. http://dx.doi.org/10.1257/aer.101.5.1649.

[92] Muller, N.Z. (2014). Boosting GDP growth by accounting for the environment. Science *345*, 873–874. http://dx.doi.org/10.1126/science.1253506.

[93] Muller, N.Z. (2018). AP3 (AP2, APEEP) Model. https://public.tepper.cmu.edu/nmuller/APModel.aspx.

[94] Stein, J.S., Holmgren, W.F., Forbess, J., and Hansen, C.W. (2016). PVLIB: Open source photovoltaic performance modeling functions for Matlab and Python. Proceedings of the IEEE Photovoltaic Specialist Conference *43*, 3425–3430. http://dx.doi.org/10.1109/PVSC.2016.7750303.

[95] Dobos, A.P. (2014). PVWatts Version 5 Manual. Technical report, National Renewable Energy Laboratory. https://www.nrel.gov/docs/fy14osti/62641.pdf.

[96] National Renewable Energy Laboratory (2018). PVWatts Calculator - Version 5. http://pvwatts.nrel.gov/version_5.php.

[97] Bolinger, M., Seel, J., and Lacommare, K.H. (2017). Utility-Scale Solar 2016: An Empirical Analysis of Project Cost, Performance, and Pricing Trends in the United States. Technical report, Lawrence Berkeley National Laboratory. https://emp.lbl.gov/publications/utility-scale-solar-2015-empirical.

[98] Lorenzo, E., Narvarte, L., and Muñoz, J. (2011). Tracking and back-tracking. Progress in Photovoltaics: Research and Applications *19*, 747—-753. http://dx.doi.org/10.1002/pip.1085.

[99] Reindl, D., Beckman, W., and Due, J. (1990). Diffuse fraction correlations. Solar Energy *45*, 1–7. http://dx.doi.org/10.1016/0038-092X(90)90060-P.

[100] Loutzenhiser, P.G., Manz, H., Felsmann, C., Strachan, P.A., Frank, T., and Maxwell, G.M. (2007). Empirical validation of models to compute solar irradiance on inclined surfaces for building energy simulation. Solar Energy *81*, 254–267. http://dx.doi.org/10.1016/j.solener.2006.03.009.

[101] Reda, I. and Andreas, A. (2004). Solar position algorithm for solar radiation applications. Solar Energy *76*, 577–589. http://dx.doi.org/10.1016/j.solener.2003.12.003.

[102] Reda, I. and Andreas, A. (2008). Solar Position Algorithm for Solar Radiation Applications (Revised). Technical report, National Renewable Energy Laboratory. https://www.nrel.gov/docs/fy08osti/34302.pdf.

[103] King, D.L., Boyson, W.E., and Kratochvil, J.A. (2004). Photovoltaic array performance model. Technical report, Sandia National Laboratories. http://dx.doi.org/10.2172/919131.

[104] Garver, L.L. (1966). Efective Load Carrying Capability of Generating Units. IEEE Transactions on Power Apparatus and Systems *PAS-85*, 910–919. http://dx.doi.org/10.1109/TPAS.1966.291652.

[105] Keane, A., Milligan, M., Dent, C.J., Hasche, B., D'Annunzio, C., Dragoon, K., Holttinen, H., Samaan, N., Söder, L., and O'Malley, M. (2011). Capacity value of wind power. IEEE Transactions on Power Systems *26*, 564–572. http://dx.doi.org/10.1109/TPWRS.2010.2062543.

[106] Madaeni, S.H., Sioshansi, R., and Denholm, P. (2012). Comparison of Capacity Value Methods for Photovoltaics in the Western United States. Technical Report July, National Renewable Energy Laboratory. http://dx.doi.org/10.2172/1046871.

[107] Madaeni, S.H., Sioshansi, R., and Denholm, P. (2013). Comparing capacity value estimation techniques for photovoltaic solar power. IEEE Journal of Photovoltaics *3*, 407–415. http://dx.doi.org/10.1109/JPHOTOV.2012.2217114.

[108] Dent, C.J., Sioshansi, R., Reinhart, J., Wilson, A.L., Zachary, S., Lynch, M., Bothwell, C., and Steele, C. (2016). Capacity value of solar power: Report of the IEEE PES task force on capacity value of solar power. In 2016 International Conference on Probabilistic Methods Applied to Power Systems (PMAPS) (IEEE, Beijing), pp. 1–7. http://dx.doi.org/10.1109/PMAPS.2016.7764197.

[109] Bothwell, C. and Hobbs, B.F. (2017). Crediting Wind and Solar Renewables in Electricity Capacity Markets: The Effects of Alternative Definitions upon Market Efficiency. The Energy Journal *38*, 173–188. 10.5547/01956574.38.SI1.cbot.

[110] Byers, C., Levin, T., and Botterud, A. (2018). Capacity market design and renewable energy: Performance incentives, qualifying capacity, and demand curves. The Electricity Journal *31*, 65–74. http://dx.doi.org/10.1016/j.tej.2018.01.006.

[111] California ISO (CAISO) (2018). Renewables and emissions reports. http://www.caiso.com/market/Pages/ReportsBulletins/RenewablesReporting.aspx.

[112] Electric Reliability Council of Texas (ERCOT) (2018). Hourly Aggregated Wind Output. http://www.ercot.com/gridinfo/generation.

[113] PJM Interconnection (2018). Wind Generation. https://dataminer2.pjm.com/feed/wind_gen/definition.

[114] ISO New England (ISONE) (2018). Daily Generation by Fuel Type. https://www.iso-ne.com/isoexpress/web/reports/operations/-/tree/daily-gen-fuel-type.

[115] Gami, D., Sioshansi, R., and Denholm, P. (2017). Data Challenges in Estimating the Capacity Value of Solar Photovoltaics. IEEE Journal of Photovoltaics *7*, 1065–1073. http://dx.doi.org/10.1109/JPHOTOV.2017.2695328.

[116] U.S. Energy Information Administration (2018). Henry Hub Natural Gas Spot Price. https://www.eia.gov/dnav/ng/hist/rngwhhdA.htm.

Supplementary Information

SI Note 1 Input and background data

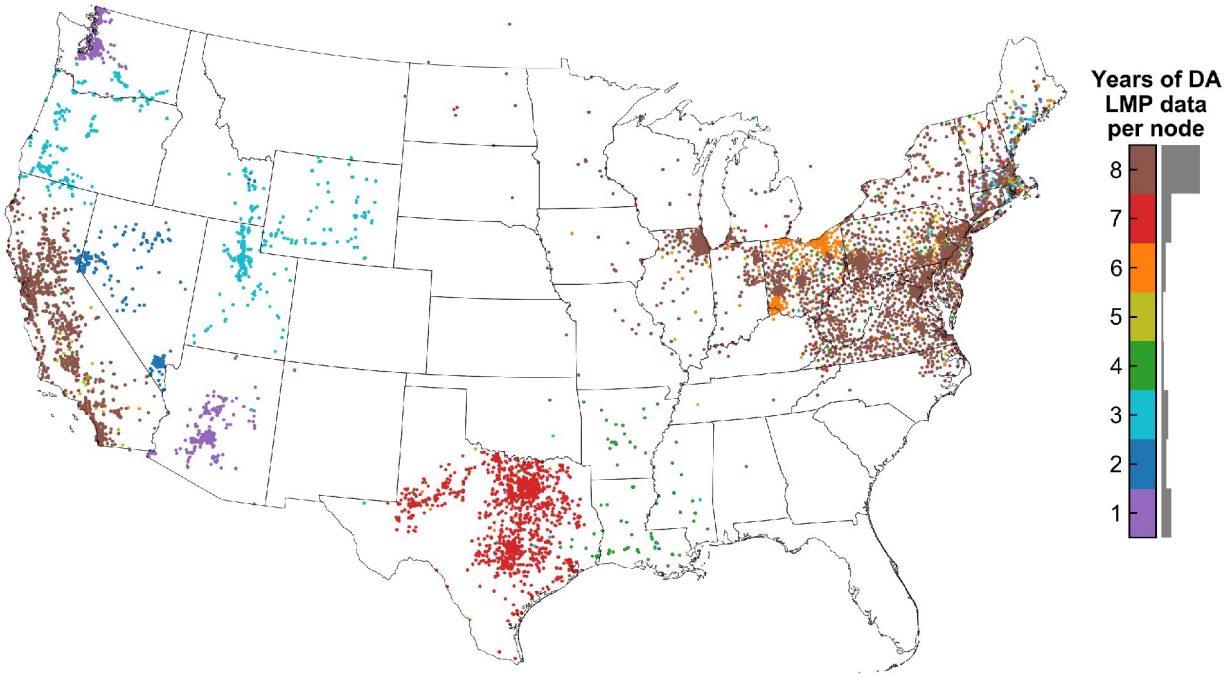

Figure SI.1: Number of complete years of day-ahead LMP data available per node.

Table SI.1: Nodal day-ahead LMP and geographic data availability by ISO and year. Data are reported in terms of the number of nodes in each ISO-year with complete data availability. The label "non-CAISO WECC" refers to nodes that lie outside of the CAISO system territory but have LMP and geographic data reported by CAISO.

RTO	2010	2011	2012	2013	2014	2015	2016	2017
CAISO	2118	2121	2150	2204	2234	2236	2237	2209
non-CAISO WECC						1049	1824	3461
ERCOT		1559	1563	1567	1569	1570	1570	1563
MISO	179	192	197	200	368	370	386	378
PJM	4288	4366	4967	5044	4936	4857	4741	4686
NYISO	402	412	424	430	434	435	436	436
ISONE	409	437	499	593	612	746	829	966

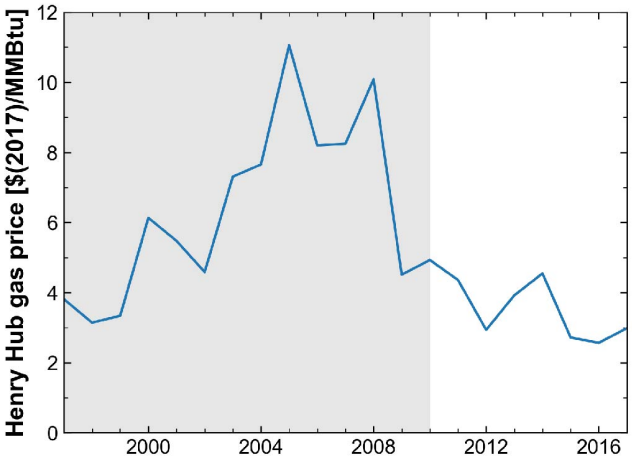

Figure SI.2: Annual Henry Hub natural gas price over time, measured in 2017 U.S. dollars per million British thermal units (MMBTU). [116] The period of time corresponding to the period of time analyzed in the rest of this study is signified by the white background from 2010–2017.

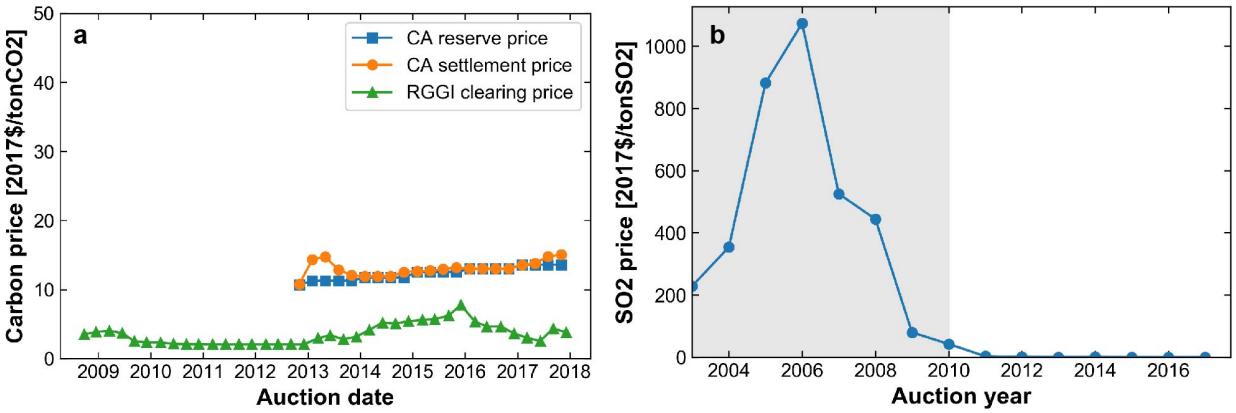

Figure SI.3: Cap-and-trade allowance prices. **a**, CO_2 on the California Cap and Trade market (blue squares and orange circles) and on the Regional Greenhouse Gas Initiative market (green triangles); [47, 48] **b**, SO_2 on the EPA Air Markets Program. [49]

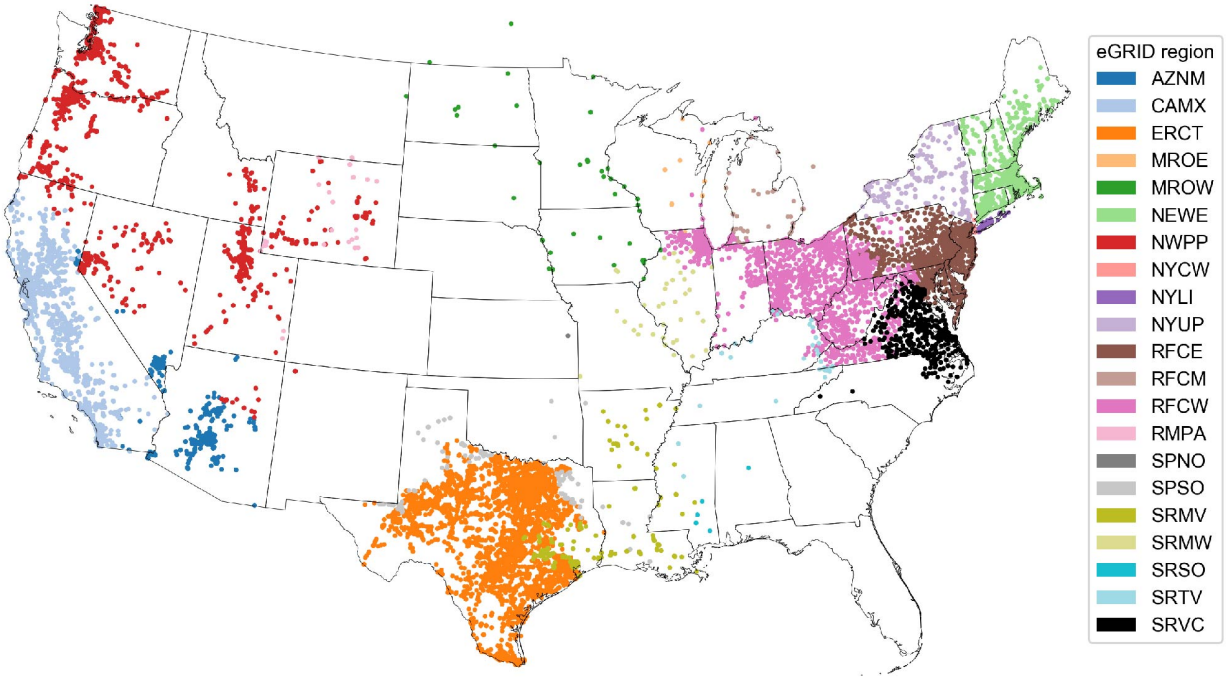

Figure SI.4: Mapping of LMP nodes to EPA eGRID zones [33] used for marginal emissions offset analysis.

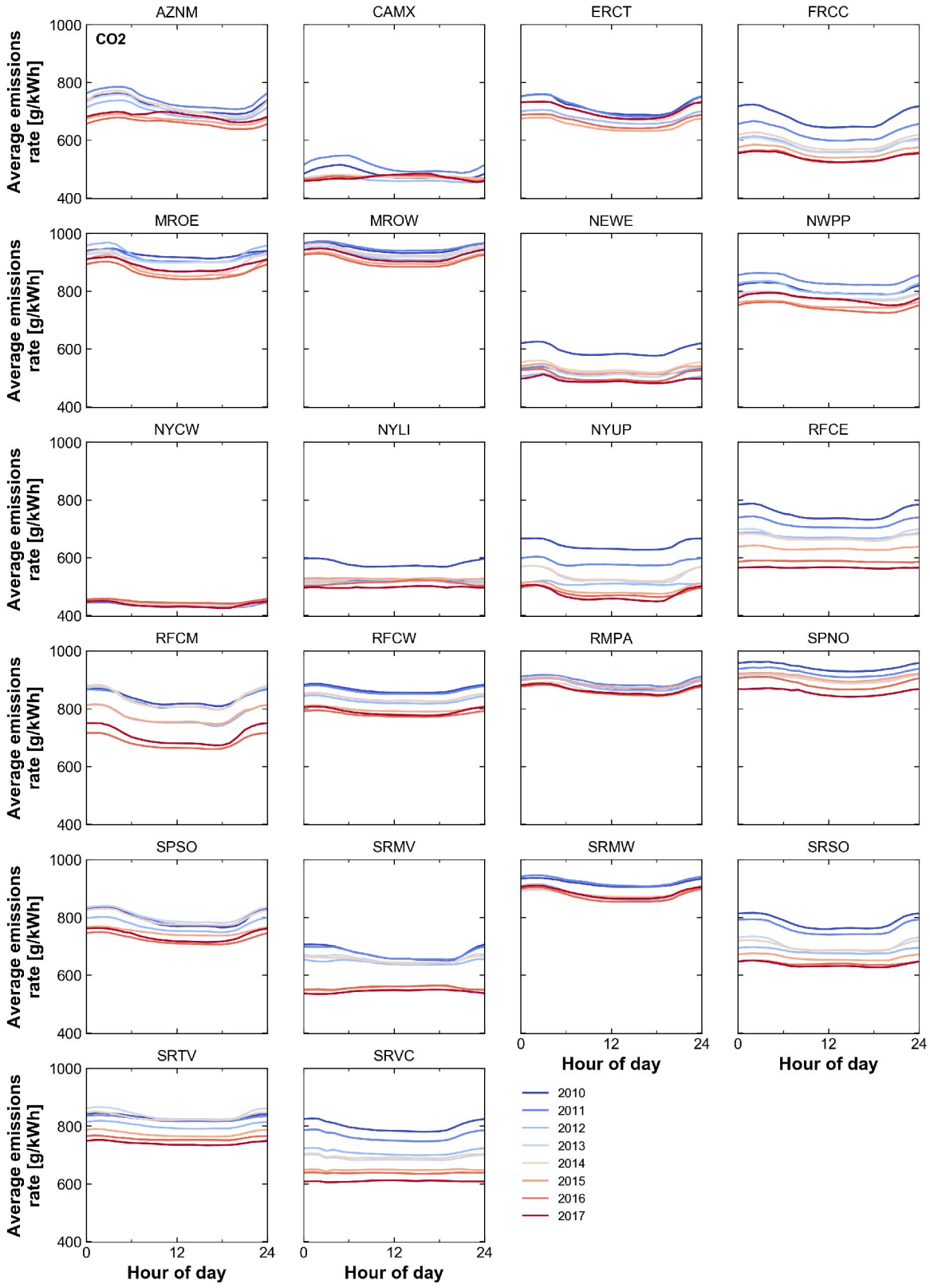

Figure SI.5: Average emissions rates of CO_2 by eGRID region. Data are from Azevedo et al. [31]

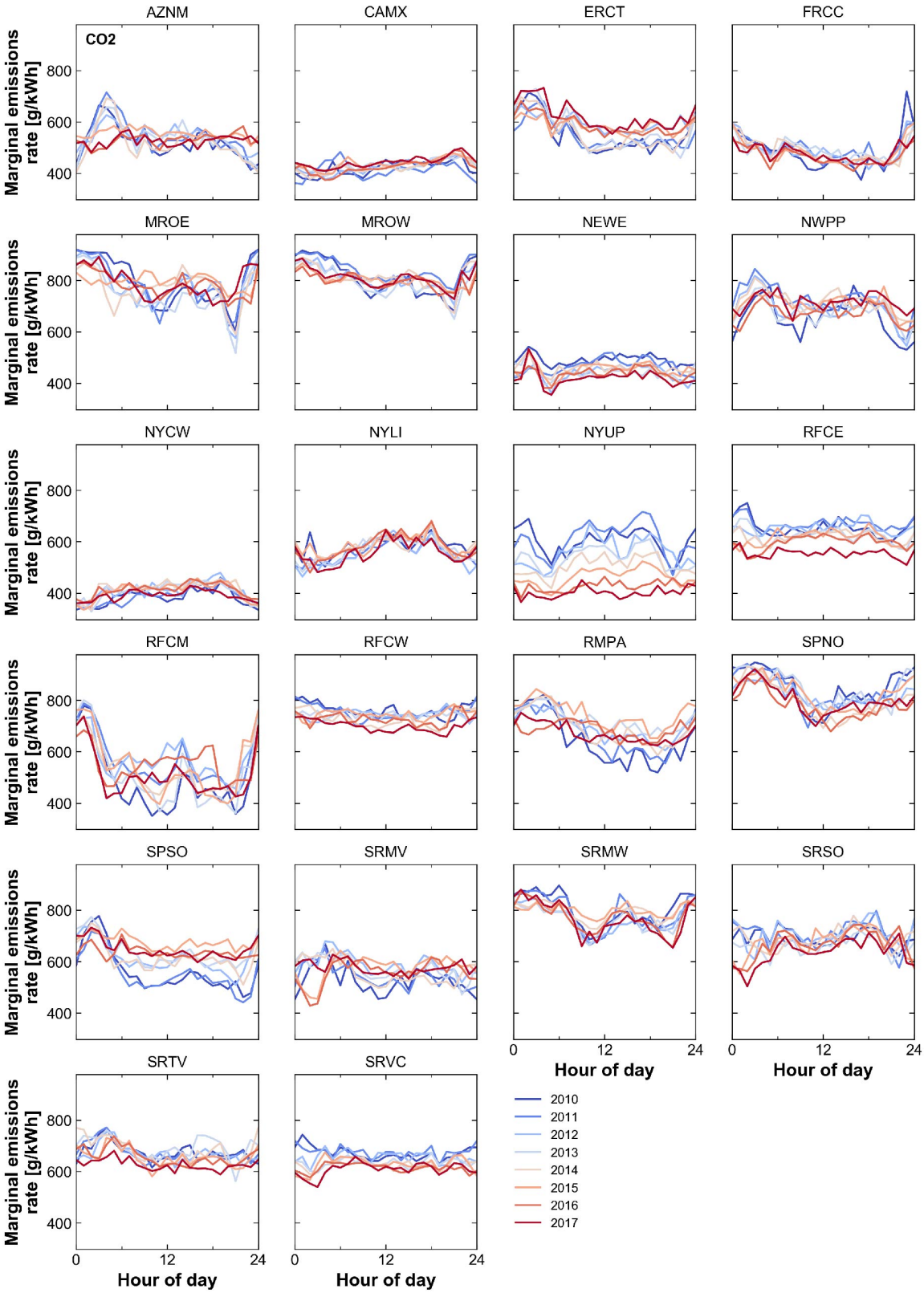

Figure SI.6: Marginal emissions rates of CO_2 by eGRID region. Data are from Azevedo et al. [31]

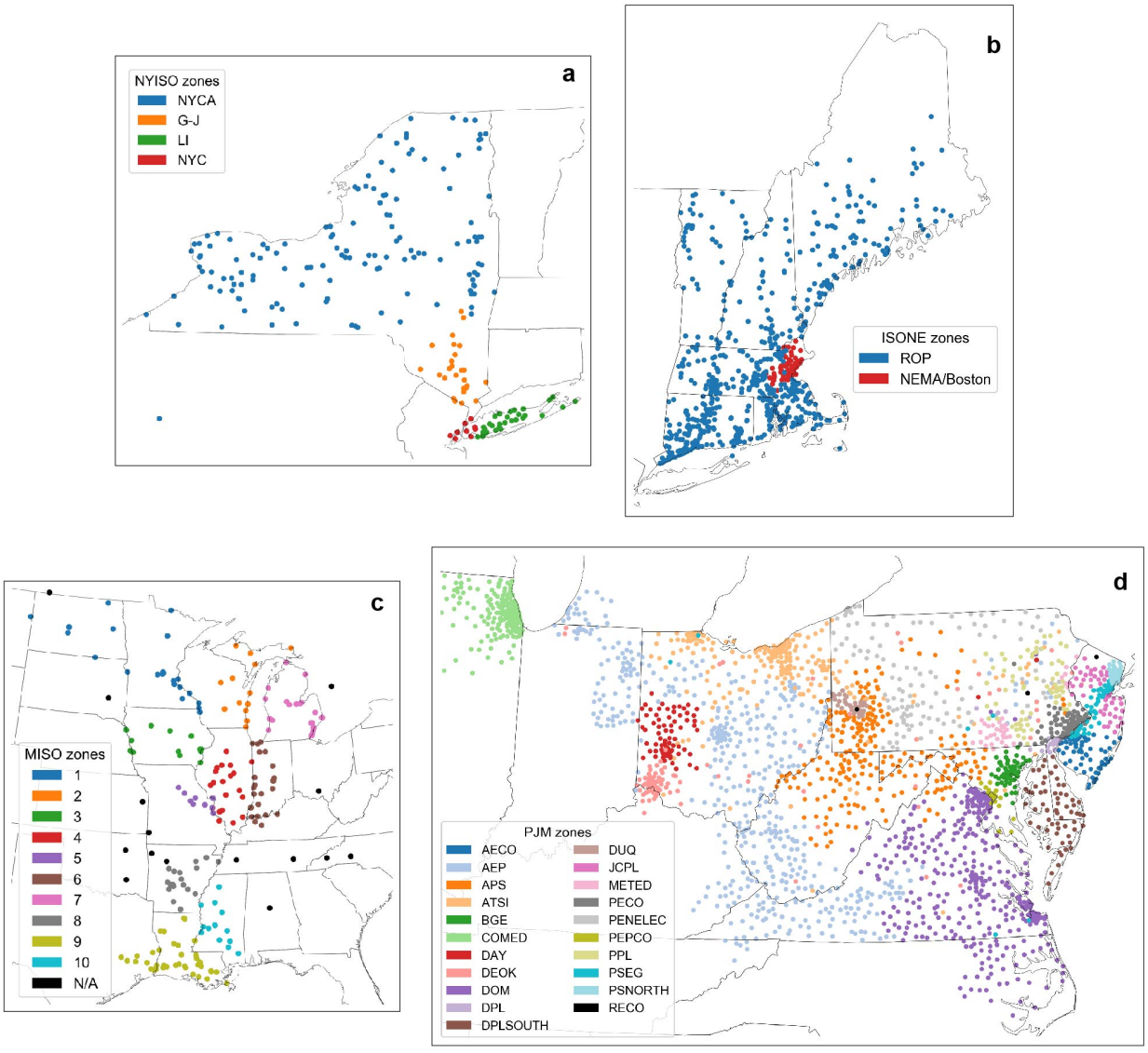

Figure SI.7: Map of capacity market zones for NYISO (a), ISONE (b), MISO (c), and PJM (d).

SI Note 2 Model characterization

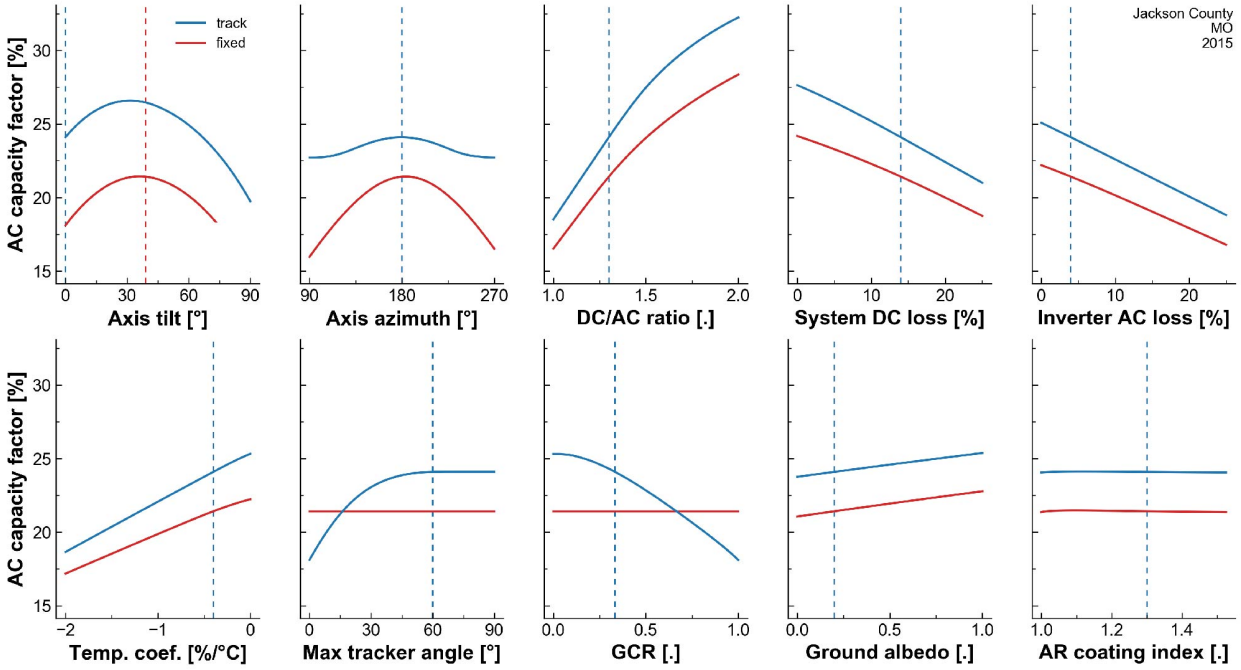

Figure SI.8: Sensitivity of PV capacity factor to input assumptions. Results are shown for a 1-axis-tracking array (blue traces) and a fixed-tilt array (red traces) located in Jackson County, MO in 2015. The dashed vertical line in each panel denotes the value of the respective parameter in all of the other panels, and is taken from Table 2 in the Methods section. "GCR" refers to ground coverage ratio (κ).

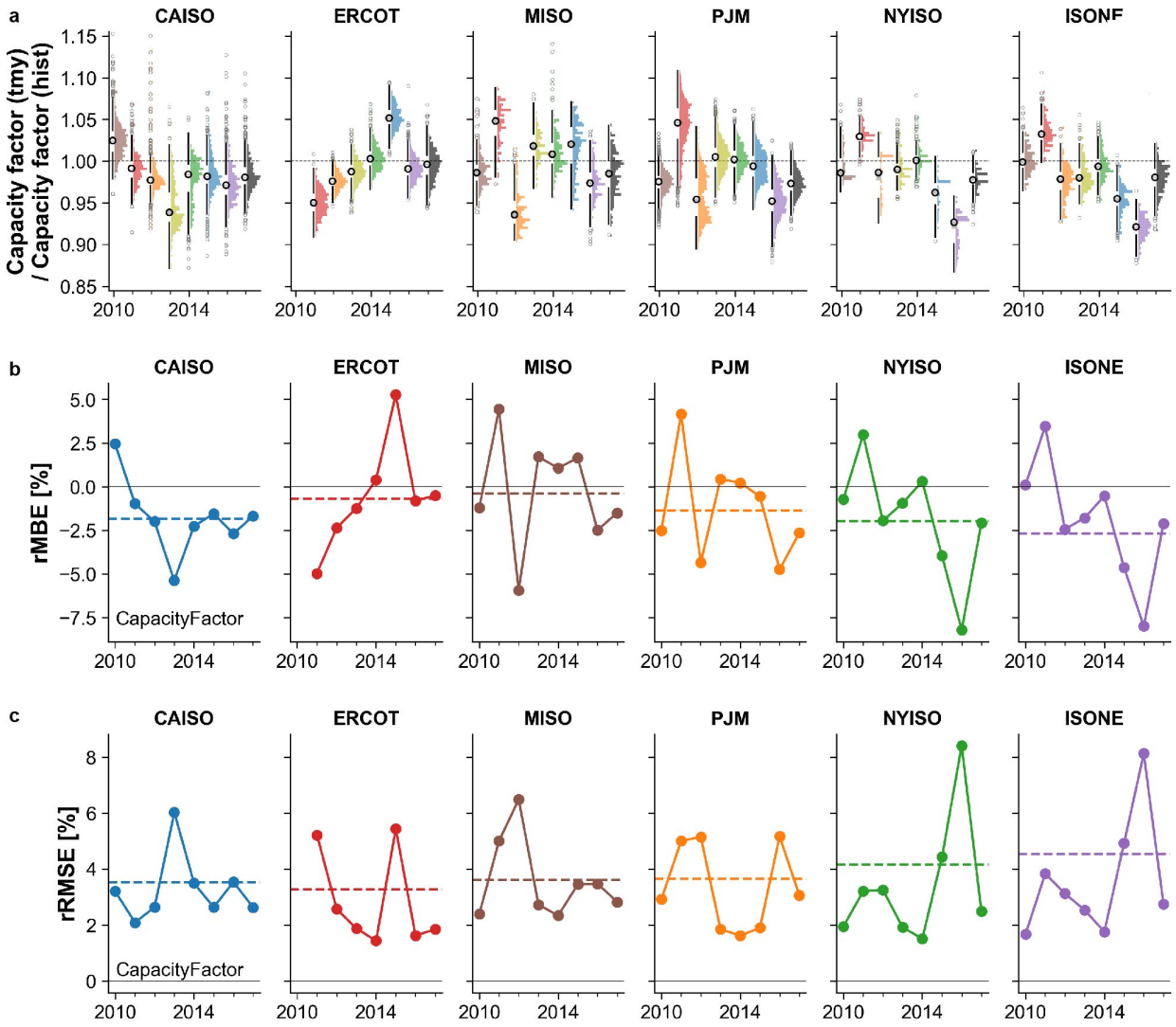

Figure SI.9: Comparison of modeled capacity factors using historical irradiance and typical meteorological year (TMY) irradiance. All modeled capacity factors are for a 1-axis-tracking PV array ($\theta = 0°$, $\phi = 180°$). For **b** and **c**, x^{sim} in (SI.4) and (SI.6) is the calculated capacity factor under TMY irradiance and x^{meas} is the calculated capacity factor under historical irradiance. Replicates are node-years within the labeled ISO. **a**, Distribution of ratios of capacity factor under historical TMY irradiance to capacity factor under historical irradiance by ISO and year. **b**, Relative mean bias error (rMBE) of capacity factor using TMY irradiance to capacity factor using historical irradiance. **b**, Relative root mean square error (rRMSE) of capacity factor using TMY irradiance to capacity factor using historical irradiance.

SI Note 3 Model validation

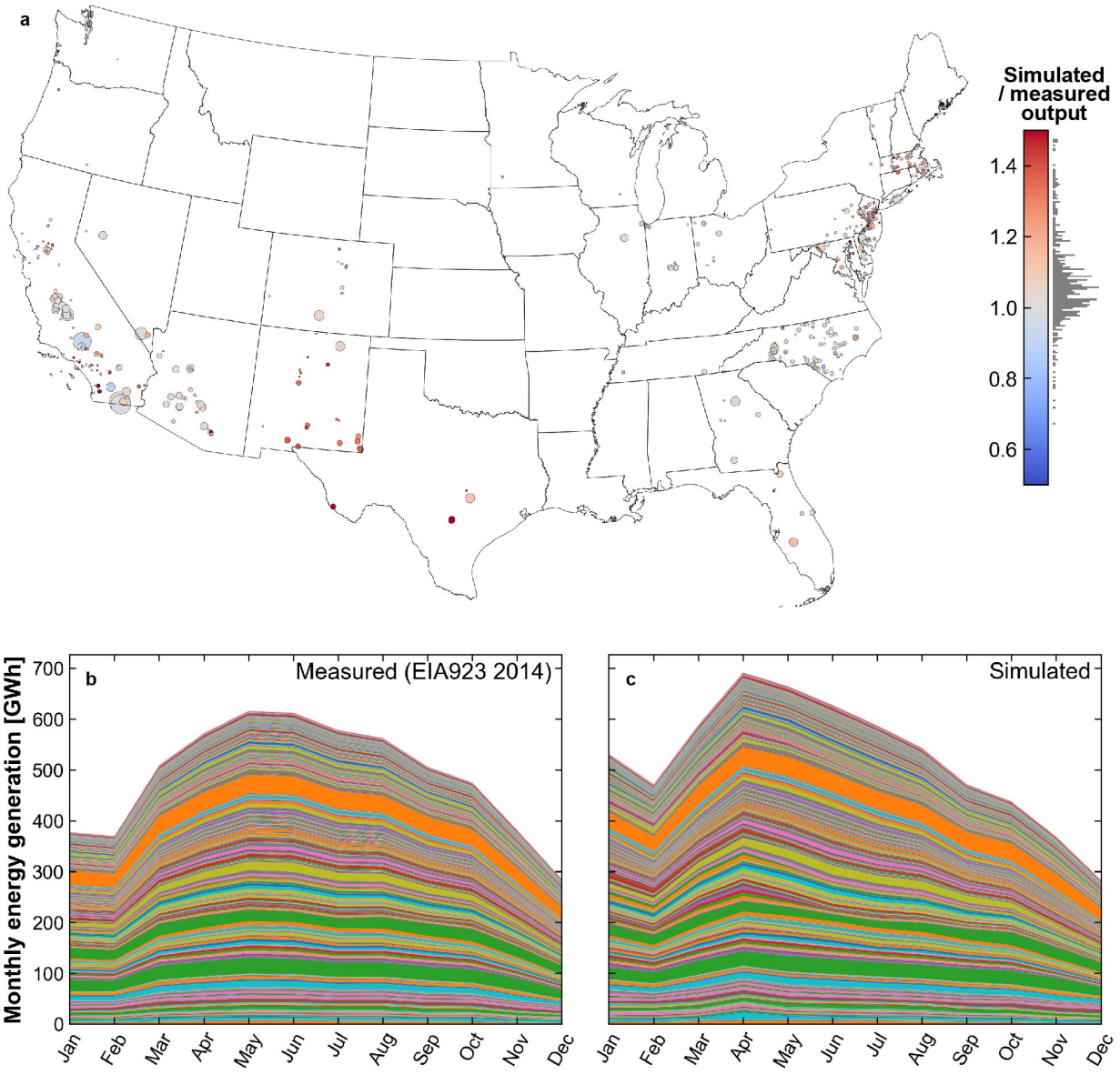

Figure SI.10: Location, capacity, and simulation accuracy of PV plants simulated for validation purposes in 2014. **a**. Location, capacity (indicated by marker size), and yearly simulation accuracy (indicated by marker color) of 542 utility-scale PV plants compared with reported monthly generation data from EIA forms 860 and 923. [18, 24] **b**. Reported monthly generation for each of the 542 plants, and **c**, simulated monthly generation for each of the 542 plants. Each filled band in **b** and **c** represents a single measured and simulated plant.

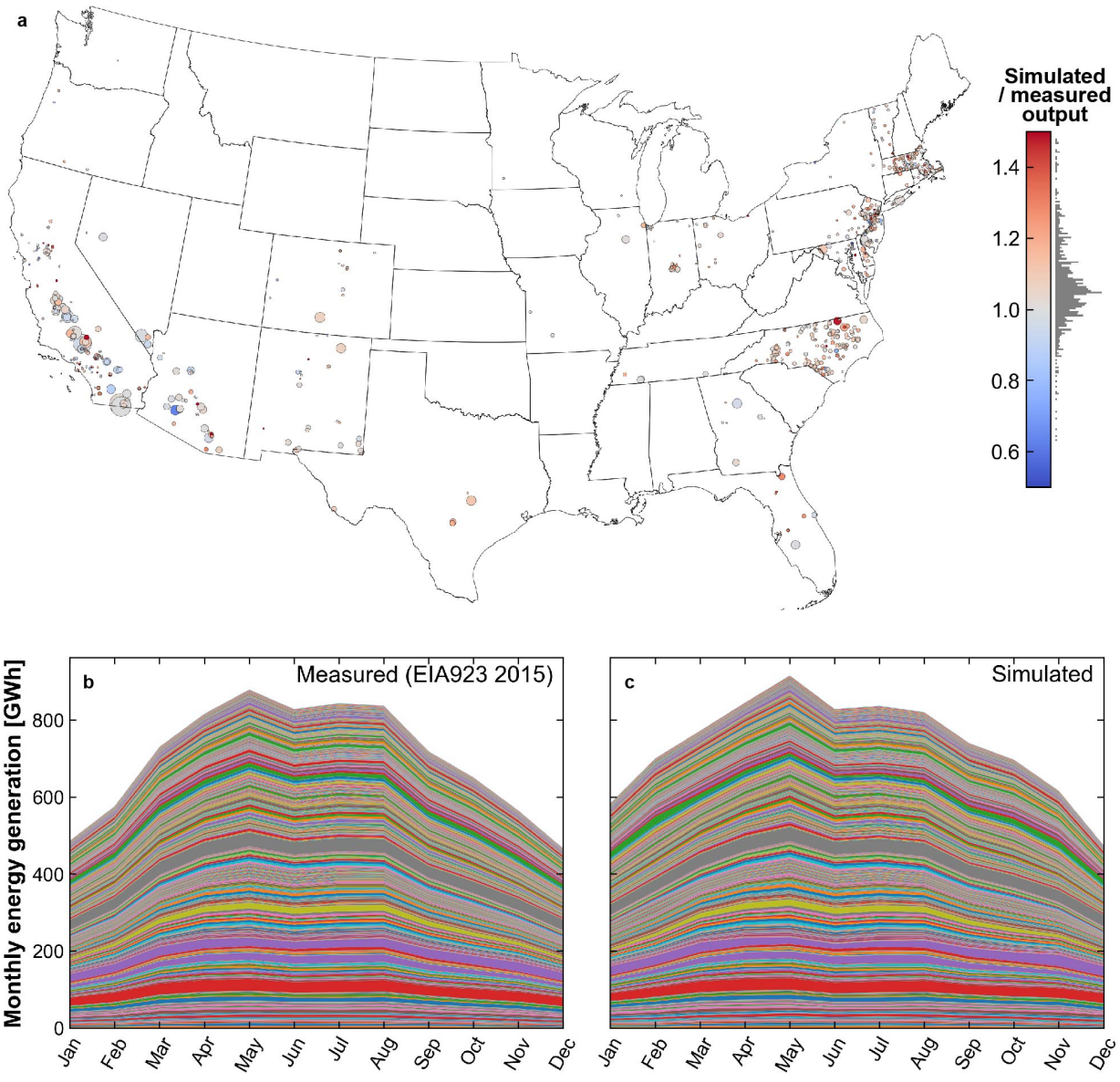

Figure SI.11: Location, capacity, and simulation accuracy of PV plants simulated for validation purposes in 2015. **a**. Location, capacity (indicated by marker size), and yearly simulation accuracy (indicated by marker color) of 800 utility-scale PV plants compared with reported monthly generation data from EIA forms 860 and 923. [18, 24] **b**. Reported monthly generation for each of the 800 plants, and **c**, simulated monthly generation for each of the 800 plants. Each filled band in **b** and **c** represents a single measured and simulated plant.

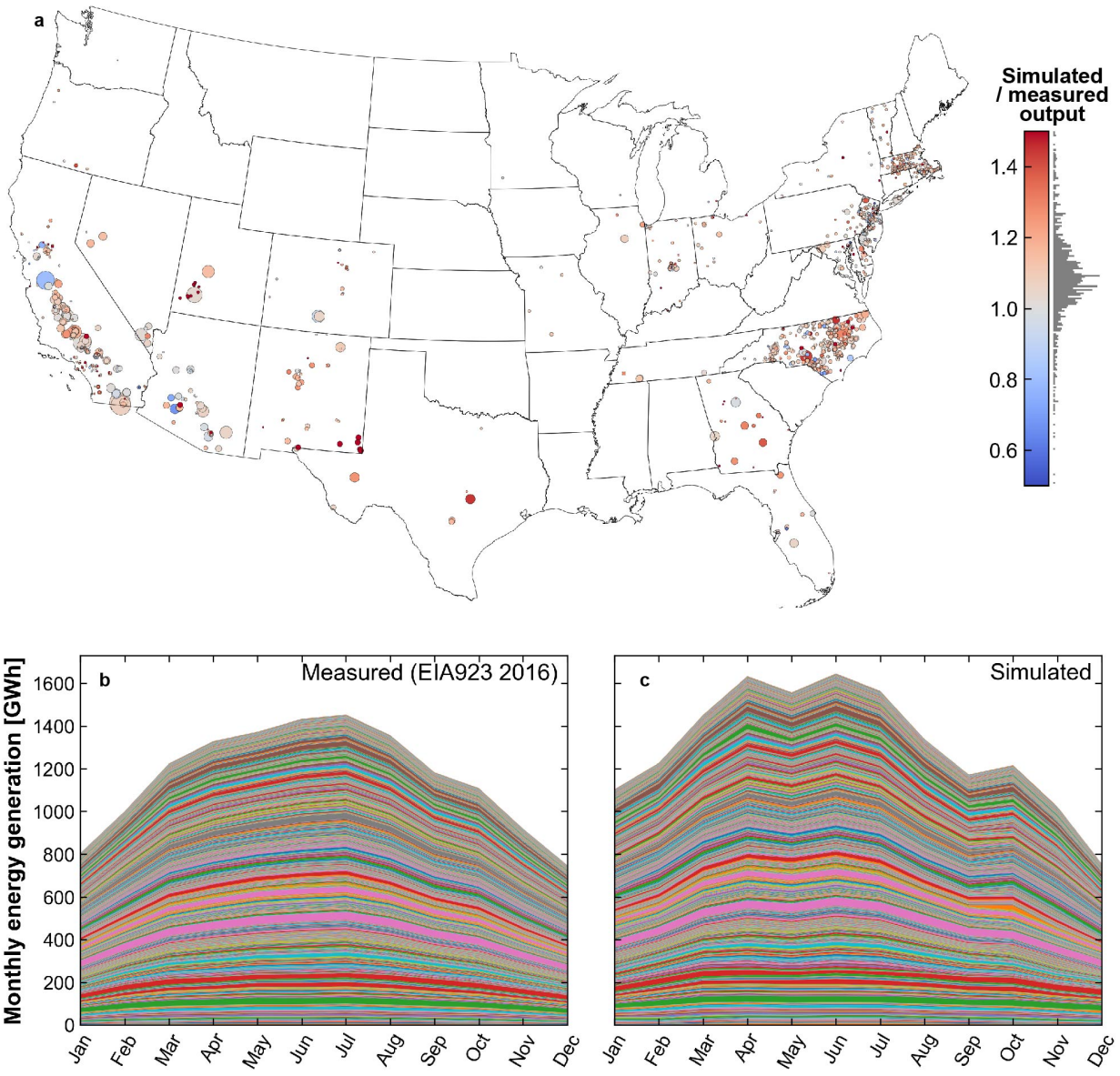

Figure SI.12: Location, capacity, and simulation accuracy of PV plants simulated for validation purposes in 2016. **a**. Location, capacity (indicated by marker size), and yearly simulation accuracy (indicated by marker color) of 1170 utility-scale PV plants compared with reported monthly generation data from EIA forms 860 and 923. [18, 24] **b**. Reported monthly generation for each of the 1170 plants, and **c**, simulated monthly generation for each of the 1170 plants. Each filled band in **b** and **c** represents a single measured and simulated plant.

Monthly model validation metrics

Model validation metrics are defined as in [20], with x_{meas} indicating the measured or reported value, x_{sim} indicating the simulated value, and n indicating the sample size:

$$\mathrm{CC} = \frac{\sum_{i=1}^{n}\left(\left(x_i^{sim} - \overline{x^{sim}}\right) \times \left(x_i^{meas} - \overline{x^{meas}}\right)\right)}{\sqrt{\sum_{i=1}^{n}\left(x_i^{sim} - \overline{x^{sim}}\right)^2} \times \sqrt{\sum_{i=1}^{n}\left(x_i^{meas} - \overline{x^{meas}}\right)^2}} \tag{SI.1}$$

$$\mathrm{MAE} = \frac{1}{n}\sum\left|x_{sim} - x_{meas}\right| \tag{SI.2}$$

$$\mathrm{MBE} = \frac{1}{n}\sum\left(x_{sim} - x_{meas}\right) \tag{SI.3}$$

$$\mathrm{rMBE} = \frac{\sum\left(x_{sim} - x_{meas}\right)}{\sum x_{meas}} \tag{SI.4}$$

$$\mathrm{RMSE} = \sqrt{\frac{1}{n}\sum\left(x_{sim} - x_{meas}\right)^2} \tag{SI.5}$$

$$\mathrm{rRMSE} = \sqrt{\frac{\sum\left(x_{sim} - x_{meas}\right)^2}{\sum x_{meas}^2}} \tag{SI.6}$$

Monthly validation results are differentiated by PV plant capacity (Figure SI.13), tracking strategy (Figure SI.14), and year of plant construction (Figure SI.15). Simulations for plants with capacity $\geq 10\,\mathrm{MW}$ are more accurate than for plants with capacity $< 10\,\mathrm{MW}$; this result is to be expected, as larger installations are also less likely to be subject to environmental shading losses and may have better maintenance practices. Simulations for fixed-tilt PV plants are more accurate than for 1-axis-tracking PV plants; this result is also intuitive, as the output of 1-axis tracking plants depends on assumptions that are not reported in EIA Form 860, [18] including ground coverage ratio, maximum tracker angler, and the presence or lack of backtracking to avoid self-shading. The only discernible trend with year of construction is that generation from the oldest PV plants, those constructed in 2009, tends to be overestimated. Seasonally, errors tend to be highest during the winter and early spring months. The overestimation in capacity factor at the beginning of each year likely arises from snow cover, which is not included in our model.

Combining results across all months, the yearly rMBE varies between $+4.3\,\%$ to $+6.6\,\%$ across all system sizes and $-0.1\,\%$ to $+5.6\,\%$ for $> 10\,\mathrm{MW}$ systems, depending on the year.

The rRMSE varies between 18 % to 27 % across all system sizes depending on the year. This level of accuracy is similar to that of the input NSRDB dataset itself, which demonstrates a rMBE of ±5 % for GHI and ±10 % for DNI, and a rRMSE of up to 20 % for GHI and up to 40 % for DNI. [20] The similar level of accuracy between our modeled results and the input meteorological data, particularly given our unadjusted assumptions for system losses and inverter losses and the possibility of inaccuracies from reporting error and curtailment or outages in the reported EIA data, lends credence to the PV power output simulation methodology employed here.

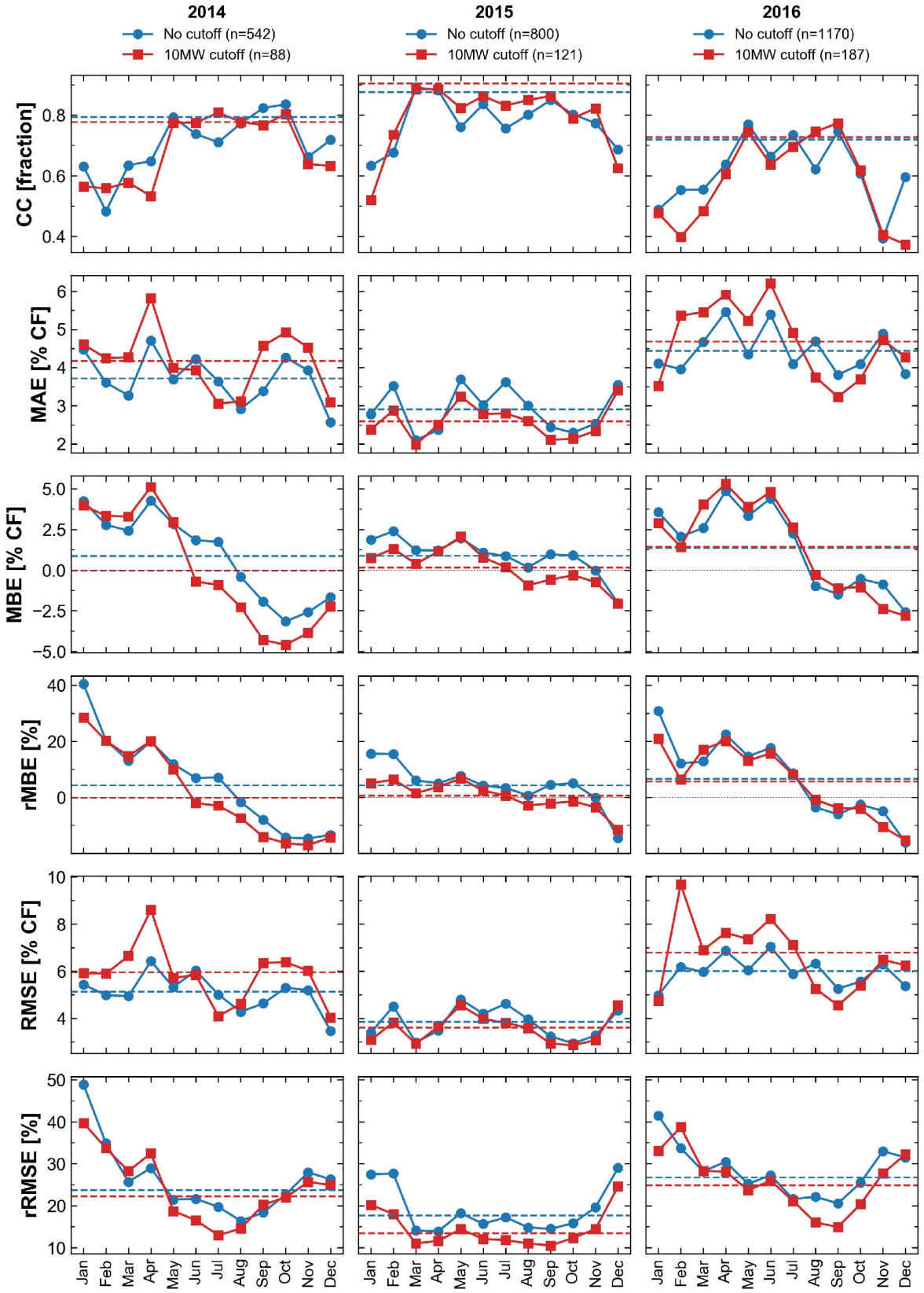

Figure SI.13: Monthly model validation statistics, differentiated by PV plant nameplate capacity. Dashed lines represent the value across all months.

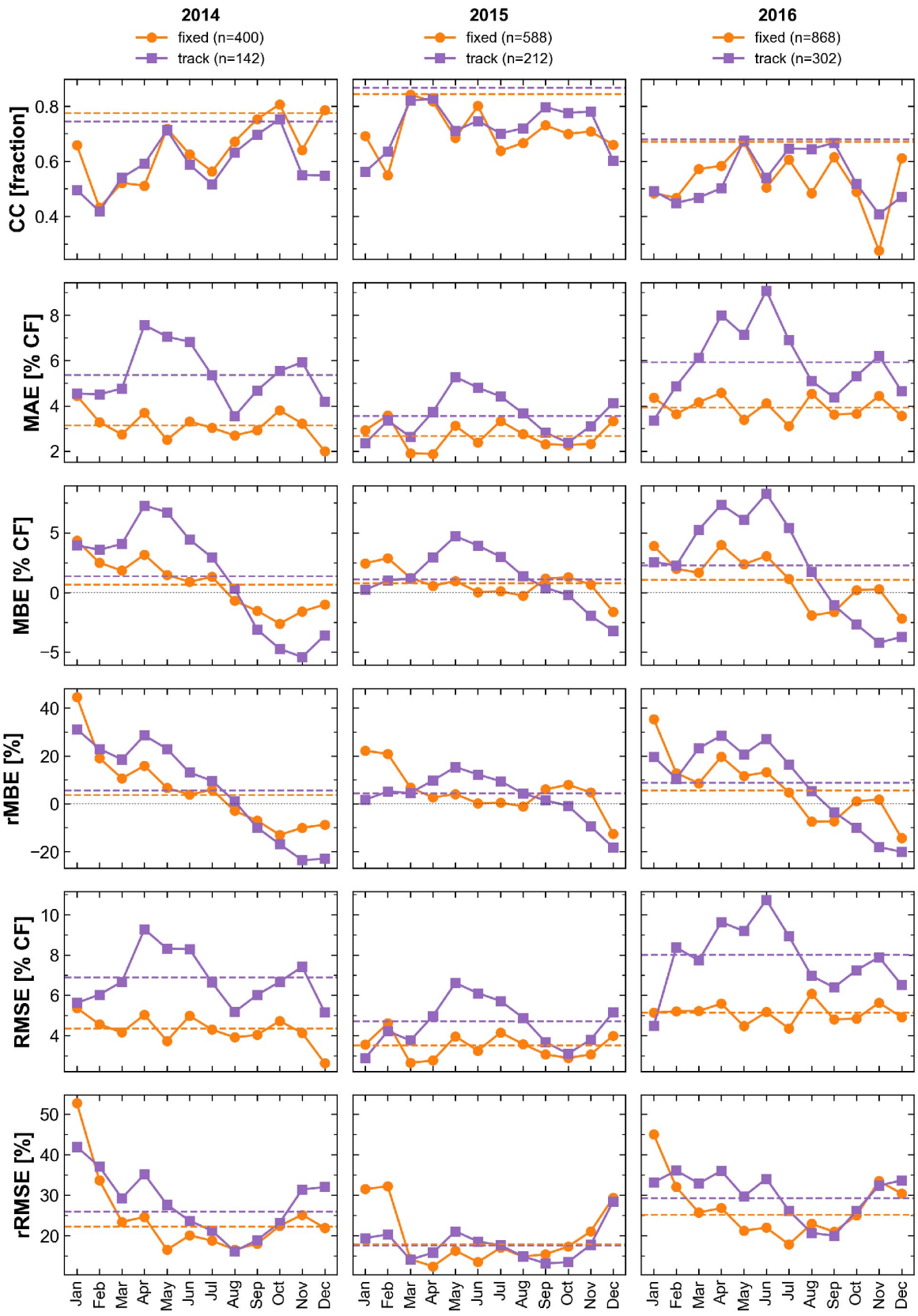

Figure SI.14: Monthly model validation statistics, differentiated by PV plant tracking strategy. Dashed lines represent the value across all months.

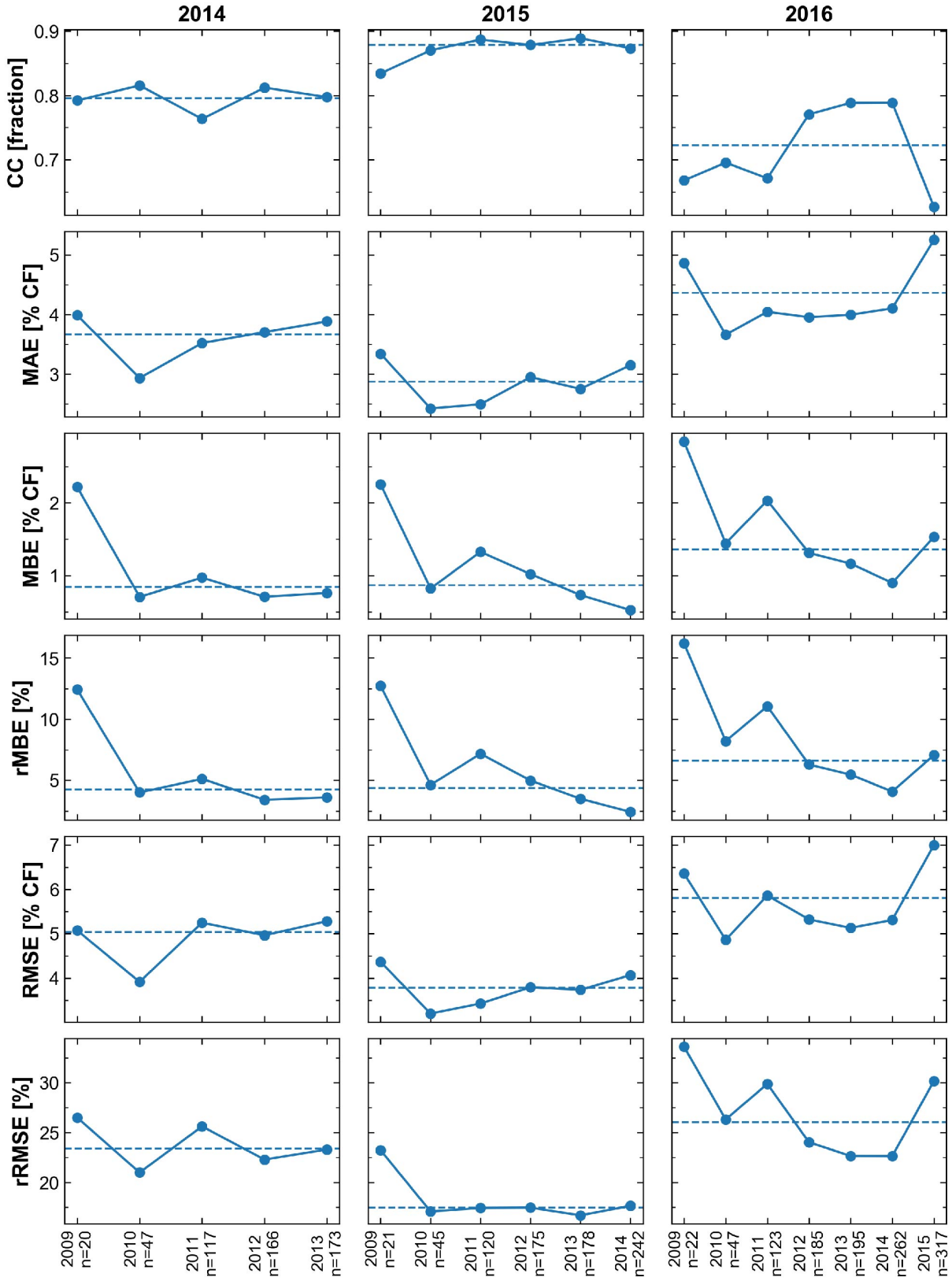

Figure SI.15: Monthly model validation statistics, differentiated by PV plant vintage. Plants are binned along the x-axis by year of construction. Dashed lines represent the value across all vintages.

Hourly model validation metrics

Hourly measured [25] and simulated PV profiles are displayed in Figures SI.16 and SI.17, and validation metrics as defined above are displayed in Figure SI.18 binned by month and in Figure SI.19 binned by hour of day. As observed above for the monthly validation, simulated results are overestimated in the winter months. The effect of snow cover on measured output is expected to be significant for this array, which has a small tilt angle ($\theta = 16.77°$) and is located in a region with relatively high annual snowfall compared to the rest of the continental U.S. Across the years analyzed, the summer rMBE across all hours ranges from +0.9 % in 2015 to +2.4 % in 2014 and the winter rMBE ranges from +30 % in 2014 to +42 % in 2015; the summer hourly rRMSE across all hours ranges from 24 % to 29 % and winter hourly rRMSE ranges from 54 % to 62 % (Figure SI.19). The low rMBE across all hours (except for sunrise and sunset) in summer, which is again comparable to the rMBE for the NSRDB input data, [20] builds confidence in the results presented here for the value factor of PV electricity, which depends on the relationship between the time-resolved PV generation and price profiles.

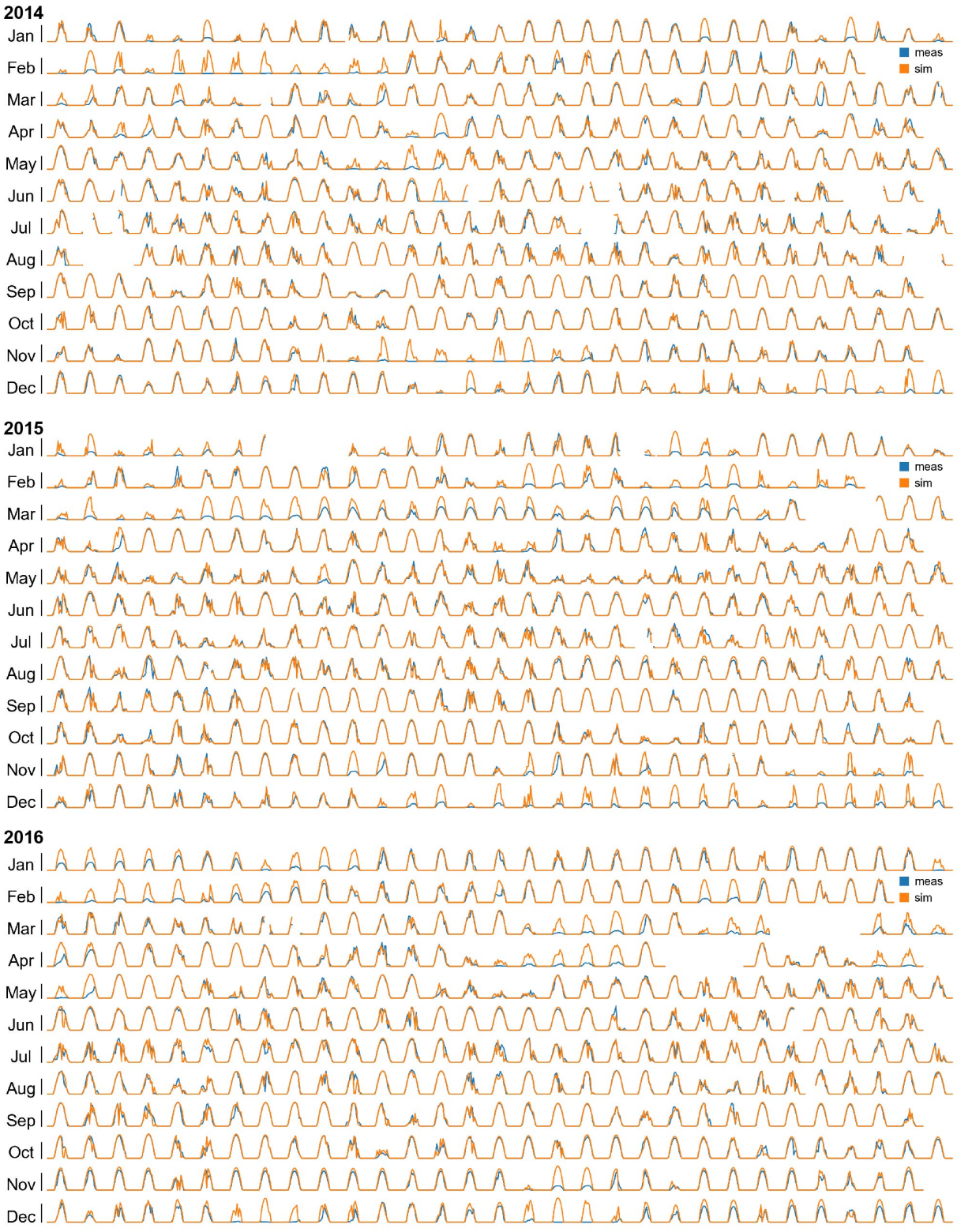

Figure SI.16: Hourly simulated and measured AC output as a fraction of nameplate AC capacity for a single PV array. "Measured" data (blue curve) are from the NREL PVDAQ database, site number 1332 (NREL parking garage). "Simulated" data are from our model, with panel orientation, inverter loading ratio, PV cell type, and installation location taken from the PVDAQ database. The height of the y-axis scale bar in each month corresponds to an AC output of 50 % of nameplate capacity.

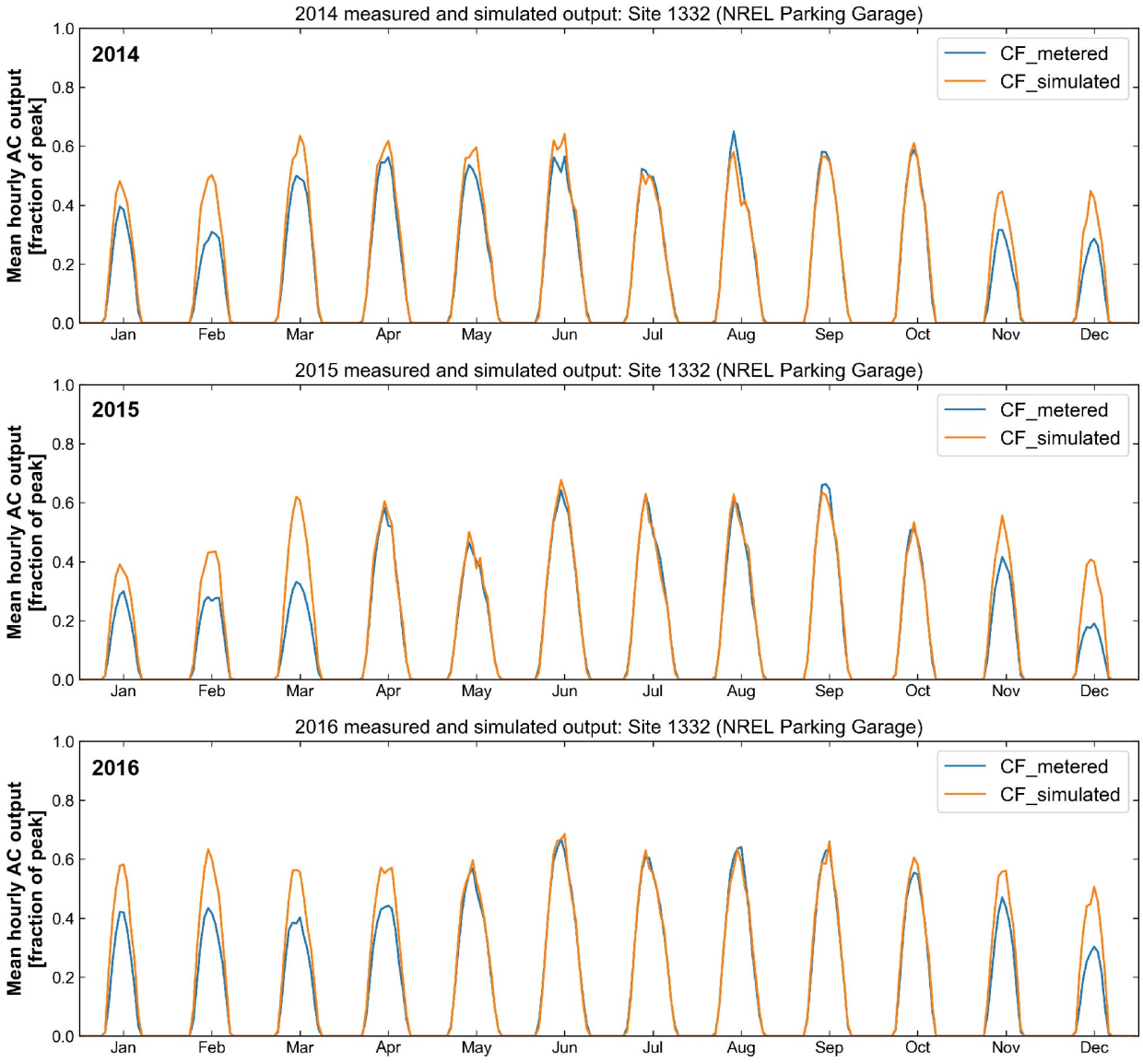

Figure SI.17: Hourly timeseries data for simulated and measured output for a single PV array. Monthly average of hourly measured and simulated data. "Measured" data (blue curve) are from the NREL PVDAQ database, site number 1332 (NREL parking garage). "Simulated" data are from our model, with panel orientation, inverter loading ratio, and PV cell type taken from the PVDAQ database.

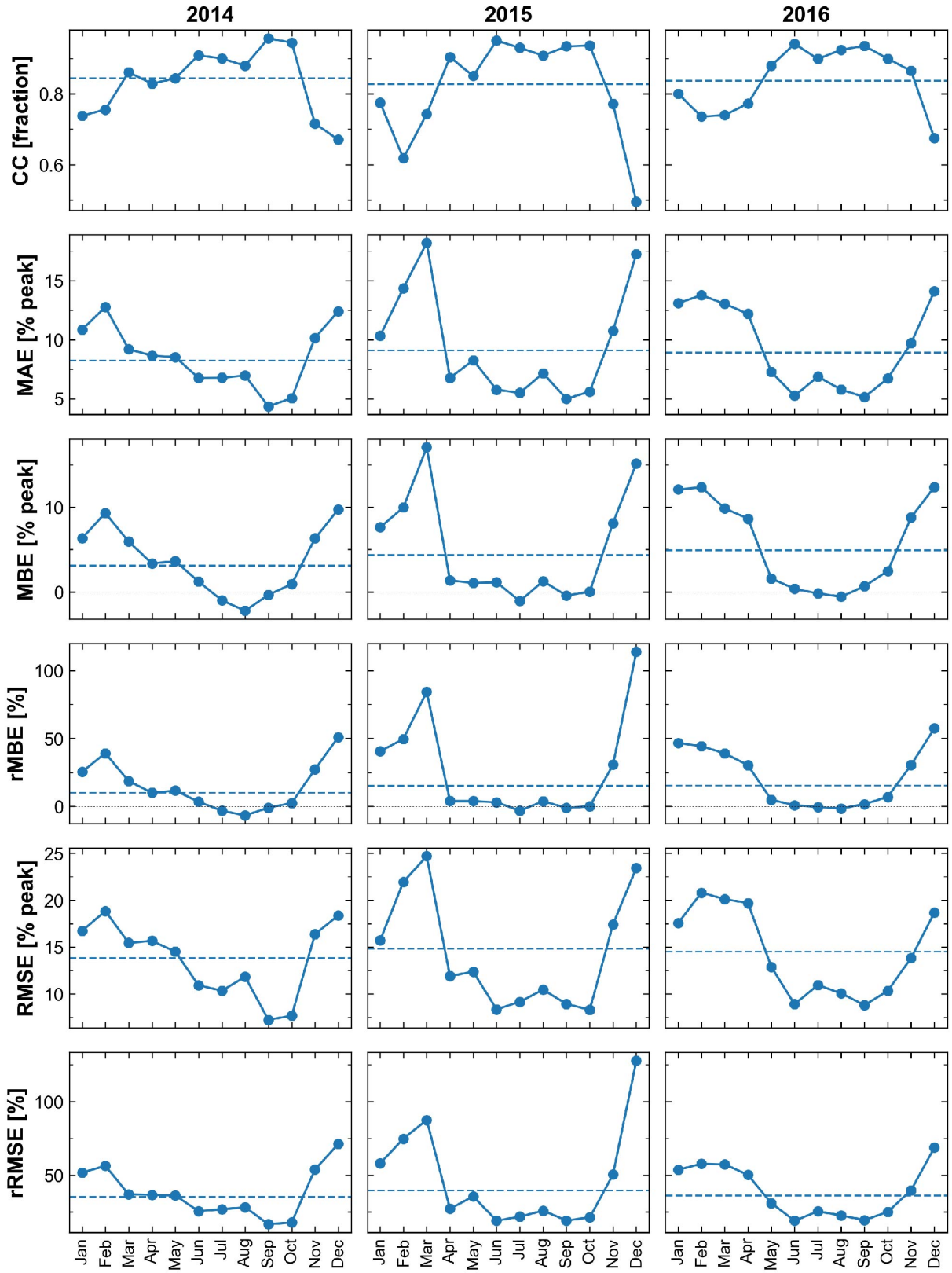

Figure SI.18: Hourly model validation statistics, sorted by month of year. Dashed lines represent the value across all months.

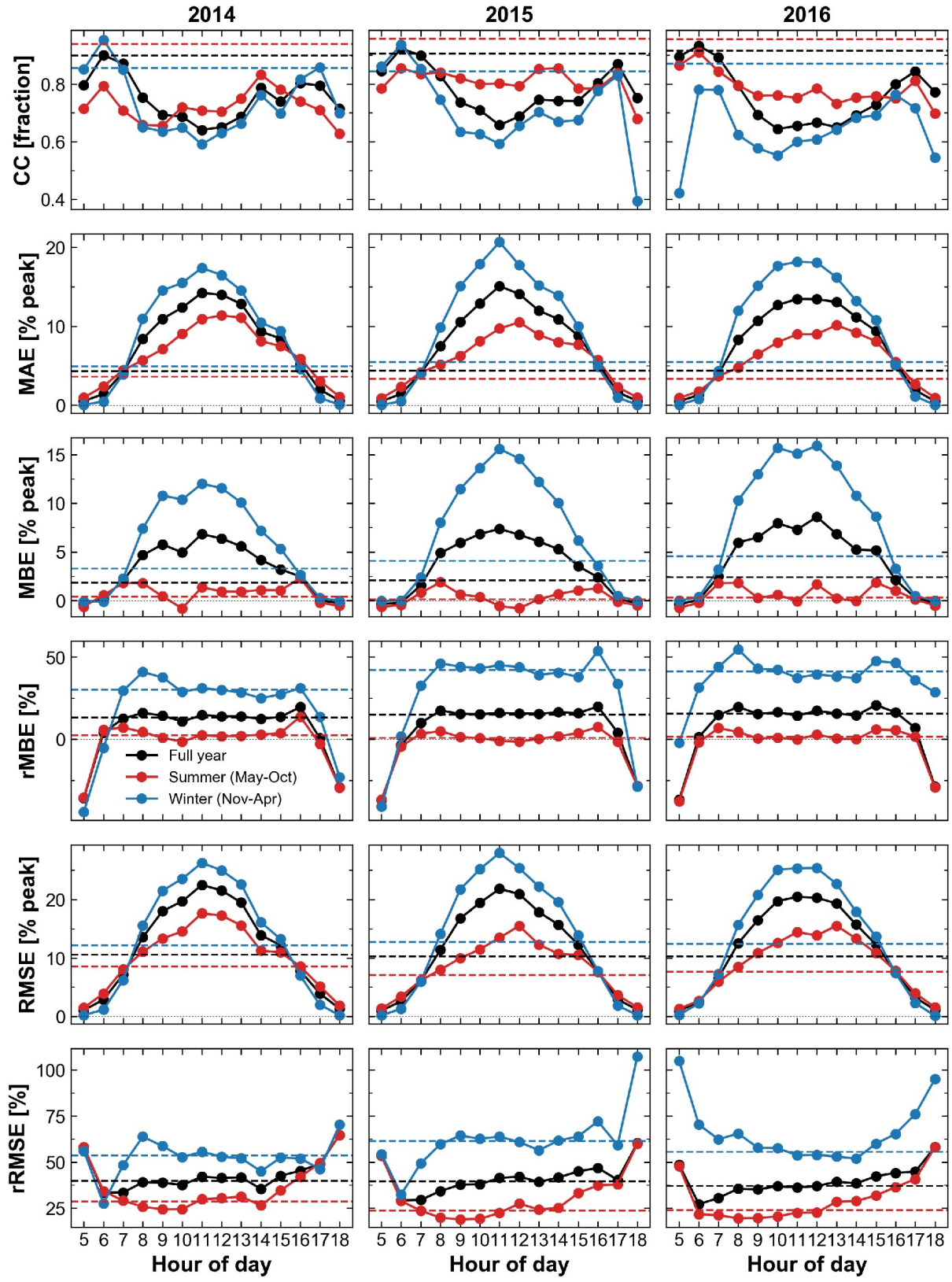

Figure SI.19: Hourly model validation statistics, sorted by hour of day and season of year. Dashed lines represent the value across all hours.

SI Note 4 Supplemental results: Energy value

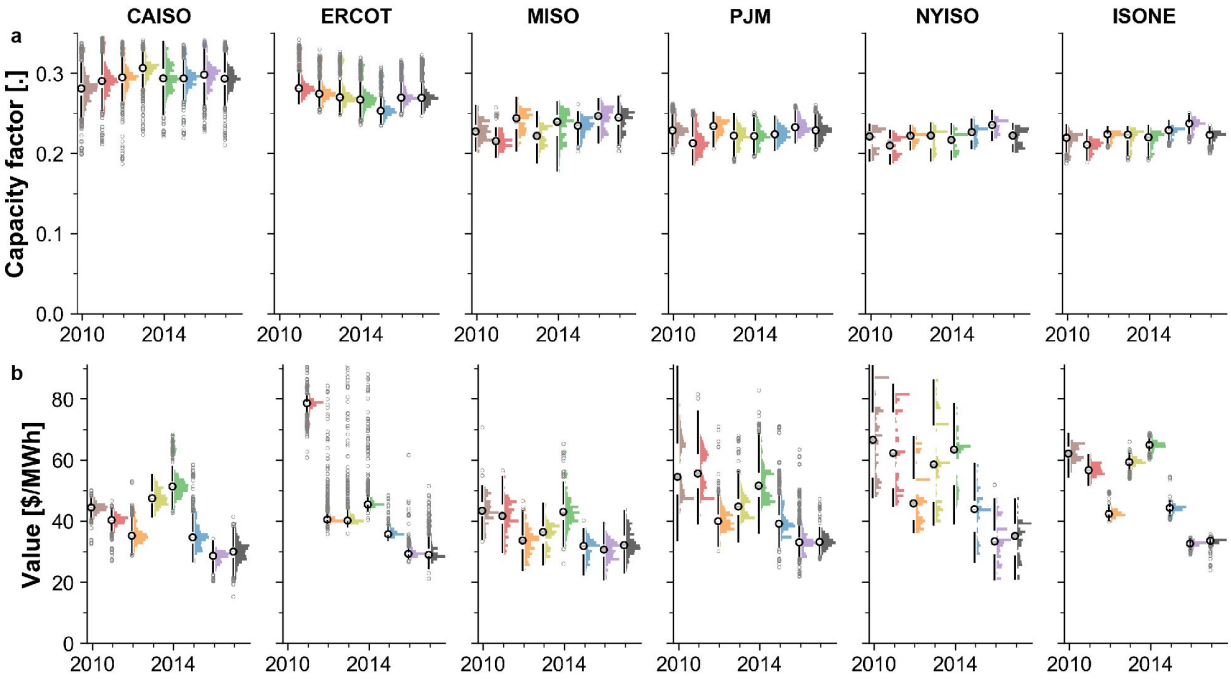

Figure SI.20: Modeled nodal PV capacity factor for a 1-axis tracking array (a) and yearly average energy value (b) sorted by ISO and year.

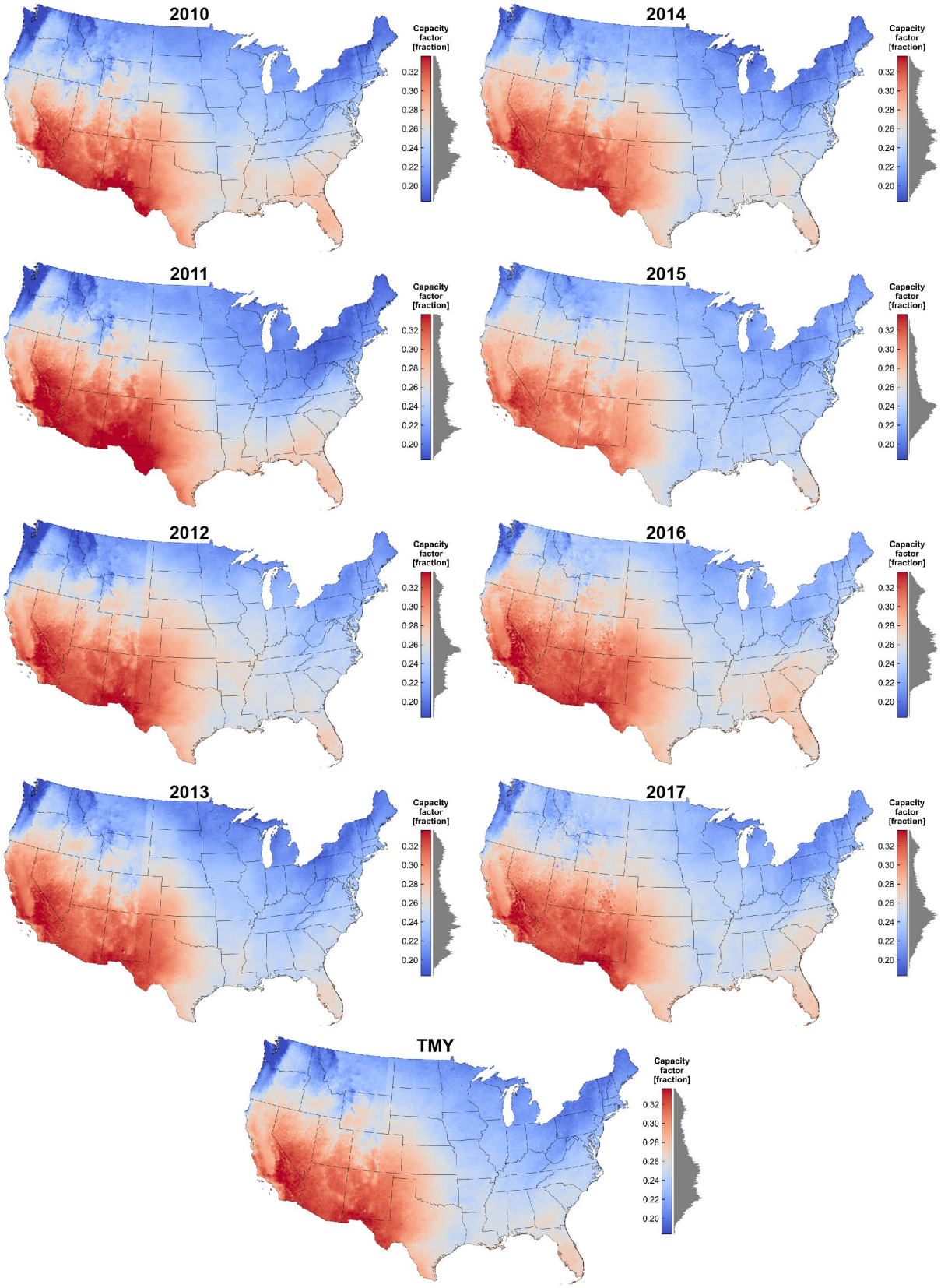

Figure SI.21: Yearly modeled capacity factor for 2010–2017 and TMY. Results assume 1-axis tracking with $\theta = 0^\circ$ and $\phi = 180^\circ$. The same color axis scale is used in all years.

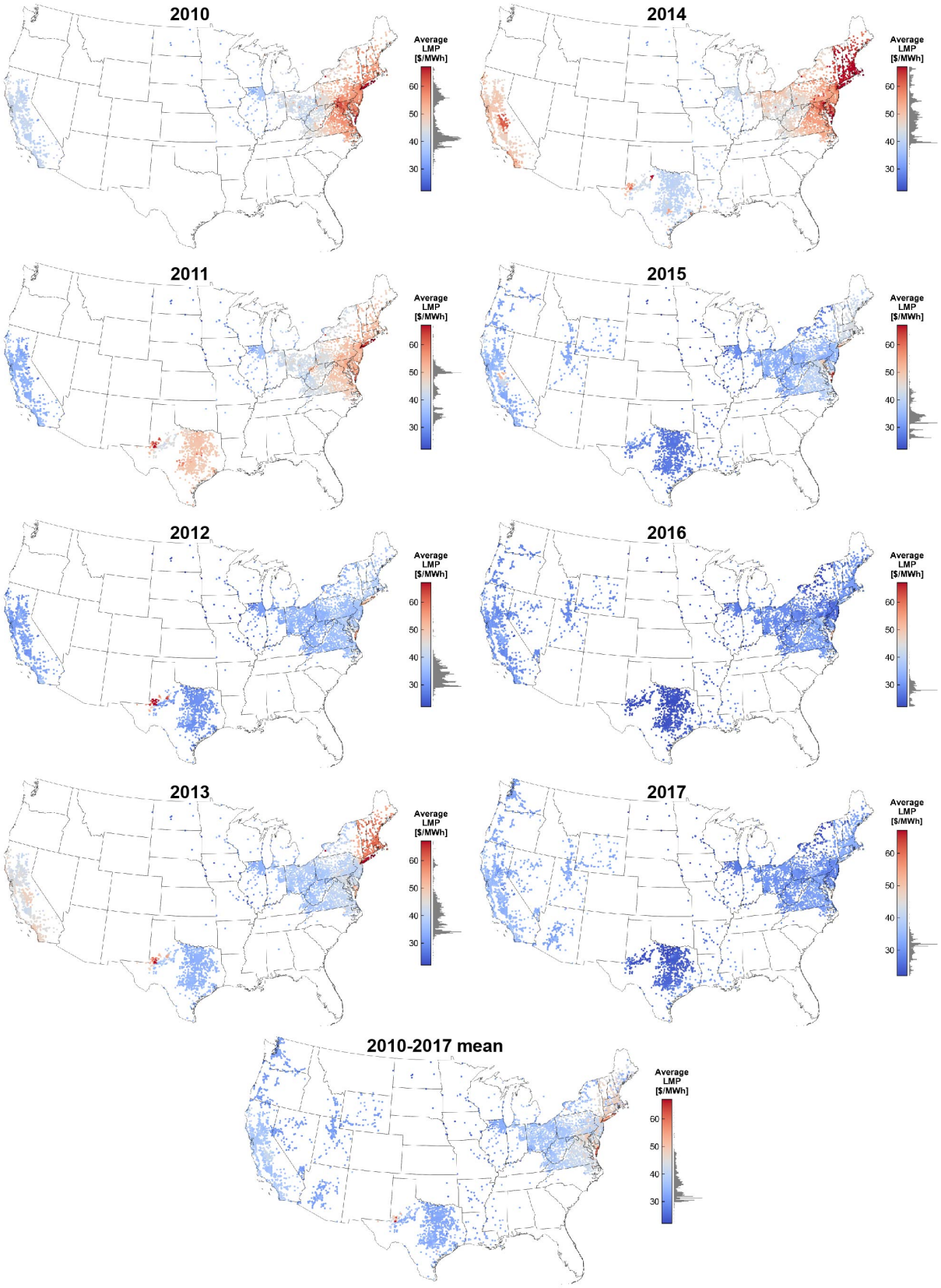

Figure SI.22: Yearly average day-ahead locational marginal price (LMP). The same color axis scale is used in all years. Note that mean values (bottom plot) include all available years of data for each node; available years of data are shown in Figure SI.1.

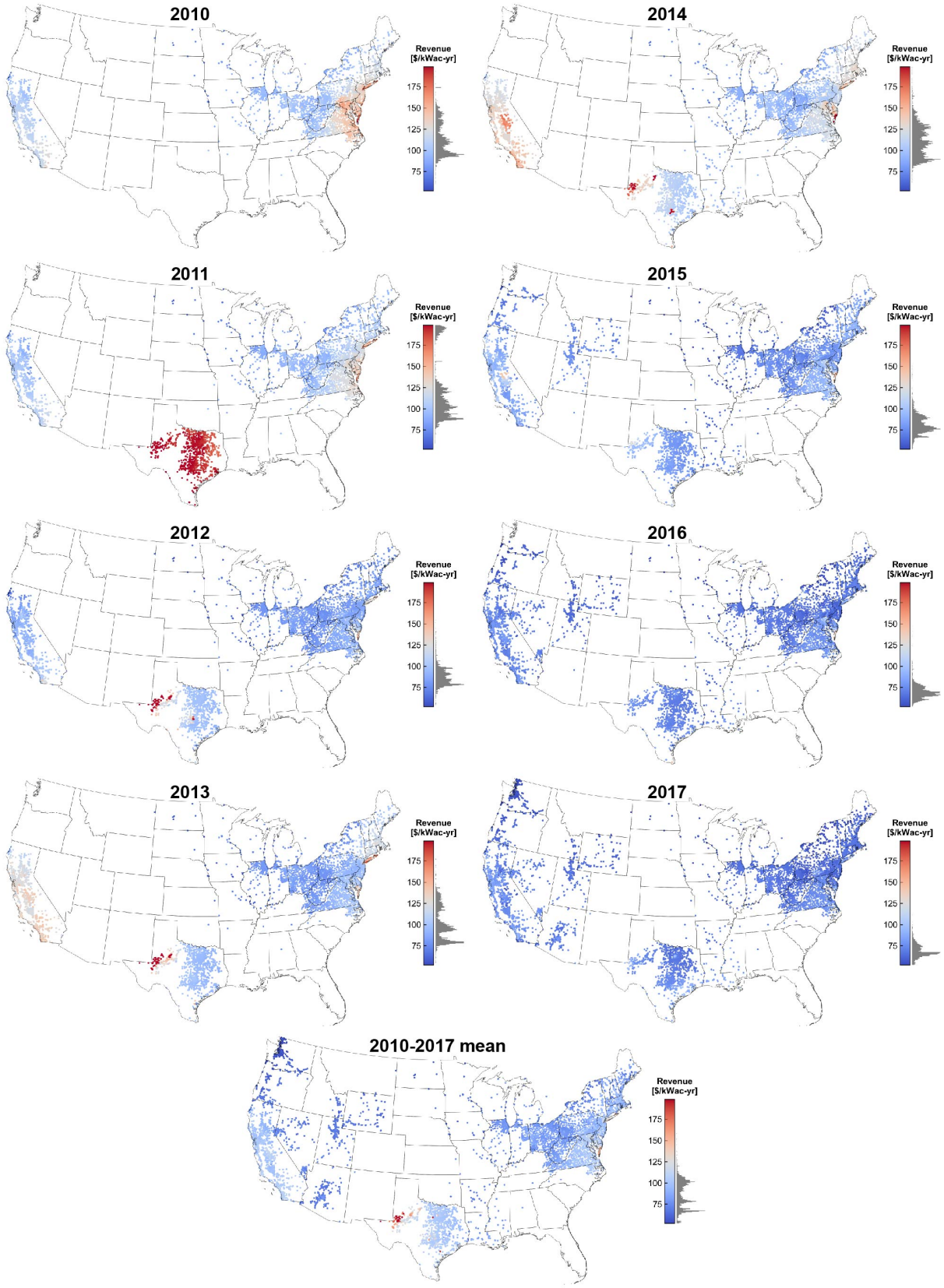

Figure SI.23: Modeled yearly revenue of 1-axis tracking PV installations ($\theta = 0°$, $\phi = 180°$) on the day-ahead market without curtailment. The same color axis scale is used in all years. Note that mean values (bottom plot) include all available years of data for each node; available years of data are shown in Figure SI.1.

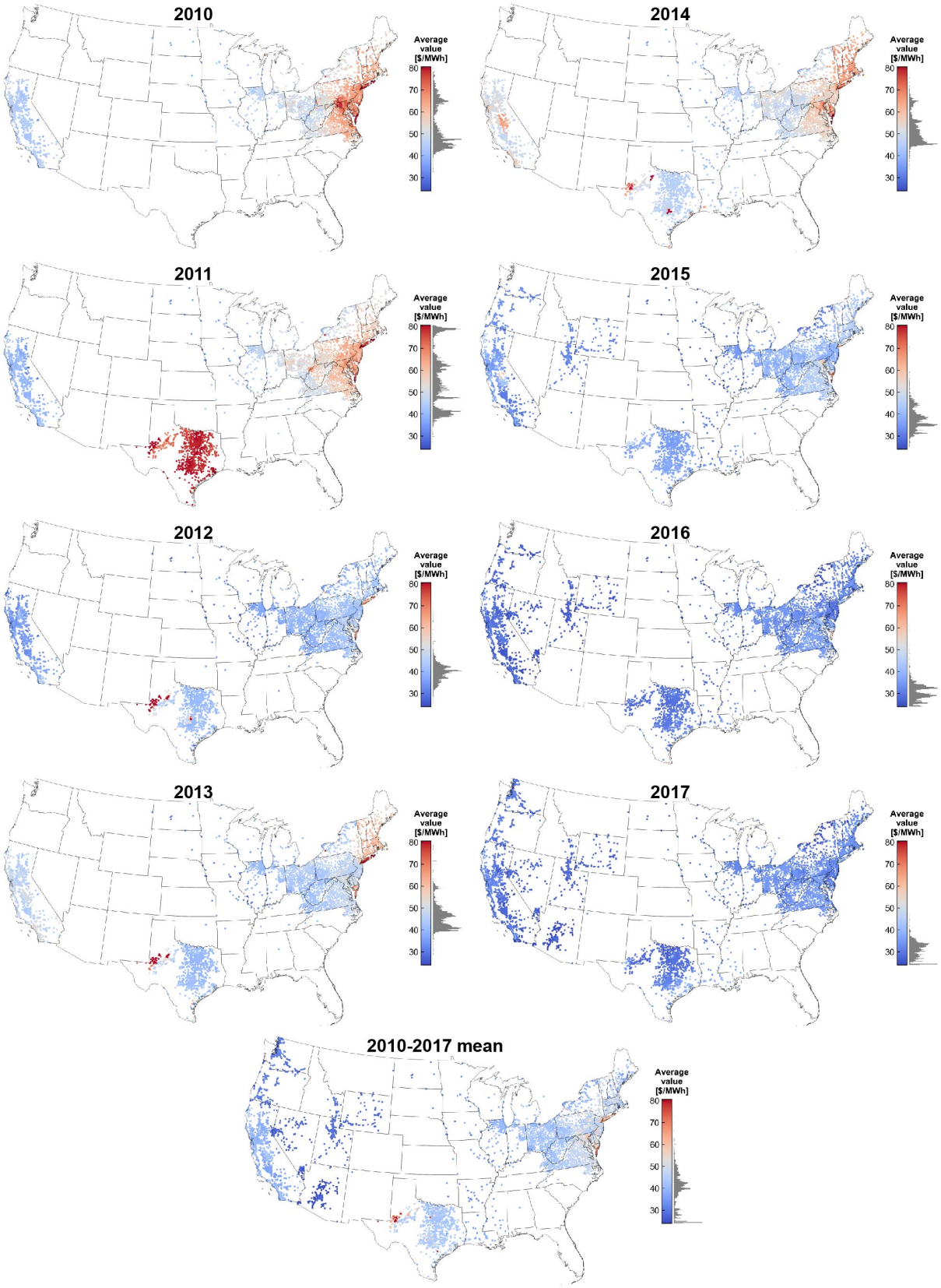

Figure SI.24: Modeled average value of electricity from a 1-axis tracking PV installation ($\theta = 0°$, $\phi = 180°$) on the day-ahead market without curtailment. The same color axis scale is used in all years. Note that mean values (bottom plot) include all available years of data for each node; available years of data are shown in Figure SI.1.

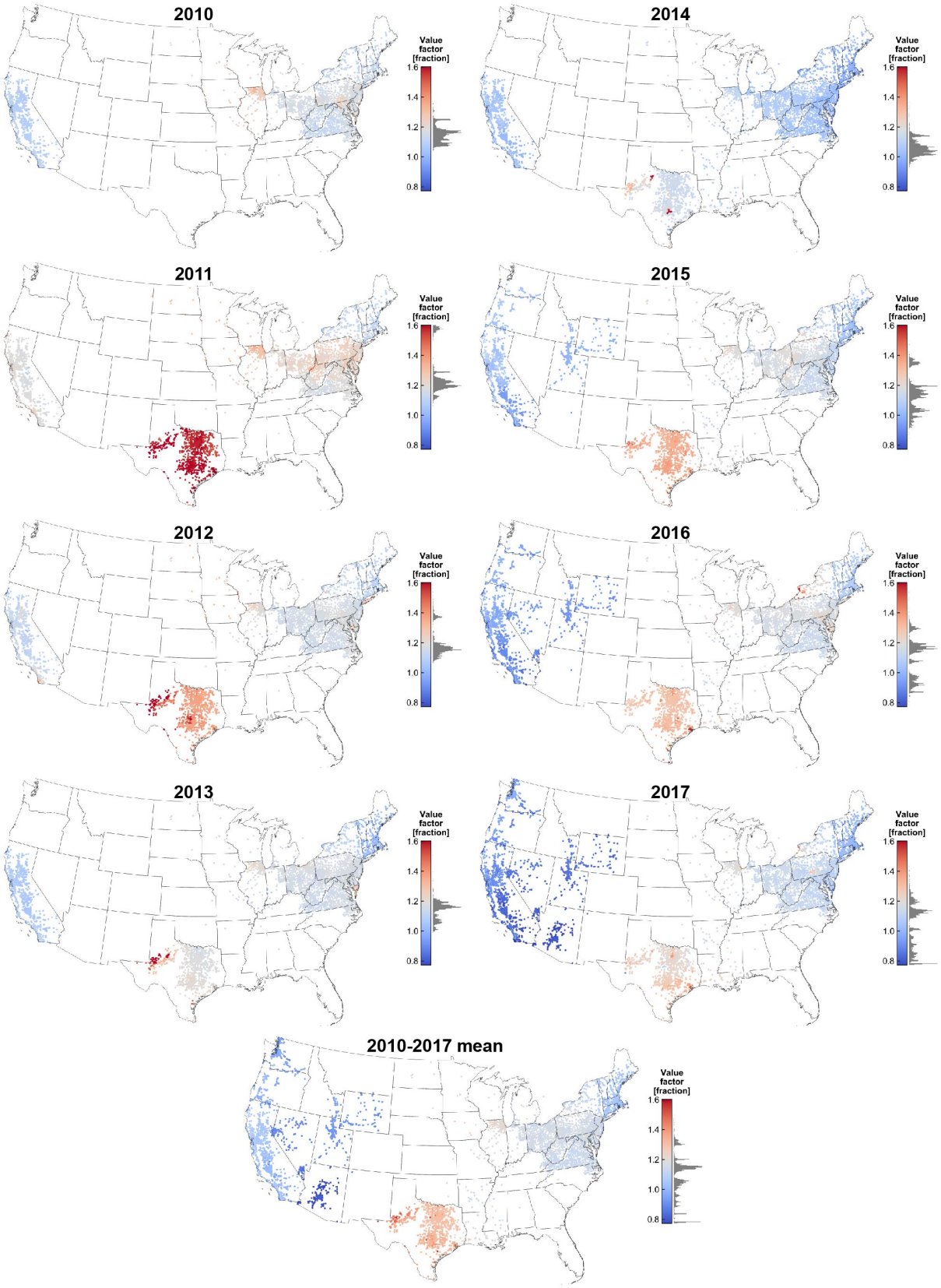

Figure SI.25: Modeled value factor of a 1-axis tracking PV installation ($\theta = 0°$, $\phi = 180°$) on the day-ahead market without curtailment. The same color axis scale is used in all years. Note that mean values (bottom plot) include all available years of data for each node; available years of data are shown in Figure SI.1.

SI Note 5 Long-term trends in nodal energy value

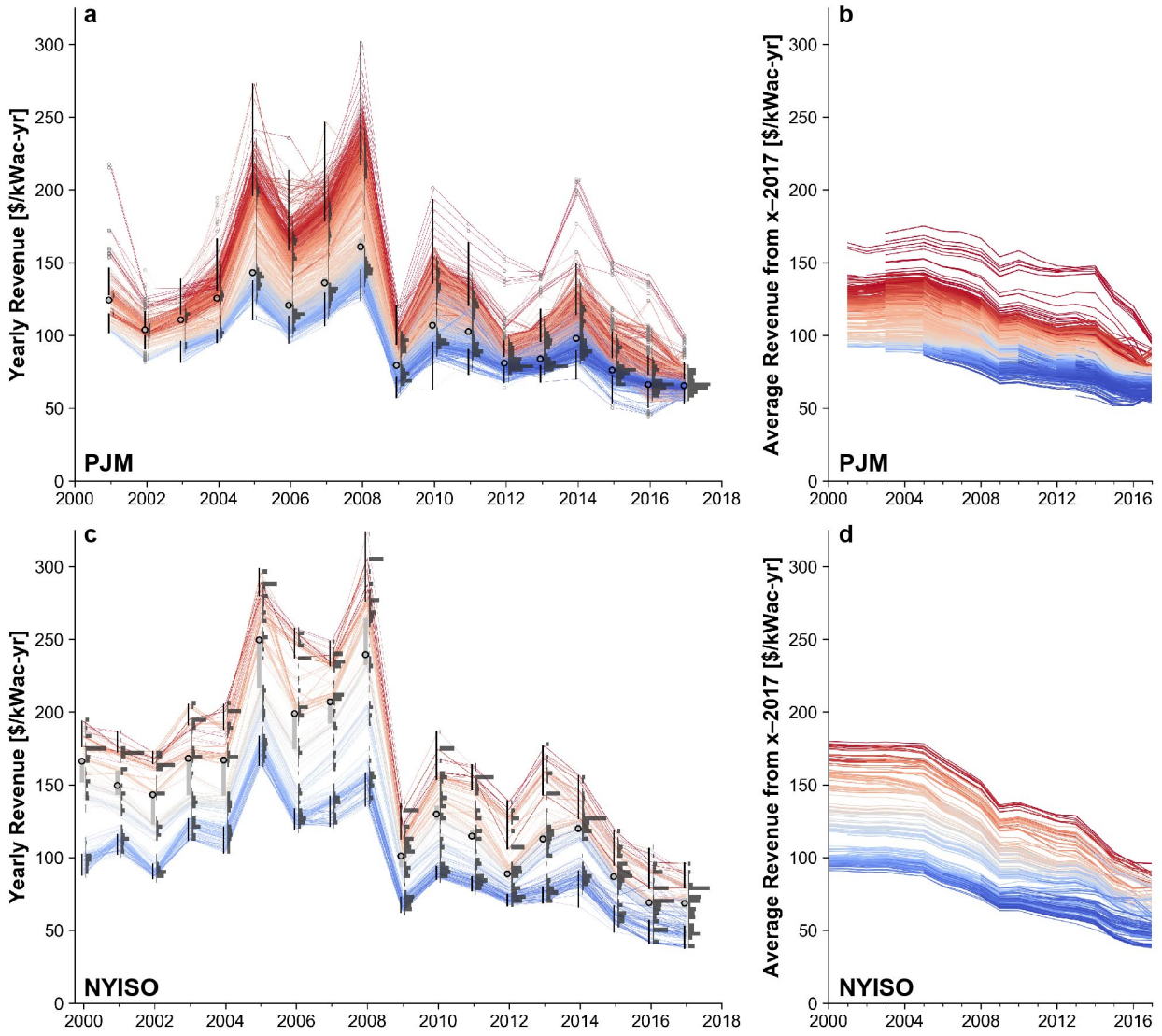

Figure SI.26: Long-term trends in nodal PV energy revenue in PJM (a-b) and NYISO (c-d). **a,c**, Yearly nodal revenue distributions. **b,d**, Multi-year average nodal revenues. Each line represents one node. Nodes are colored by their mean revenue over all available years: the highest-revenue node is reddest and lowest-revenue node is bluest. In **a** and **c**, the values in a given year represent the average revenue between that year and 2017. As shown by the persistent color distribution, the highest-revenue nodes in a particular year tend to remain at the top of the revenue distribution across all collections of years analyzed.

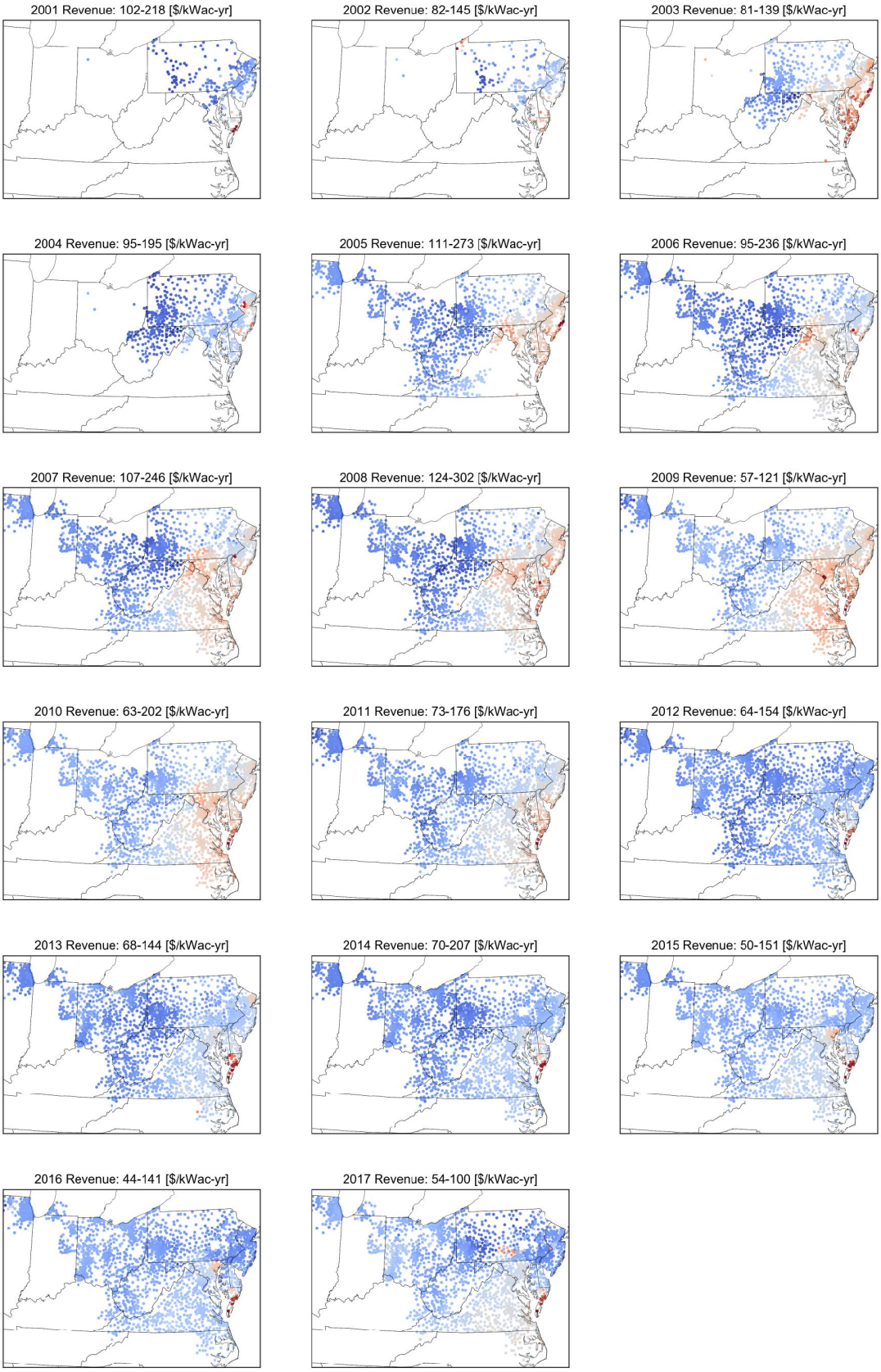

Figure SI.27: Nodal PV energy revenue in PJM from 2001–2017. Color axis scales vary between plots; minimum (blue) and maximum (red) values are listed above each plot.

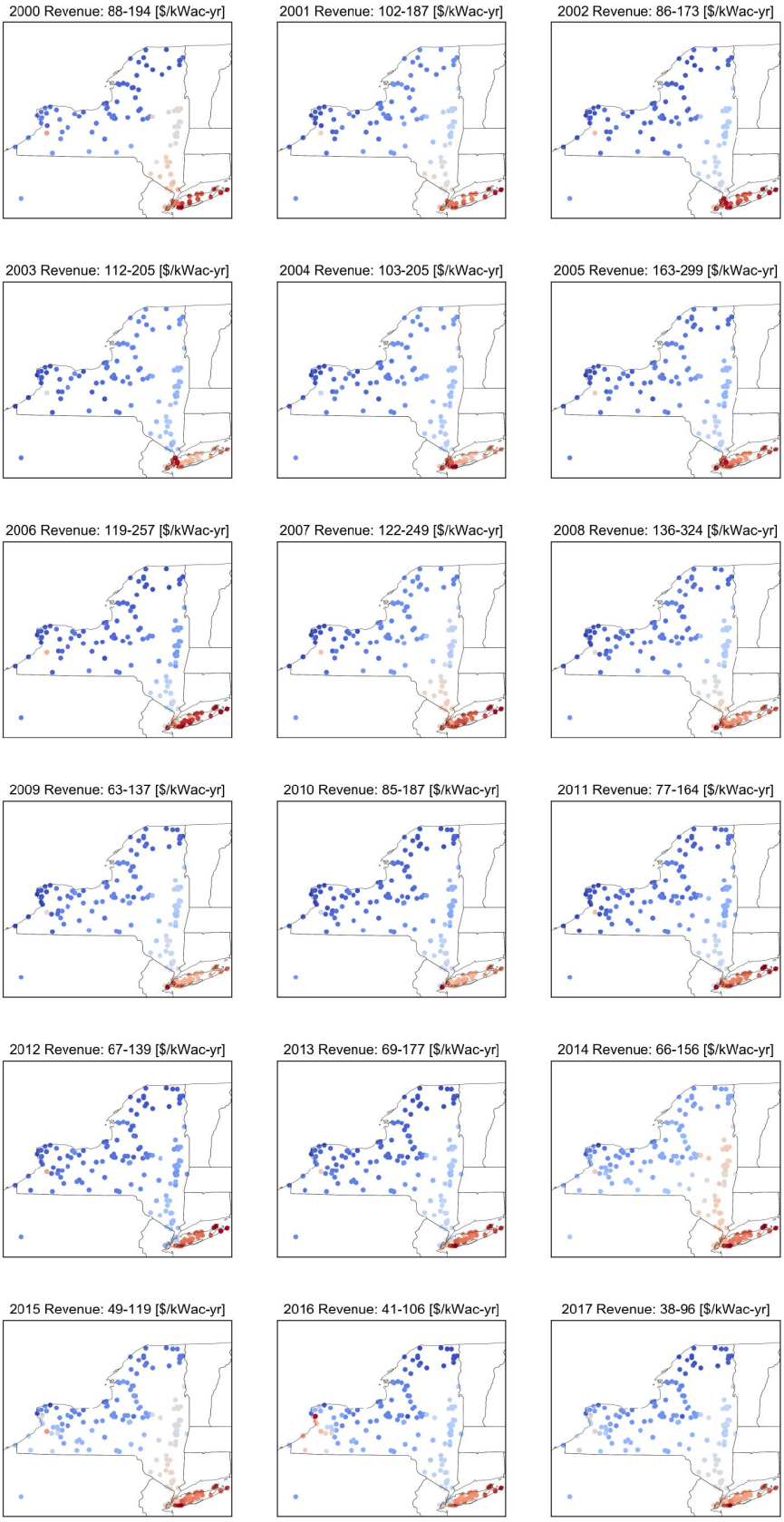

Figure SI.28: Nodal PV energy revenue in NYISO from 2000–2017. Color axis scales vary between plots; minimum (blue) and maximum (red) values are listed above each plot.

SI Note 6 LMP disaggregation

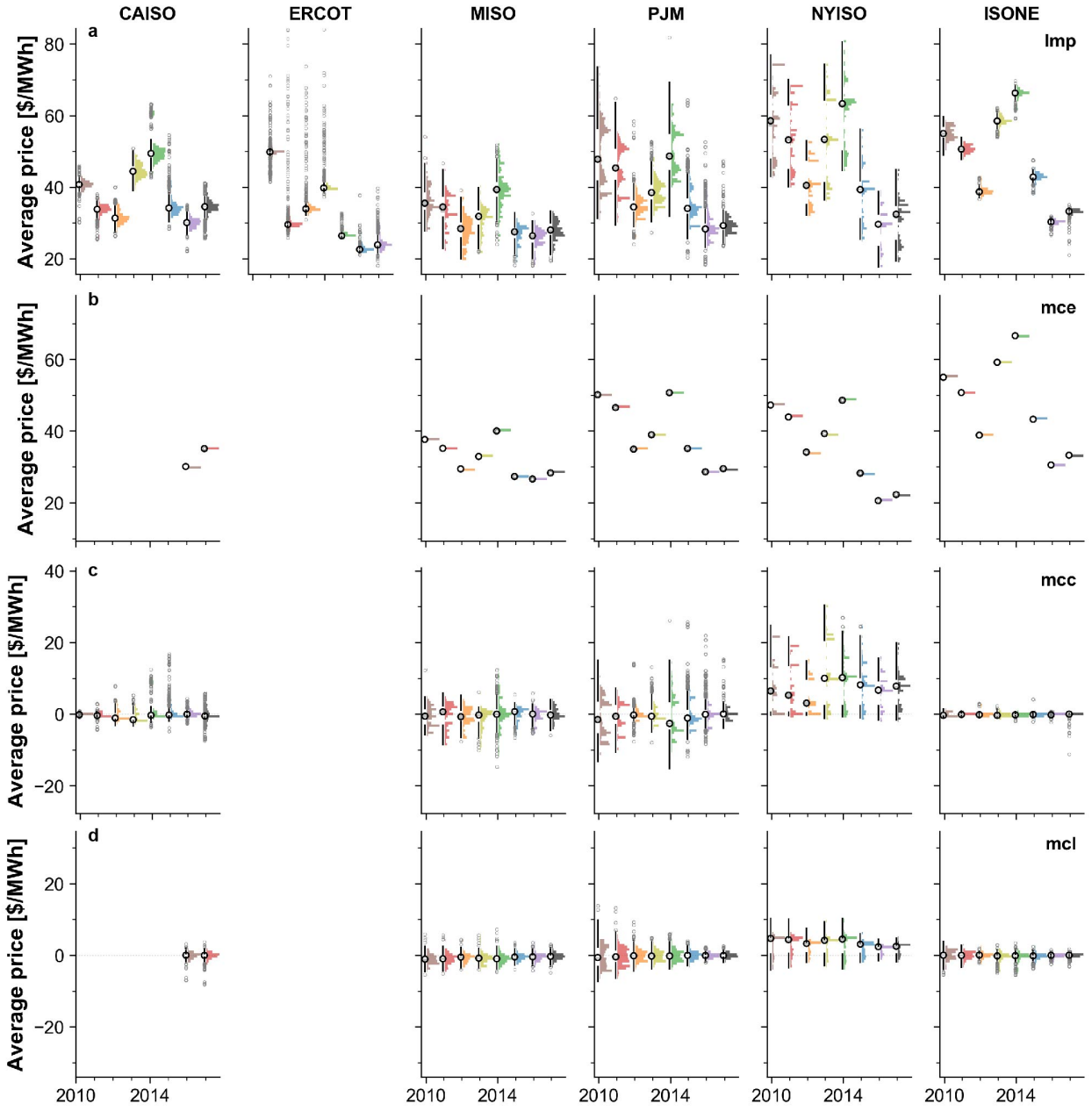

Figure SI.29: Nodal trends in electricity price disaggregated by LMP component. **a**, Full locational marginal price (LMP); **b**, marginal cost of energy (MCE); **c**, marginal cost of congestion (MCC); **d**, marginal cost of losses (MCL). For a given node, LMP = MCE + MCC + MCL. MCE and MCL data for CAISO prior to 2016 are not available. [77] All plots share the same y-axis scaling, but rows differ in y-axis offset.

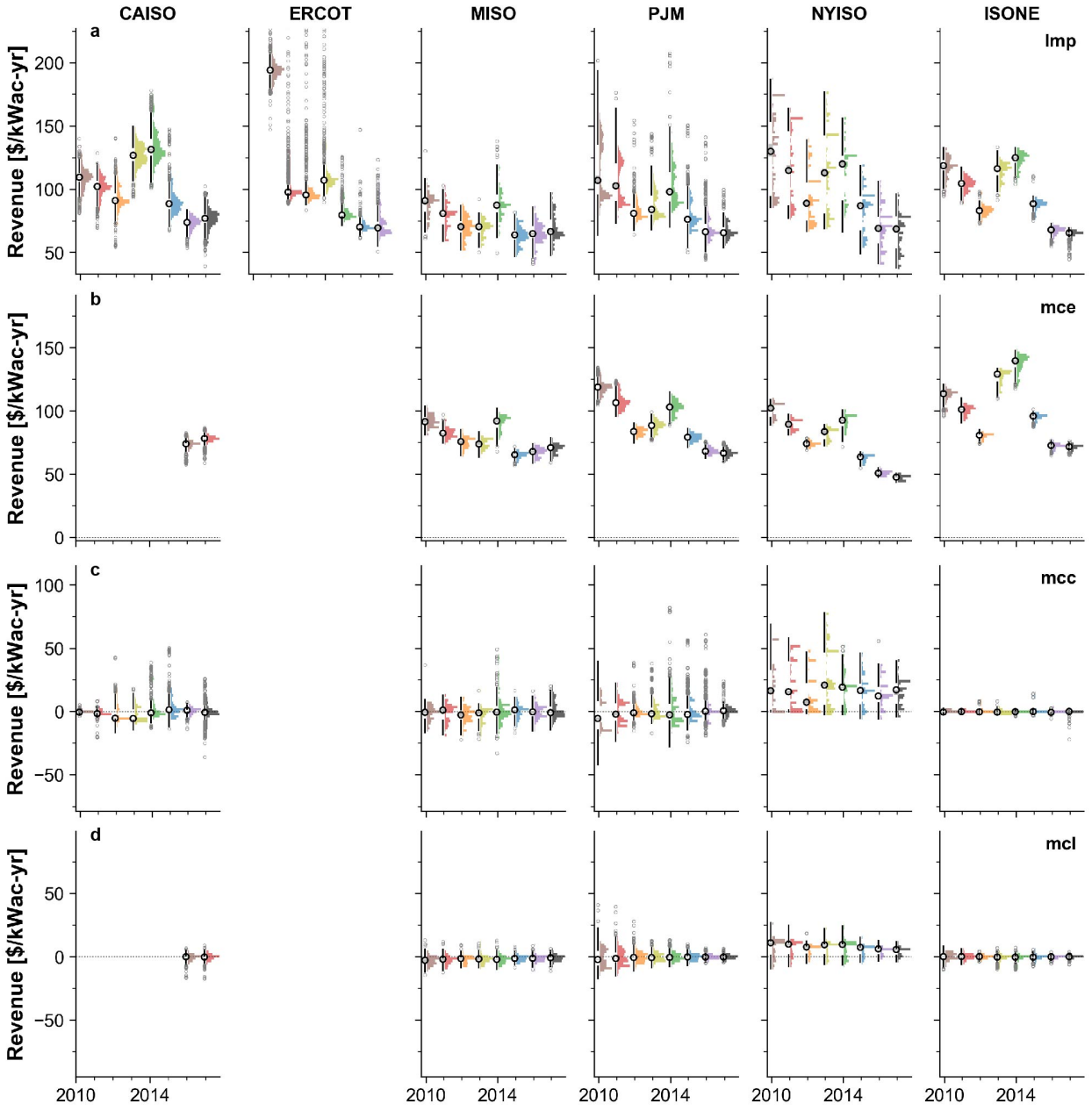

Figure SI.30: Nodal trends in PV energy revenue disaggregated by LMP component. **a**, Full locational marginal price (LMP); **b**, marginal cost of energy (MCE); **a**, marginal cost of congestion (MCC); **a**, marginal cost of losses (MCL). MCE and MCL data for CAISO prior to 2016 are not available. [77] All plots share the same y-axis scaling, but rows differ in y-axis offset.

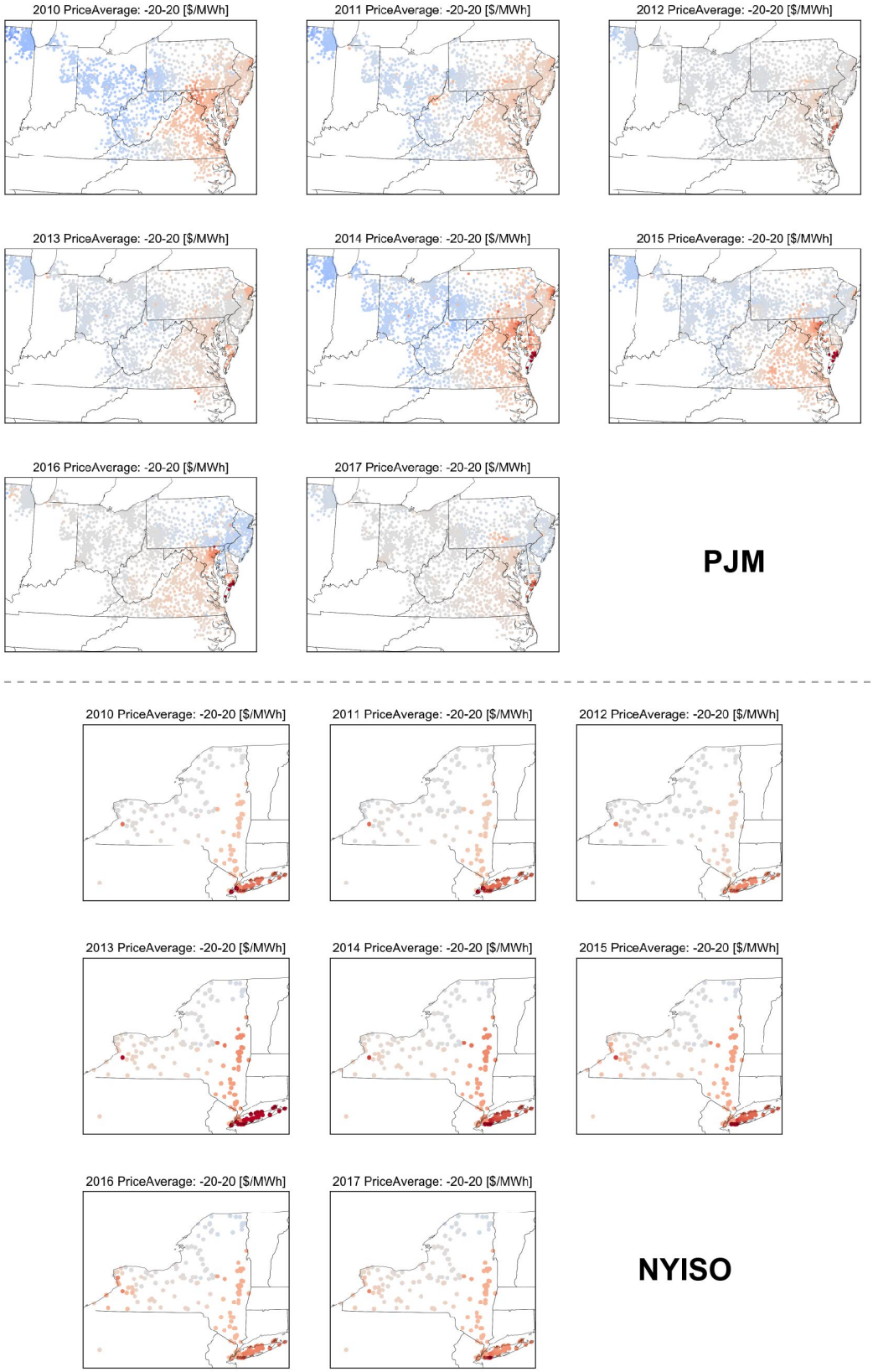

Figure SI.31: Maps of nodal marginal congestion costs (MCC) in PJM (a) and NYISO (b) over 2010–2017.

SI Note 7 Alternative assumptions for capacity credit

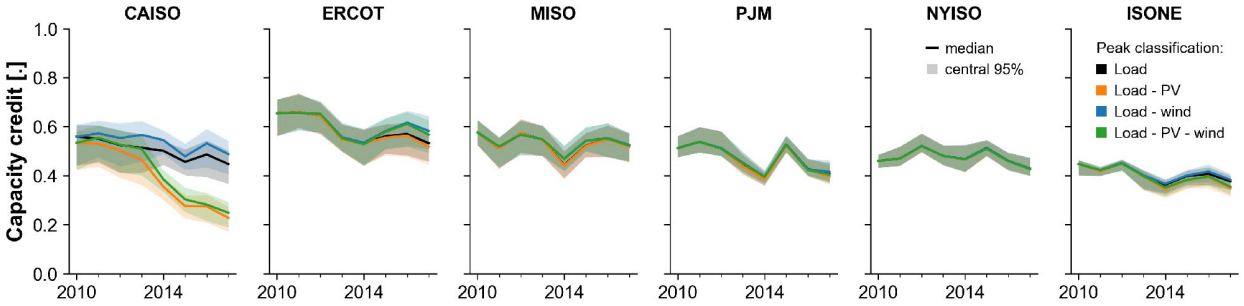

Figure SI.32: Dependence of calculated PV capacity credit on load metric. All traces use the top 7.04 % of load hours, with load defined as ISO-wide load (black), load minus utility-scale solar generation (orange), load minus ISO-reported wind generation (blue), and load minus utility-scale solar generation minus ISO-reported wind generation (green). The data associated with the green trace (load minus solar minus wind) is used in the main text and is equivalent to the blue trace in Figure 3b.

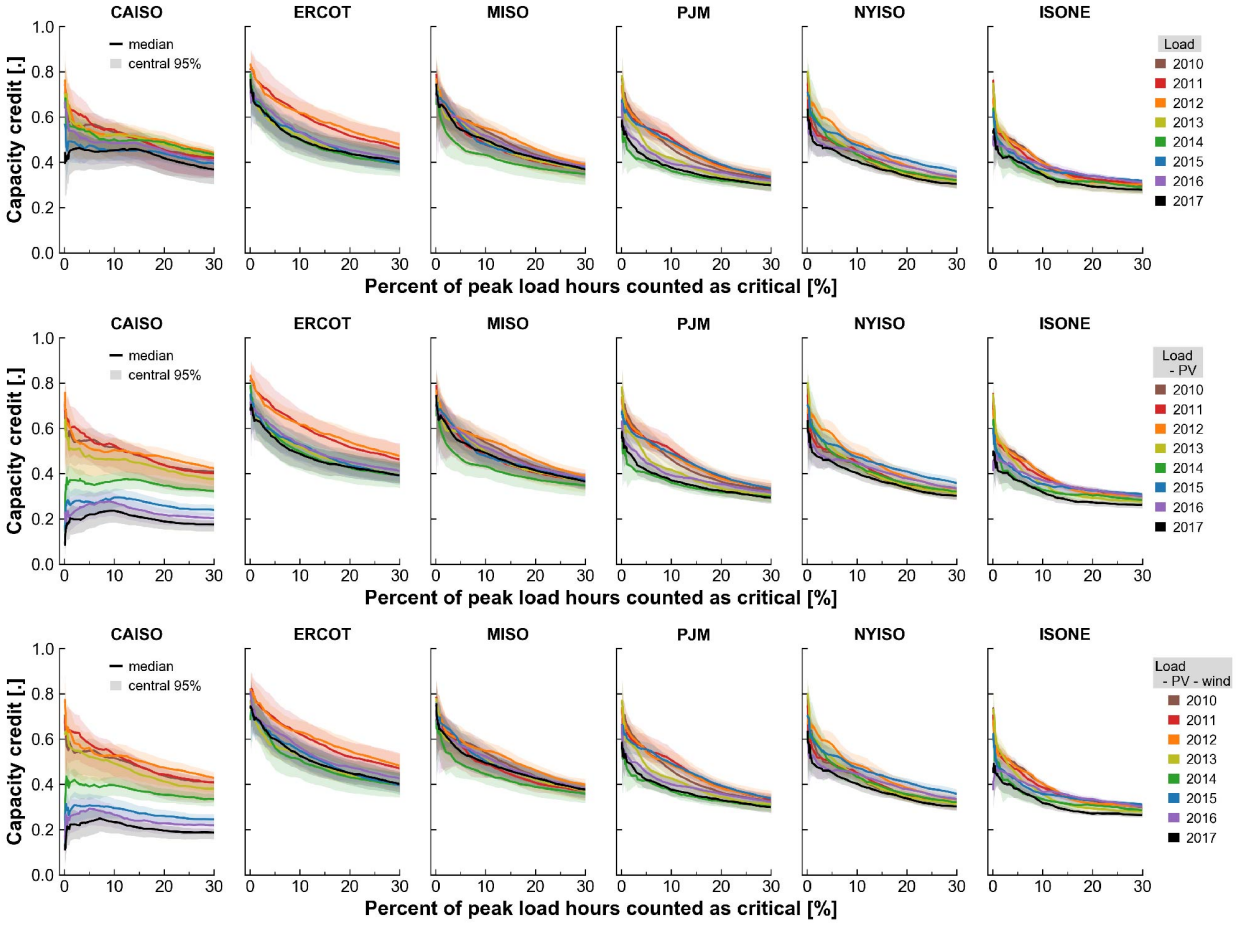

Figure SI.33: Dependence of calculated PV capacity credit on percentage of hours counted as critical. Load is defined as ISO-wide load (**a**), load minus utility-scale solar generation (**b**), or load minus utility-scale solar generation minus ISO-reported wind generation (**c**).

SI Note 8 Supplemental results: Health benefits

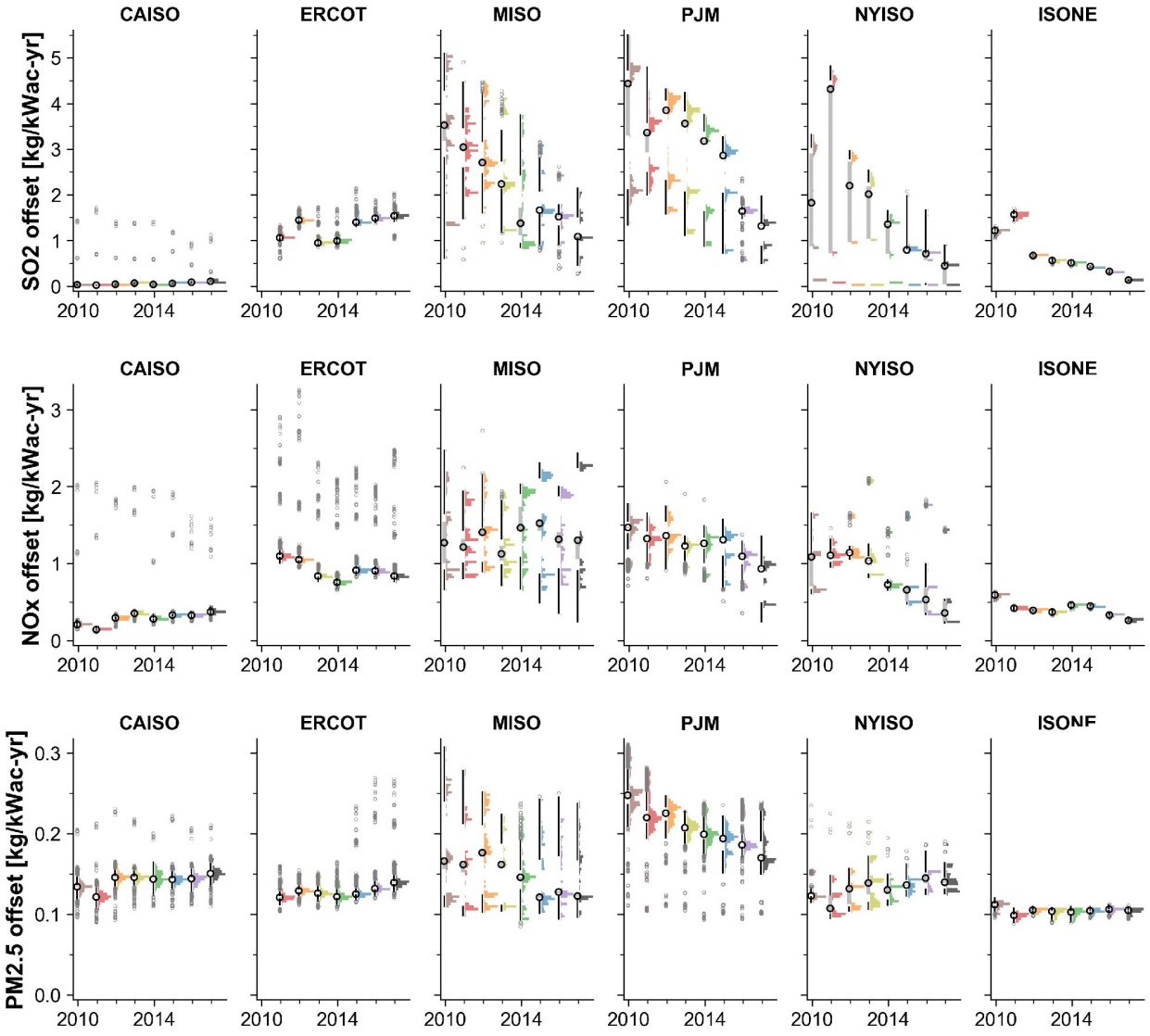

Figure SI.34: Distribution of nodal PV air pollution emissions offsets disaggregated by pollutant.

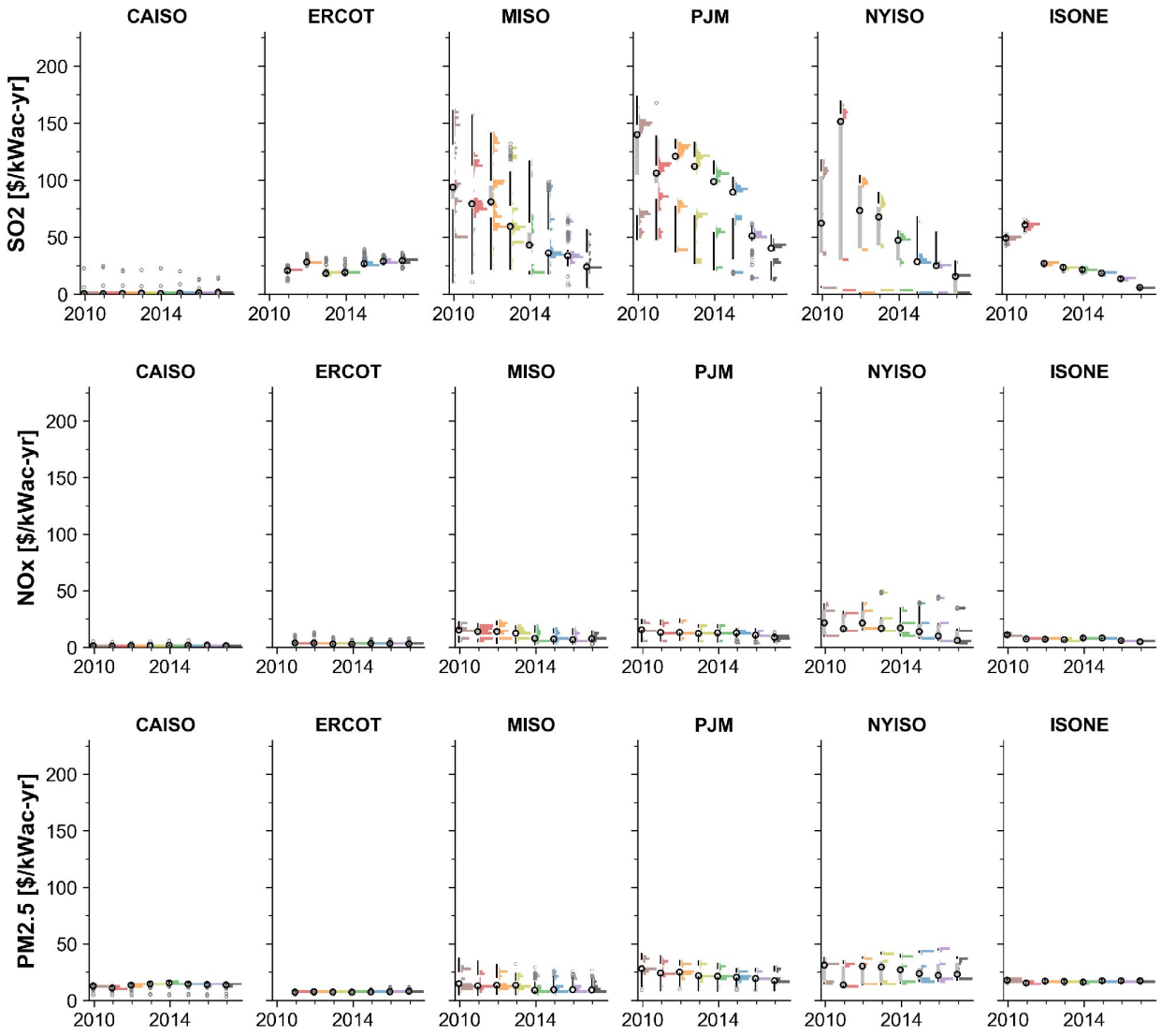

Figure SI.35: Distribution of nodal PV public health benefits from air pollution mitigation disaggregated by pollutant.

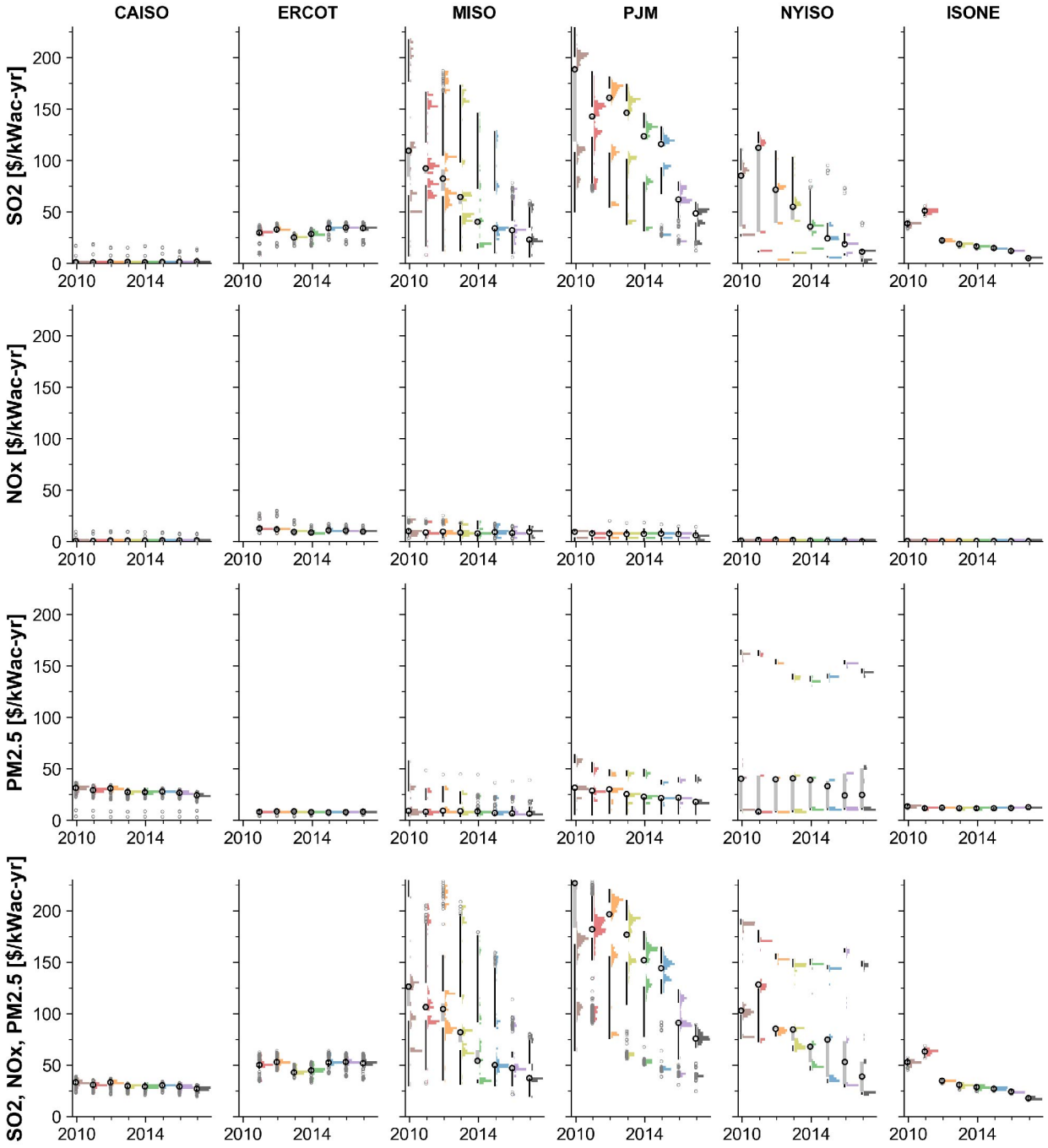

Figure SI.36: Distribution of nodal PV public health benefits from air pollution mitigation using the AP2 model. [91, 92, 93, 31] Median PV marginal health benefits calculated using AP2 in 2017 range from +64 % (in CAISO) to −37 % (in ISONE) of the benefits calculated using EASIUR. In a multi-model comparison, Millstein et al. [10] conclude that the EASIUR model is best-suited for the purposes of the present analysis, and find that EASIUR results are within 10 % of the central estimate across the five models examined. We therefore use EASIUR results (Figures 4 and SI.35) in the present analysis.

SI Note 9 Alternative assumptions for breakeven cost

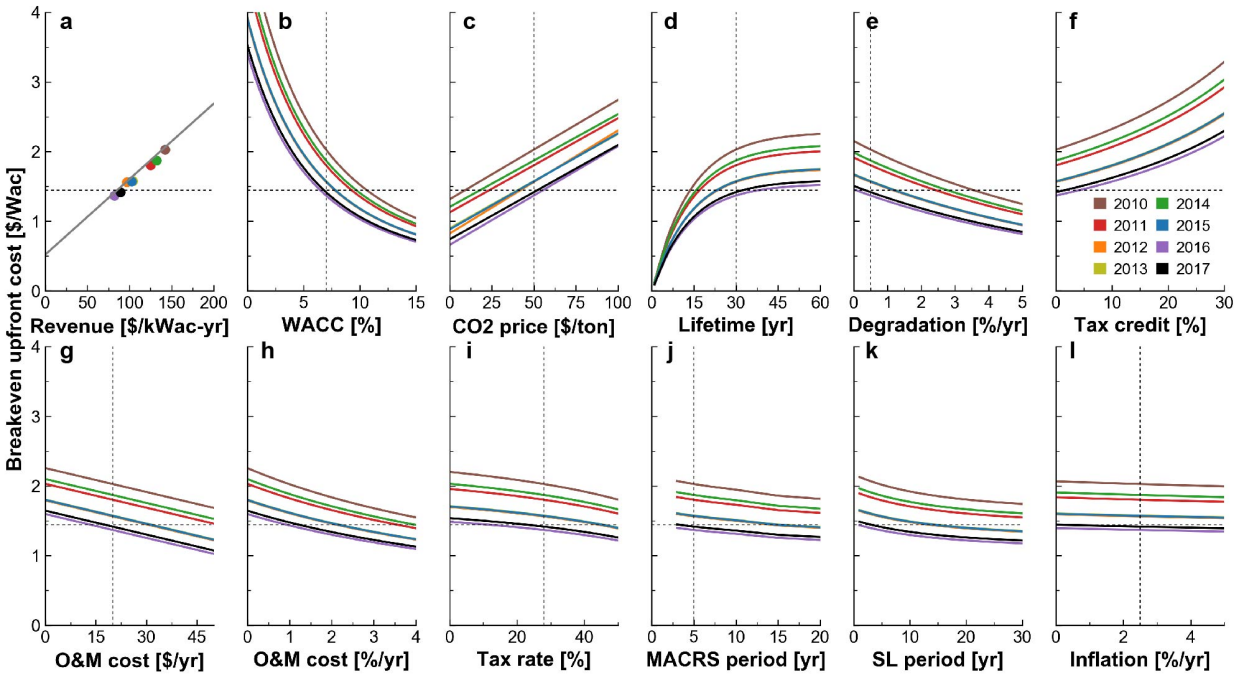

Figure SI.37: Sensitivity of calculated breakeven upfront cost to financial assumptions. Results are for a horizontal 1-axis tracking PV array ($\theta = 0°, \phi = 180°$) including revenue from the day-ahead wholesale energy market and capacity market and the value of abated carbon emissions (leaving out public health benefits) and are calculated according to (1). The gray line in **a** utilizes the median marginal carbon displacement M_{CO_2} across all years; colored markers in **a** utilize the median M_{CO_2} from the corresponding year. Each trace in **b**–**l** represents the breakeven cost for the median value of PV revenue R and marginal carbon displacement M_{CO_2} for each year. Horizontal dashed lines indicate the observed PV upfront system cost in 2017. [1] Vertical dashed lines in each panel indicate the value assumed in Figure 5 and used in each of the other panels. "SL period" refers to straight-line depreciation as an alternative to MACRS depreciation; an SL period of 5 years indicates nominal depreciation of 20 % per year.

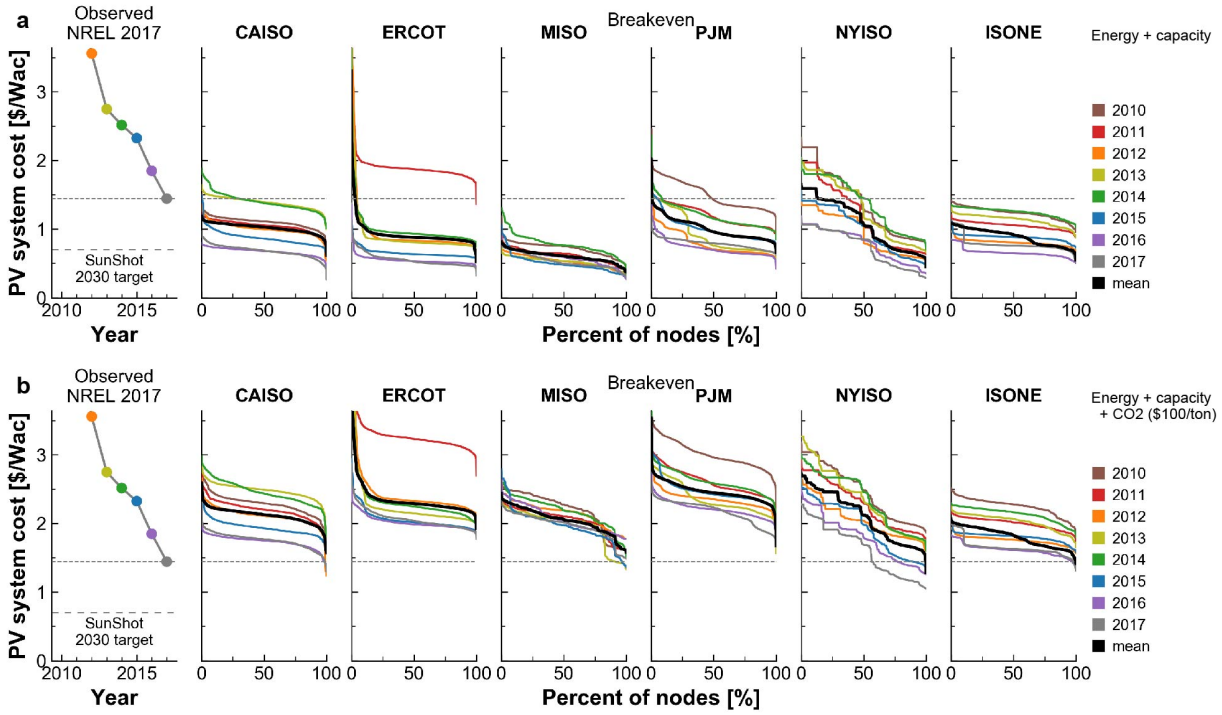

Figure SI.38: Breakeven upfront PV costs for 2010–2017 profile years. Results are presented as in Figure 5. Quantified benefits include (**a**), energy and capacity; (**b**), energy, capacity, and CO_2 abatement at 100 \$/tonCO_2;

MIT CEEPR

MIT Center for Energy and Environmental Policy Research

Since 1977, the Center for Energy and Environmental Policy Research (CEEPR) has been a focal point for research on energy and environmental policy at MIT. CEEPR promotes rigorous, objective research for improved decision making in government and the private sector, and secures the relevance of its work through close cooperation with industry partners from around the globe. Drawing on the unparalleled resources available at MIT, affiliated faculty and research staff as well as international research associates contribute to the empirical study of a wide range of policy issues related to energy supply, energy demand, and the environment.

An important dissemination channel for these research efforts is the MIT CEEPR Working Paper series. CEEPR releases Working Papers written by researchers from MIT and other academic institutions in order to enable timely consideration and reaction to energy and environmental policy research, but does not conduct a selection process or peer review prior to posting. CEEPR's posting of a Working Paper, therefore, does not constitute an endorsement of the accuracy or merit of the Working Paper. If you have questions about a particular Working Paper, please contact the authors or their home institutions.

MIT Center for Energy and Environmental Policy Research
77 Massachusetts Avenue, E19-411
Cambridge, MA 02139
USA

Website: ceepr.mit.edu

MIT CEEPR Working Paper Series is published by the MIT Center for Energy and Environmental Policy Research from submissions by affiliated researchers.

For inquiries and/or for permission to reproduce material in this working paper, please contact:

Email ceepr@mit.edu
Phone (617) 253-3551
Fax (617) 253-9845